INAUGURAL–DISSERTATION
zur
Erlangung der Doktorwürde
der
Naturwissenschaftlich–Mathematischen
Gesamtfakultät
der
Ruprecht–Karls–Universität
Heidelberg

vorgelegt von
M.Sc. Mathematics Rana Muhammad Humza
aus Gujranwala, Pakistan

Tag der mündlichen Prüfung:

Numerical Investigation of Non-reactive and Reactive Turbulent Spray Flows

Advisor: Prof. Dr. Eva Gutheil

Acknowledgements

I must acknowledge the great opportunity to study at University of Heidelberg, which enabled me to learn and develop in the best academic atmosphere possible. The Faculty of Mathematics at this university is well known and highly ranked. I also pay my gratitude to Interdisciplinary Center of Scientific Computing (IWR) and Heidelberg Graduate School of Mathematics and Computational Sciences (HGS-MathComp) for their great research facilities and environment. I would also thank the financial support from HGS-MathComp and Kohat University of Science and Technology, Pakistan.

I would like to thank Prof. Dr. Eva Gutheil for her continuous support and guidance during all the time of my Ph.D. work. She always guided me with patience and helped me to complete the thesis. Her valuable suggestions and prompt feedbacks were a source of motivation. During all the time of my Ph.D., she was always there whensoever I needed help. I am also thankful for the financial and moral support that she provided me.

I would extend my cordial thanks to Prof. Dr. Gabriel Wittum. He always helped me to go through this period of Ph.D.. His precious remarks made me complete this thesis. I am grateful to him for his help in documentation and his comments on the thesis.

I was an alien in Heidelberg, I am obliged to thank all of my colleagues and friends who made my stay in Heidelberg so special, the people whom I will always share the cheerful memories with. They simply made me feel at home and became part of my family. I am thankful to Mrs. Vogel, Mrs. Cramer-Langer, Daniela, Cui, Fenfen, Hai-Wen, Gerit, Chandan, Srikanth, James, Yong Hu, Hernan, Manfred, and Stefan for their cooperation and help as a nice colleague.

I do have the emotions but not the words to thank my parents Mr. Rana Muhammad Ali and Mrs. Riffat Jahan. Their prayers, love, warmth feelings and kindness was and will remain the most precious asset of my life. I can not count their favors and help, but I do count on them. In short, I consider myself lucky to be their son. I would also thank my sisters, brothers-in-law, nephews and nieces for their love and affection.

Contents

Abstract I

Zusammenfassung III

1. Introduction 1

2. Governing Equations 7
2.1 Gas phase flow 7
2.1.1 Conservation equations 7
2.1.2 Chemical reactions modeling 13
2.2 Probability density function methods 15
2.2.1 Presumed PDF methods 15
2.2.2 Transported PDF methods 19
2.2.3 Boundary conditions 22
2.3 Liquid phase flow 23
2.3.1 Direct quadrature method of moments (DQMOM) 23
2.3.2 Discrete droplet model (DDM) 25
2.3.3 Droplet dynamics 25
2.3.4 Droplet evaporation 26
2.3.5 Droplet heating 28
2.3.6 Droplet collisions 28
2.3.7 Source terms 29

3. Numerical Schemes 31
3.1 Finite volume method for gas phase conservation equations 32
3.1.1 Discretized formulation 36
3.1.2 Solution algorithm 41
3.1.3 Stability 41
3.2 Monte-Carlo particle method for the PDF transport equation 43
3.3 Liquid phase 46
3.3.1 Stochastic parcel method for DDM 46
3.3.2 Finite difference scheme for DQMOM 47

4. Results and Discussion 51
4.1 Evaporating Water/Air Spray 51
4.1.1 Experimental setup 51
4.1.2 Initial data generation 52
4.1.3 Results 54
4.2 Methanol/Air Spray Flame 61
4.2.1 Experimental Setup 63
4.2.2 Results 63

5. Conclusions and Outlook 73

Appendix 75

A. Trivariate Transported PDF 77
A.1 Derivation of PDF transport equation 77
A.2 Velocity model 79

B. Nomenclature 81

Abstract

The droplet size distribution and interaction of the liquid phase and the gas flow are key features in the modeling of evaporating spray flows, which are important because of their vast range of industrial and engineering applications. Two-phase effects and poly-dispersity of droplet size distributions dominate the structure of any spray and related applications such as spray flames, end products of spray drying processes, or medical applications. The spray dynamics depends on various physical processes such as droplet inertia, evaporation, and gas phase characteristics. Thus, it is important to have reliable models and numerical techniques in order to be able to describe the physics of two-phase flows, where the dispersed phase consists of droplets of various sizes that may evaporate, coalesce, breakup as well as have their own inertia and size-conditioned dynamics.

In the present thesis, an evaporating water/air spray is modeled using direct quadrature method of moments (DQMOM) and discrete droplet model (DDM) in an axisymmetric geometrical configuration. In DDM, the two-phase effects are captured by resolving the gas phase conservation equations considering the droplets as point sources. The system of conservation equations is closed using an extended $k - \epsilon$ model. The system of equations is solved using a hybrid finite volume - Lagrangian particle tracking method. DQMOM is not yet coupled to gas phase fully, rather the inlet gas flow properties are used to compute the drag force exerted on droplet velocity. For both DDM and DQMOM, appropriate initial and boundary conditions as well as the starting values for simulations are generated from experimental data, which have been carried out by the group of Prof. G. Brenn at TU Graz, Austria. The simulation results are compared with experiment and found in good agreement.

Furthermore, a turbulent methanol air jet spray flame is investigated. A detailed methanol/air combustion mechanism consisting of 23 species and 168 elementary reactions is implemented through a spray flamelet model. The process of molecular mixing is treated following probability density function (PDF) modeling, where two approaches are used i.e., presumed PDF and transported PDF. The standard β distribution is used as the base case to describe the process of molecular mixing. Its shape parameters and distribution characteristics are known and well established.

A bivariate joint PDF of the mixture fraction and enthalpy is applied for turbulent

spray flames. The PDF transport equation is deduced. The mixture fraction and enthalpy are described using an extended Interaction-by-Exchange-with-the-Mean (IEM) model and modified Curl's model. The PDF transport equation is closed through coupling with an extended $k - \epsilon$ model, and it is solved using a hybrid finite volume/Lagrangian Monte-Carlo particle method. The numerical results of the gas velocity, the gas temperature, and the Sauter mean radius are compared with experimental data from the literature and good agreement with the experiment is observed. Furthermore, the shapes of the PDF of the mixture fraction and enthalpy at different positions, which are computed by the transported PDF method, are presented and analyzed. For the sake of comparison, the presumed PDF method is also applied, where statistical behavior of mixture fraction is described using standard β function. A comparison of the results of the transported PDF method using modified Curl's and IEM models with the standard β function shows that the standard β function fails to describe the statistical behavior of mixture fraction accurately. Effect of a four parameter modified β distribution instead of a standard β distribution are also discussed. A trivariate joint PDF of enthalpy, gas velocity and mixture fraction is proposed for future simulations, and its transport equation is derived, where the gas velocity is modeled using an extended simplified Langevin model.

Zusammenfassung

Die Tröpfchengrößenverteilung und die Wechselwirkung der flüssigen und der Gasphase sind wesentliche Merkmale bei der Modellierung von Spray Geladenen Strömungen, die wichtig sind aufgrund ihrer Vielzahl von industriellen und technischen Anwendungen. Zweiphasen-Effekte und Poly-Dispersität von Tröpfchengrößenverteilungen dominieren die Struktur eines jeglichen Sprays und verwandter Anwendungen wie beispielsweise Sprayflammen, Endprodukten von Sprühtrocknungsverfahren oder medizinische Anwendungen. Die Spraydynamik hängt von verschiedenen physikalischen Prozessen ab wie Tröpfchenträgheit, Verdampfung und Gasphasen-Characteristika. Somit ist es wichtig, zuverlässige Modelle und numerische Verfahren zu haben, um die Physik von Zweiphasenströmungen zu beschreiben, bei denen die dispergierte Phase aus Tröpfchen unterschiedlicher Größe besteht, die verdampfen, koalieren und aufbrechen können, wobei sie ihre eigene Dynamik besitzen.

In der vorliegenden Arbeit wird ein verdampfenes Wasser/Luft Spray modelliert mittels *direct quadrature method of moments* (DQMOM) und einen *discrete droplet model* (DDM) in einer axialsymmetrischen Konfiguration. Bei dem DDM werden die Zweiphasen-Effekte durch Lösen der Gasphasen-Erhaltungsgleichungen unter Berücksichtigung der Tröpfchen als Punktquellen beschrieben. Das System der Erhaltungsgleichungen wird geschlossen durch ein erweitertes $k - \epsilon$ Modell. Die Gleichungen werden mittels einer *hybrid finite volume - Lagrangian particle tracking method* gelöst. DQMOM ist noch nicht vollständig an die Gasphase gekoppelt, stattdessen werden die Eigenschaften des einströmenden Gases zur Berechnung der einwirkenden Trägheitskraft auf die Tröpfchengeschwindigkeit verwendet. Geeignete Anfangs- und Randbedingungen sowie die Startwerte für die Simulationen werden aus experimentellen Daten generiert, die von der Arbeitsgruppe von Prof. G. Brenn an der TU Graz, Österreich, erarbeitet wurden. Die Simulationsergebnisse wurden mit den experimentellen Ergebnissen verglichen und ergeben gute Übereinstimmung.

Weiterhin wird eine turbulente Methanol/Luft Freistrahlflamme untersucht. Ein detaillierter Methanol/Luft-Verbrennungsmechanismus bestehend aus 23 Spezies und 168 Elementarreaktionen wird durch ein Spray-Flamelet-Modell implementiert. Der Prozess des molekularen Mischens wird mittels *probability density function* (PDF) Modellierung behandelt, wobei zwei Ansätze verwendet werden, die *presumed* PDF und *transported* PDF. Die Standard β-Verteilung wird als Basisfall verwendet, um den Prozess des molekularen Mischens zu beschreiben, da diese Funktion sehr gut bekannt und etabliert ist.

Eine Zweidimensional gebundene PDF des Mischungsbruchs und der Enthalpie wird auf turbulente Sprayflammen angewendet. Die PDF-Transportgleichung wird

hergeleitet. Der Mischungsbruch und die Enthalpie werden beschrieben unter Verwendung eines erweiterten *Interaction-by-Exchange-with-the-mean* (IEM)-Modells und des *modified Curl*-Modells. Die PDF-Transportgleichung wird durch Kopplung mit einem erweiterten $k - \epsilon$ Modell und mittels einer *hybrid finite volume/Lagrangian Monte-Carlo* Methode gelöst. Die numerischen Ergebnisse der Gasgeschwindigkeit, der Gastemperatur und des Sauter Radius werden mit experimentellen Daten aus der Literatur verglichen und es wird gute Übereinstimmung gefunden. Ferner werden die Formen der PDF des Mischungsbruchs und der Enthalpie, die durch die *transported* PDF-Methode berechnet werden an unterschiedlichen Positionen, dargestellt und analysiert. Für Vergleichszwecke wird das *presumed* PDF Verfahren ebenfalls angewendet, wobei das statistische Verhalten des Mischungsbruchs mittels der Standard β-Funktion beschrieben wird. Ein Vergleich der Ergebnisse der *transported* PDF Methode unter Anwendung der *modified Curl*- und IEM-Modelle mit der Standard β-Funktion zeigt, dass die Standard β-Funktion das statistische Verhalten des Mischungsbruchs nicht genau beschreiben kann. Die Auswirkungen einer modifizierten Vier-Parameter β-Verteilung anstelle einer Standard β-Verteilung werden ebenfalls diskutiert. Weiterführende Arbeiten sollten eine *trivariate joint* PDF von Enthalpie, Gasgeschwindigkeit und Mischungsbruch beinhalten, dazu wird deren Transportgleichung hergeleitet, indem die Gasgeschwindigkeit mit einem erweiterten vereinfachten Langevin-Modell beschrieben wird.

List of Figures

3.1 Particle-Source-in-Cell (PSIC) model [95] 34
3.2 Staggered grids in two dimensions: $\rightarrow = \tilde{u}_x$; $\uparrow = \tilde{u}_r$; $\bullet$ = scalar variables [158]. 35
3.3 Control volume of the grid nodes [158]. 37
3.4 Control volume of axial velocity (left) and radial velocity (right) [158]. . 39

4.1 Schematic of experimental setup 52
4.2 Profile of effective cross-section area of the probe volume for measured droplet size. 52
4.3 Experimental and DQMOM approximation of droplet number density for a water spray. 53
4.4 Experimental and numerical profiles of the Sauter mean diameter at the cross section of 0.12 m distance from the nozzle exit for 80 kg/h. 54
4.5 Experimental and numerical profiles of the Sauter mean diameter at the cross section of 0.16 m distance from the nozzle exit for 80 kg/h. 55
4.6 Experimental and numerical profiles of the Sauter mean diameter at the cross section of 0.12 m distance from the nozzle exit for 120 kg/h. . . . 56
4.7 Experimental and numerical profiles of the Sauter mean diameter at the cross section of 0.16 m distance from the nozzle exit for 120 kg/h. . . . 56
4.8 Experimental and numerical profiles of the mean droplet diameter at the cross section of 0.12 m distance from the nozzle exit for 80 kg/h. . 57
4.9 Experimental and numerical profiles of the mean droplet diameter at the cross section of 0.16 m distance from the nozzle exit for 80 kg/h. . 58
4.10 Experimental and numerical profiles of the mean droplet diameter at the cross section of 0.12 m distance from the nozzle exit for 120 kg/h. . 59
4.11 Experimental and numerical profiles of the mean droplet diameter at the cross section of 0.16 m distance from the nozzle exit for 120 kg/h. . 59
4.12 Experimental and numerical profiles of the mean droplet velocity at the cross section of 0.12 m distance from the nozzle exit. 60
4.13 Experimental and numerical profiles of the mean droplet velocity at the cross section of 0.16 m distance from the nozzle exit. 61

4.14 Schematic of the methanol/air experimental setup. 62
4.15 Sketch of the fuel injector. 62
4.16 Experimental and numerical profiles of the axial gas velocity at the cross section of 0.025 m distance from the nozzle exit. 64
4.17 Experimental and numerical profiles of the axial gas velocity at the cross section of 0.05 m distance from the nozzle exit. 64
4.18 Experimental and numerical profiles of the axial gas velocity at the cross section of 0.075 m distance from the nozzle exit. 65
4.19 Experimental and numerical profiles of the axial gas velocity at the cross section of 0.1 m distance from the nozzle exit. 66
4.20 Experimental and numerical profiles of the axial gas velocity at the cross section of 0.15 m distance from the nozzle exit. 66
4.21 Experimental and numerical profiles of the gas temperature at the cross section of 0.025 m distance from the nozzle exit. 67
4.22 Experimental and numerical profiles of the gas temperature at the cross section of 0.05 m distance from the nozzle exit. 67
4.23 Experimental and numerical profiles of the gas temperature at the cross section of 0.075 m distance from the nozzle exit. 68
4.24 Experimental and numerical profiles of the gas temperature at the cross section of 0.1 m distance from the nozzle exit. 69
4.25 Experimental and numerical profiles of the gas temperature at the cross section of 0.15 m distance from the nozzle exit. 69
4.26 Experimental and numerical profiles of Sauter mean radius at the cross section of 0.025 m distance from the nozzle exit. 70
4.27 Transported and presumed PDF shapes at axial location of 0.025 m and radial location of 0.01 m (left) as well as at axial location of 0.05 m and radial location of 0.01 m (right). 71
4.28 Comparison of modified β with standard β and transported PDF methods for gas temperature at the cross section of 0.05 m distance from the nozzle exit. 71

List of Tables

3.1 Governing equations of the gas flow with a dilute spray [67]. 33

1. Introduction

Turbulent spray flows have been a topic of interest of researchers for decades due to their wide range of applications in a diverse variety of fields. Limited possibilities of precise study of turbulent spray flows in available experimental facilities have added to the value of spray modeling. The physical processes that govern the dynamics and size distribution of the spray such as application of drag by surrounding gas, droplet collisions leading to breakup, coalescence or mass transfer and turbulence are important to be considered to reach a feasible model.

The droplet size distribution and interaction of the liquid phase and the gas flow are key features in the modeling of evaporating spray flows, which are important because of their vast range of industrial and engineering applications. Two-phase effects and poly-dispersion of droplet size distributions dominate the structure of any spray and related applications such as spray flames, spray drying processes, or in spray inhalers of medical applications. An improved understanding of the physical processes that influence the spray characteristics is essential because of the complexity of the corresponding mathematical problem. The spray dynamics depend on various physical processes such as droplet inertia, evaporation, and gas phase characteristics. Thus, it is important to have reliable models and numerical techniques in order to be able to describe the physics of two-phase flows where the dispersed phase is constituted of droplets of various sizes that may evaporate, coalesce, breakup as well as have their own inertia and size-conditioned dynamics.

In regards with physical assumptions, the spray models may be categorized in *locally homogeneous flow* (LHF) models [1–3] and *separated flow* (SF) models [4, 5]. LHF models assume the two phases to be in dynamic and thermodynamic equilibrium i.e., at each position in the flow field, droplet has the same velocity and temperature as the surrounding gas. The slip effect between the liquid phase and gas phase is neglected. The LHF condition is the limiting case with infinitely small droplets. This makes the modeling and simulation relatively easy but most of the practical cases cannot be accounted for.

The SF models are a suitable alternative, which take the effects of the finite rate exchange of properties between the two phases into account. In general, there are different approaches in the SF model namely continuous droplet model (CDM) [6–13] and discrete droplet model (DDM) [14–21].

CDM assumes that the droplets have a continuous behavior characterized by their statistical properties with negligible deviation from spherical shape [22]. In this approach, the dispersed phase is treated as a continuous fluid. Therefore, in order to represent droplets in continuous formulation, a number of scalar fields are introduced such as weights [23]. The droplet properties are defined at grid nodes, which coincide with those for the gas phase. The mean flow field equations are derived for both phases. Thus, they result in more global or macroscopic description of the dispersed phase.

There are several Eulerian methods that have been developed based upon Williams' spray equation [22] and applied extensively in recent years. For instance, in the multi-fluid approach [6], the distribution function is discretized using a finite volume technique that yields conservation equations for mass and momentum of droplets in fixed size intervals called sections or fluids [7]. This approach has recently been improved to higher order of accuracy [8], but discretization of droplet size phase - space is still a problem that needs to be addressed. The efficiency and the applicability of moment based methods [9, 10] for poly-disperse systems have remained a question of interest [11]. In order to address these issues, direct quadrature method of moments (DQMOM) has turned out to be an attractive and suitable approach [12].

Even though DQMOM has been tested to model non-evaporating sprays [24–26], few studies have been carried out on evaporating sprays [23, 27, 28]. However, these studies consider a very simplified evaporation model to calculate the change in droplet size with time i.e., either as a linear function of droplet volume or non-linear function of droplet volume, which is similar to the well established but very simplified d^2 law. This has been improved [13] by implementing the advanced evaporation model.

On the contrary, DDM or Lagrangian approach focusses on rather microscopic level. In the Lagrangian approach, the mean field equations are used only for the continuous gas phase. The droplet properties are defined along the path lines followed by the droplet. The trajectories of droplets are tracked for each droplet group by using a set of equations that describe their physical transport in flow field. In case the gas phase is also described using a Lagrangian formulation, the stochastic particles are introduced and tracked to reproduce the same statistics as the real one. Their time evolution is solved by using stochastic differential equations. In this case, the gas phase may be solved by either Eulerian formulation or a Lagrangian formulation [15]. The effects of the liquid phase are considered by including appropriate spray source terms into the governing equations of the gas phase. The errors due to numerical diffusion in the solution of liquid phase are minimized in DDM. Furthermore, it is rather convenient to obtain a physical model and construct a numerical algorithm based on DDM [20, 30]. As far as droplet-turbulence interaction is considered, SF models can be further sub-categorized as *deterministic separated flow* (DSF) and *stochastic separated flow* (SSF)

models. In DSF models, the droplet-turbulence interaction is neglected, which may not be a physically feasible assumption in most of the cases. The resulting profiles predict only laminar behavior of the droplets. Therefore, SSF models turn out to be a suitable choice [18, 20].

In either the classical Eulerian or Lagrangian approach, the continuous gas phase is modeled using the Navier – Stokes equations. Considering the presence of turbulence in the system, these equations can be solved following a number of ways such as direct numerical simulation (DNS) [31–41], large eddy simulation (LES) [42–53] or Reynolds-averaged Navier – Stokes (RANS) numerical simulation [54, 55]. In DNS, the conservation equations are solved directly without any turbulence model, thus all the spatial and temporal scales of turbulence must be resolved. In LES method, the filtering implies that the scales below the filter width are not resolved and must be modeled. However, in reactive flows, molecular mixing and kinetics occur at small unresolved scales. Therefore, modeling these small scales and their coupling with LES resolved scales imposes additional challenges [43]. Hencce in reactive flows, RANS with density weighted averaged such as Favre-average is preferred.

An important aspect of the spray flows is the modeling of gas-liquid interactions i.e., study of the processes at the interface of liquid and gas. There are several physical processes dominating the droplet characteristics at the interface such as energy transfer, mass transfer and drag force. The coupling between continuum gas phase and dispersed droplet phase can be done in a number of ways, the simplest being one-way coupling. In one-way coupling, the behavior of transported droplets is described within a given turbulent gas flow. The effects of carrier phase on the dispersed particles are taken into account explicitly. However, the effects of droplet characteristics on the gas phase are not negligible in many cases. The turbulence influences the behavior of droplets, which in return effect turbulence. This is because of the micro turbulence, which is produced due to the presence of the droplets. In particular, boundary layers are formed at the interface of the droplets and gas i.e., droplet surface, due to relative motion of the droplet and the surrounding gas, which is commonly described as the drag force effect. If there is heat and mass transfer between droplets and surrounding gas, which is quite common in spray flows then the two-way coupling is the suitable choice. In two-way coupling, the effects of droplet properties are considered in evolution of gas phase flow and vice versa. It is well established that a two-way coupling is suitable for droplets interacting with turbulent carrier phase, particularly at low Mach number [56, 57].

In turbulent spray flames, the detailed chemistry may be included by using flamelt based model. In this approach, a turbulent flame is considered as an ensemble of laminar flames [58]. Flamelet model was originally proposed for gas flames [58]. This assumption is valid for high Damköhler numbers, which is fulfilled in many technical

combustion applications. The success of flamelet based models in the simulation of turbulent gas flames has motivated their application in the simulation of turbulent spray flames [59]. However, the classical flamelet model includes very strict assumptions regarding the different combustion regimes that may occur in turbulent flames. In general, either non-premixed or premixed combustion are considered, whereas the partially premixed regime is discarded. Recently, several multi-regime flamelet models have been developed in order to overcome the limitations related with classical flamelet models [60–62]. In general, multi-regime flamelet models based on laminar gas structures are able to predict the flame characteristics in zones where no evaporation occurs, since these regions are not considerably affected by spray processes [63], but they are not suitable to properly describe the flame structure in zones where both evaporation and combustion occur, since they are dominated by evaporation effects. Therefore, a separation of the regimes with pure gas combustion, i.e. all droplets have vaporized, and a regime where both evaporation and combustion occur simultaneously [63], solve the question of the pure gas combustion regime, but not the region, where both evaporation and chemical reactions occur simultaneously [65].

Hollmann and Gutheil [65] and Gutheil [63] proposed an extension of the classical non-premixed flamelet model [58] for spray flames, which consistently uses a library based on laminar spray structures. It is found that spray flamelets are not only determined by the mixture fraction and its scalar dissipation rate (associated with the strain rate) as in counterflowing laminar gas diffusion flames, but they also depend on the initial droplet size and velocity and the equivalence ratio on the spray side of the configuration [58].

In flamelet models, the chemistry and turbulence are coupled through the statistical discription of characteristic variables. This can be done by using the probability density function (PDF) methods. These include presumed PDF method and transported PDF method. In presumed PDF method, the statistical distribution of mixture fraction and scalar dissipation rate is calculated considering their mutual statistical independence. The β distribution is applied to presume mixture fraction [66, 67]. Ge and Gutheil [68] and Luo *et al.* [32] reported that a modified four parameter β distribution is a better approximation than standard two parameter β distribution. But the choice of additional parameters namely the minimum and maximum of PDF domain is still an open question. The scalar dissipation rate is presumed to follow log-normal distribution [69, 70].

In the transported PDF methods [64], the shape of PDF is calculated by solving its transport equation. Earlier studies have favored PDF transport equation [71], which was applied to gas flames. The advantage is that no additional modeling for chemical reactions or turbulence is required. This approach was extended to account for spray

flows as well [94]. In transported PDF method, the term for molecular mixing requires to be closed through an additional model. Therefore, in order to analyze the effects of molecular mixing and evaluate the existing mixing models, the PDF transport equation serves as a suitable ground. For gas flames, the simplest model is interaction by exchange with the mean (IEM) model [72], which is extended to account for spray flames [68, 94]. In gas flames, there are other mixing models available in literature, which include Curl's particle interaction model [73], modified Curl's model [74, 75] and Eucleadian minimal spanning tree (EMST) [76]. But these models are not yet formulated for spray flows.

In the present work, two different spray systems i.e., an evaporating water/air spray and reactive methanol/air spray flame have been considered. The evaporating water/air spray is modeled using DQMOM and DDM in an axisymmetric, two-dimensional configuration. In DDM, the effects of the two-phase flow are captured by solving the gas phase conservation equations considering the droplets as point sources. DQMOM considers the inlet gas flow properties to compute the drag force exerted on droplet velocity. Droplet collisions are also included in DQMOM. The methanol/air flame is modeled using presumed and transported PDF methods. The gas phase is resolved using Favre averaged conservation equations with appropriate source terms due to spray evaporation. The chemical reactions are included using laminar flamelet library [65, 83]. In presumed PDF method, the standard β distribution is applied and different choices for additional two parameters for four parameter modified β distribution are analyzed. In transported PDF method, modified Curl's model is extended to account for spray flows. The spray source terms in extended IEM are rederived. The results from transported and presumed PDF methods are compared with experiment at various positions.

In this dissertation, the governing equations of mathematical models are described in chapter 2. The applied numerical schemes are discussed in chapter 3. The results are presented and discussed in chapter 4. The conclusions and perspective work is given chapter 5.

2. Governing Equations

The mathematical model to treat two phase flows and their inter-coupling is explained in this chapter. Taking the advantages of locally detailed information into account, both reactive and non-reactive spray flows are treated using Euler-Lagrangian formulation. The gas phase is treated as a continuum phase while the liquid phase flow is modeled by applying discrete droplet model. The non-reactive (water) spray is modeled using DQMOM as well. The governing equations for gas flow, DQMOM and DDM are given in this chapter.

2.1 Gas phase flow

2.1.1 Conservation equations

Mathematical description of the considered spray system is achieved by resolving the gas phase equations where the effect of dispersed phase is taken into account through inclusion of source terms [77], where droplets are considered are point sources. under the assumptions of dilute spray and low Mach number, the compressible form of conservation equations of mass and momentum may be written as

$$\frac{\partial \rho}{\partial t} + \frac{\partial (\rho u_j)}{\partial x_j} = S_{l,1}, \tag{2.1}$$

$$\frac{\partial (\rho u_i)}{\partial t} + \frac{\partial (\rho u_i u_j)}{\partial x_j} = -\frac{\partial p}{\partial x_i} + \frac{\partial \tau_{ij}}{\partial x_j} + \rho g_i + S_{l,u_i}, \tag{2.2}$$

where $\rho, \mathbf{u}$ and p are the density, velocity and pressure of the gas flow. g_i is the acceleration due to gravity and the quantities $S_{l,1}$ and S_{l,u_i} are the source terms due to spray evaporation [67]. τ_{ij} is the viscous stress tensor given by

$$\tau_{ij} = \mu \left(\frac{\partial u_i}{\partial x_j} + \frac{\partial u_j}{\partial x_i} - \frac{2}{3} \frac{\partial u_k}{\partial x_k} \delta_{ij} \right), \tag{2.3}$$

where δ is the tensorial Kronecker delta given by

$$\delta_{ij} = \begin{cases} 1 & : \quad i = j \\ 0 & : \quad i \neq j. \end{cases} \tag{2.4}$$

Neglecting the processes of radiation, friction heating, Dufour effect and the viscous heating, the conservation equation of total stagnant enthalpy can be written as

$$\frac{\partial(\rho h)}{\partial t}+\frac{\partial(\rho u_j h)}{\partial x_j}=\frac{\partial p}{\partial t}-\frac{\partial J^d_{q,j}}{\partial x_j}-\frac{\partial J^c_{q,j}}{\partial x_j}+S_{l,h}, \tag{2.5}$$

where h is the enthalpy of the gas flow and the terms on the right-hand side are the change rate of the pressure, the heat diffusion term, the heat conduction term and the source term due to spray evaporation, $S_{l,h}$, respectively. The heat conduction term is expressed by the Fourier's Law

$$J^c_{q,j}=-\lambda\frac{\partial T}{\partial x_j}=\frac{\lambda}{\bar{C}_p}\left(\frac{\partial h}{\partial x_j}-\sum_{\alpha=1}^{N_s}h_\alpha\frac{\partial Y_\alpha}{\partial x_j}\right), \tag{2.6}$$

where λ, T, $\bar{C}_p$ are thermal conductivity, gas temperature and specific heat capacity respectively. N_s refers to the number of chemical species while h_α and Y_α are the enthalpy and mass fraction of species α. The heat diffusion term $J^d_{q,j}$ is written as

$$J^d_{q,j}=\sum_{\alpha=1}^{N_s}h_\alpha J^m_\alpha=-\sum_{\alpha=1}^{N_s}\rho h_{s,\alpha}D_{\alpha,M}\frac{Y_\alpha}{\partial x_j}, \tag{2.7}$$

where $h_{s,\alpha}$ and $D_{\alpha,M}$ are the specific sensible enthalpy of species α and diffusion coefficient of species α respectively. Assuming a unity Lewis number (Le = 1) and equal diffusibility of all species, the total heat flux is

$$J_q=J^c_{q,j}+J^d_{q,j}=-\frac{\lambda}{\bar{C}_p}\left(\frac{\partial h}{\partial x_j}-\sum_{\alpha=1}^{N_s}h_\alpha\frac{\partial Y_\alpha}{\partial x_j}\right)-\sum_{\alpha=1}^{N_s}\rho h_{s,\alpha}D_{\alpha,M}\frac{Y_\alpha}{\partial x_j}. \tag{2.8}$$

As it will be discussed in the next section (c.f. Eq. (2.46) – (2.56)) that

$$\frac{\lambda}{\bar{C}_p}\sum_{\alpha=1}^{N_s}h_\alpha\frac{\partial Y_\alpha}{\partial x_j}=\sum_{\alpha=1}^{N_s}\rho h_{s,\alpha}D_{\alpha,M}\frac{Y_\alpha}{\partial x_j},$$

therefore the Eq. (2.8) is reduced to

$$J_q=-\frac{\lambda}{\bar{C}_p}\frac{\partial h}{\partial x_j}=-\Gamma_h\frac{\partial h}{\partial x_j}. \tag{2.9}$$

Using Eq. (2.9) in Eq. (2.5), the energy equation can be written as

$$\frac{\partial(\rho h)}{\partial t}+\frac{\partial(\rho u_j h)}{\partial x_j}=\frac{\partial p}{\partial t}+\frac{\partial}{\partial x_j}\left(\Gamma_h\frac{\partial h}{\partial x_j}\right)+S_{l,h}. \tag{2.10}$$

The conservation equation of species mass can be written as

$$\frac{\partial(\rho Y_\alpha)}{\partial t}+\frac{\partial(\rho u_j Y_\alpha)}{\partial x_j}-\frac{\partial}{\partial x_j}\left(\rho D_\alpha\frac{\partial Y_\alpha}{\partial x_j}\right)=S_\alpha+\delta_{L,\alpha}S_{l,Y_\alpha}, \tag{2.11}$$

where D_α is the diffusion coefficient of species α while S_α and $S_{l,\alpha}$ are the source terms due to chemical reactions and spray evaporation respectively. The mass fraction may be used to form mixture fraction. The advantage of an appropriately defined mixture fraction is that the source term S_α will be zero. In the present work, two spray systems are considered i.e. water spray in air and methanol spray in air. In case of methanol spray in air, element mass fraction may be defined with reference to carbon because oxygen appears in both liquid and gaseous stream and Lewis number of hydrogen is very low. For the water spray, the only possibility is to define the mixture fraction with reference to hydrogen as oxygen appears in both gas and liquid. A detailed study of different reference elements may be referenced from [79]. Thus the mass fraction Z_{A} of element A, where A is either C or H is defined as

$$Z_{\mathrm{A}} = \sum_{i=1}^{n} \frac{a_{\mathrm{IA}} M_{\mathrm{A}}}{M_{\mathrm{I}}} Y_{\mathrm{I}}. \tag{2.12}$$

where a_{IA} is the mass of element A in molecule I and M_{A} and M_{I} are the molecular weights of element A and element I, respectively. Using this definition, mixture fraction can be defined as

$$\xi = \frac{Z_{\mathrm{A}} - Z_{\mathrm{A,min}}}{Z_{\mathrm{A,max}} - Z_{\mathrm{A,min}}}. \tag{2.13}$$

Multiplying Eq. (2.11) by $\frac{a_{\mathrm{IA}} M_{\mathrm{A}}}{a_{\mathrm{IA}} M_{\mathrm{I}}}$ and summing over total number of species under the assumption of equal diffusivity, the following conservation equation for mixture fraction is obtained

$$\frac{\partial(\rho\xi)}{\partial t} + \frac{\partial(\rho u_i \xi)}{\partial x_i} = \frac{\partial}{\partial x_i}\left(\Gamma_M \frac{\partial \xi}{\partial x_i}\right) + S_{l,\xi}, \tag{2.14}$$

where $\Gamma_M = \rho D_M$ is the mass diffusion coefficient of the mixture.

Equations (2.1), (2.2), (2.10) and (2.14) are the instantaneous conservation equations of mass, momentum, energy and mixture fraction. These need to be averaged for application to turbulent flows. For turbulent compressible flows, a density weighted average e.g. Favre average for Navier–Stokes equations is useful. Favre average of a function Φ is defend as

$$\widetilde{\Phi} = \frac{\overline{\rho\Phi}}{\bar{\rho}}. \tag{2.15}$$

The fluctuating components are then defined as

$$\Phi'' = \Phi - \widetilde{\Phi} \tag{2.16}$$

with

$$\widetilde{\Phi''} = 0. \tag{2.17}$$

Averaging the Eqs. (2.1) and (2.2) by using the Eq. (2.15), the following forms are obtained

$$\frac{\partial \bar{\rho}}{\partial t} + \frac{\partial(\bar{\rho}\widetilde{u}_j)}{\partial x_j} = \bar{S}_{l,1}, \tag{2.18}$$

and

$$\frac{\partial(\bar{\rho}\widetilde{u}_i)}{\partial t} + \frac{\partial(\bar{\rho}\widetilde{u}_i\widetilde{u}_j)}{\partial x_j} + \frac{\partial(\widetilde{\bar{\rho}u_i''u_j''})}{\partial x_j} = -\frac{\partial \bar{p}}{\partial x_i} + \frac{\partial \bar{\tau}_{ij}}{\partial x_j} + \bar{\rho}g_i + \bar{S}_{l,\tilde{u}_i}. \tag{2.19}$$

Averaging Eq. (2.10) using the Eq. (2.15) and applying gradient-diffusion hypothesis

$$\frac{\partial(\bar{\rho}\tilde{h})}{\partial t} + \frac{\partial(\bar{\rho}\widetilde{u}_j\tilde{h})}{\partial x_j} = \frac{\partial \bar{p}}{\partial t} + \frac{\partial}{\partial x_j}\left(\Gamma_{h,\text{eff}}\frac{\partial \tilde{h}}{\partial x_j}\right) + \bar{S}_{l,\tilde{h}}, \tag{2.20}$$

where the effective thermal diffusion coefficient is given by $\Gamma_{h,\text{eff}} = \Gamma_h + \Gamma_{h,\text{t}}$ with

$$\Gamma_{h,\text{t}}\frac{\partial \tilde{h}}{\partial x_j} = -\widetilde{\bar{\rho}u_j''h''}. \tag{2.21}$$

Averaging Eq. (2.14) using the definition in Eq. (2.15) and applying the gradient-diffusion hypothesis, the Favre averaged conservation equation of mixture fraction is deduced as following

$$\frac{\partial(\bar{\rho}\widetilde{\xi})}{\partial t} + \frac{(\bar{\rho}\widetilde{u}_i\widetilde{\xi})}{\partial x_i} = \frac{\partial}{\partial x_i}\left(\Gamma_{M,\text{eff}}\frac{\partial \widetilde{\xi}}{\partial x_i}\right) + \bar{S}_{l,\tilde{\xi}}, \tag{2.22}$$

where the effective diffusion coefficient of the gas mixture is given by $\Gamma_{M,\text{eff}} = \Gamma_M + \Gamma_{M,\text{t}}$ with

$$\Gamma_{M,\text{t}}\frac{\partial \widetilde{\xi}}{\partial x_i} = -\widetilde{\bar{\rho}u_j''\xi_j''}. \tag{2.23}$$

The source term $\bar{S}_{l,\tilde{\xi}}$ equals $\bar{S}_{l,1}$.

In Eqs. (2.20) and (2.22), the effective diffusion coefficients $\Gamma_{\Phi,\text{eff}}$ for $\Phi \in h, M$ need to be calculated. These are calculated using turbulent viscosity of the gas. For this purpose, an extended $k-\epsilon$ model [77] is applied in the present case. This extended $k-\epsilon$ model accounts for spray flows and it is a well established method for isotropic turbulence. The transport equations for k and ϵ are written as following,

$$\frac{\partial(\bar{\rho}\tilde{k})}{\partial t} + \frac{\partial(\bar{\rho}\widetilde{u}_j\tilde{k})}{\partial x_j} = \frac{\partial}{\partial x_j}\left(\Gamma_{k,\text{eff}}\frac{\partial \tilde{k}}{\partial x_j}\right) + G_k - \bar{\rho}\tilde{\epsilon} + \bar{S}_{l,\tilde{k}}, \tag{2.24}$$

$$\frac{\partial(\bar{\rho}\tilde{\epsilon})}{\partial t} + \frac{\partial(\bar{\rho}\widetilde{u}_j\tilde{\epsilon})}{\partial x_k} = \frac{\partial}{\partial x_j}\left(\Gamma_{\epsilon,\text{eff}}\frac{\partial \tilde{\epsilon}}{\partial x_j}\right) + c_{\epsilon,1}\frac{\tilde{\epsilon}}{\tilde{k}}G_k - c_{\epsilon,2}\bar{\rho}\frac{\tilde{\epsilon}}{\tilde{k}}\tilde{\epsilon} + \bar{S}_{l,\tilde{\epsilon}}, \tag{2.25}$$

where $c_{\epsilon,1}$, $c_{\epsilon,2}$ are model constants whose values of these model constants are taken from the literature [80]. The generation term for the turbulent kinetic energy is given by

$$G_k = \mu_t\left[\left(\frac{\partial \tilde{u}_i}{\partial x_j} + \frac{\partial \tilde{u}_j}{\partial x_i}\right) - \frac{2}{3}\frac{\partial \tilde{u}_k}{\partial x_k}\delta_{ij}\right]\frac{\partial \tilde{u}_i}{\partial x_j}. \tag{2.26}$$

$\bar{S}_{l,\tilde{k}}$ and $\bar{S}_{l,\tilde{\epsilon}}$ are the mean spray source terms, which are determined by [77] as

$$\bar{S}_{l,\tilde{k}} = \overline{S_{l,u_j} u_j''} + \frac{1}{2}\overline{S_{l,1} u_j''^2} \tag{2.27}$$

and

$$\bar{S}_{l,\tilde{\epsilon}} = C_s \bar{S}_{l,\tilde{k}}, \tag{2.28}$$

where the model constant C_s is set to 1.50 [81]. The turbulent viscosity μ_t is then given by

$$\mu_t = C_\mu \bar{\rho} \frac{\tilde{k}^2}{\tilde{\epsilon}}. \tag{2.29}$$

The effective dynamic viscosity is defined as $\mu_{\text{eff}} = \mu + \mu_t$. In Eqs. (2.20), (2.22), (2.24) and (2.25), the effective exchange coefficients $\Gamma_{\Phi,\text{eff}}$ for $\Phi \in \{h, M, k, \epsilon\}$ are given by

$$\Gamma_{\Phi,\text{eff}} = \frac{\mu_{\text{eff}}}{\sigma_\Phi}, \tag{2.30}$$

where σ_Φ are the Prandtl-Schmidt numbers.

The instantaneous conservation equation of mixture fraction given by Eq. (2.14) can be used to derive the equation for the variance of mixture fraction, $\widetilde{\xi''^2}$. Thus, Multiplying Eq. (2.1) by ξ and subtracting from Eq. (2.14), the following equation is yielded

$$\rho \frac{\partial \xi}{\partial t} + \rho u_i \frac{\partial \xi}{\partial x_i} = \frac{\partial}{\partial x_i}\left(\Gamma_M \frac{\partial \xi}{\partial x_i}\right) + S_{l,1} - \xi S_{l,1}. \tag{2.31}$$

Multiplying the above equation with $2\xi''$, the following form is obtained

$$2\xi'' \rho \frac{\partial \xi}{\partial t} + 2\xi'' \rho u_i \frac{\partial \xi}{\partial x_i} = 2\xi'' \frac{\partial}{\partial x_i}\left(\Gamma_M \frac{\partial \xi}{\partial x_i}\right) + 2\xi'' S_{l,1} - 2\xi'' \xi S_{l,1}. \tag{2.32}$$

Using the property of Favre-averaging, i.e. $\tilde{\xi} = \xi + \xi''$, the above equation can be rewritten as

$$2\xi'' \rho \frac{\partial \tilde{\xi}}{\partial t} + \rho \frac{\partial \xi''^2}{\partial t} + 2\xi'' \rho u_i \frac{\partial \tilde{\xi}}{\partial x_i} + \rho u_i \frac{\partial \xi''^2}{\partial x_i} = 2\xi'' \frac{\partial}{\partial x_i}\left(\Gamma_M \frac{\partial \xi}{\partial x_i}\right) + 2\xi'' S_{l,1}(1-\xi). \tag{2.33}$$

Multiplying Eq. (2.1) with ξ''^2 and adding to Eq. (2.33), the following can be obtained

$$2\xi'' \rho \frac{\partial \tilde{\xi}}{\partial t} + \frac{\partial (\rho \xi''^2)}{\partial t} + 2\xi'' \rho u_i \frac{\partial \tilde{\xi}}{\partial x_i} + \frac{\partial (\rho u_i \xi''^2)}{\partial x_i} = 2\xi'' \frac{\partial}{\partial x_i}\left(\Gamma_M \frac{\partial \xi}{\partial x_i}\right) + 2\xi'' S_{l,1}(1-\xi) + \xi''^2 S_{l,1}. \tag{2.34}$$

Time averaging the above equation and subsequently applying the Favre-average, the equation of variance of mixture fraction can be written as

$$\begin{aligned} \frac{\partial (\bar{\rho} \widetilde{\xi''^2})}{\partial t} \;+\; & \frac{\partial (\bar{\rho} \tilde{u}_i \widetilde{\xi''^2})}{\partial x_i} + \overline{\frac{\partial (\rho u_i \xi''^2)}{\partial x_i}} + \overline{2\xi'' \rho u_i''} \frac{\partial \tilde{\xi}}{\partial x_i} + \frac{\partial}{\partial x_i}\left(\Gamma_M \frac{\partial \widetilde{\xi''^2}}{\partial x_i}\right) \\ = \; & \overline{-2\Gamma_M \left(\frac{\partial \xi''}{\partial x_i}\right)^2} + \overline{2\xi'' S_{l,1}(1-\xi)} + \overline{\xi''^2 S_{l,1}}. \end{aligned} \tag{2.35}$$

In Eq. (2.35), the third and fourth terms on the left hand side as well as the first term on the right hand side are not closed and they must be modeled. The last two terms on the right hand side arise due to spray evaporation. Using the turbulent exchange coefficient $\Gamma_{\xi''^2,t} = \mu_t/\sigma_{\xi''^2,t}$ for the third and fourth term on the right hand side, the following is obtained [77]

$$\overline{\frac{\partial(\rho u_i \xi''^2)}{\partial x_i}} = -\frac{\partial}{\partial x_i}\left(\Gamma_{\xi''^2,t}\frac{\partial\widetilde{\xi''^2}}{\partial x_i}\right), \tag{2.36}$$

$$\overline{2\xi''\rho u_i''}\frac{\partial\tilde{\xi}}{\partial x_i} = -2\Gamma_{\xi''^2,t}\left(\frac{\partial\tilde{\xi}}{\partial x_i}\right)^2. \tag{2.37}$$

Using the gradient diffusion hypothesis, the first term on the right hand side of Eq. (2.35) is written as [77]

$$\overline{2\Gamma_M\left(\frac{\partial\xi''}{\partial x_i}\right)^2} = 2\bar{\rho}D_M\left(\frac{\partial\tilde{\xi}}{\partial x_i}\right)^2. \tag{2.38}$$

The instantaneous scalar dissipation rate χ is defined at first as

$$\chi = 2D_M\left(\frac{\partial\xi}{\partial x_i}\right)^2, \tag{2.39}$$

hence Eq. (2.38) becomes

$$\overline{2\Gamma_M\left(\frac{\partial\xi}{\partial x_i}\right)^2} = \bar{\rho}\tilde{\chi}. \tag{2.40}$$

Using the dissipation hypothesis [82], the scalar dissipation rate is described as

$$\tilde{\chi} = C_\chi\frac{\tilde{\epsilon}}{\tilde{k}}\widetilde{\xi''^2}, \tag{2.41}$$

where value of the constant C_χ is set to 2 [82]. The last two terms on the right hand side of Eq. (2.35), which arise due to spray evaporation are taken as defined by Hollmann [77] and they can be written as

$$\overline{2\xi''S_{l,1}(1-\xi)} + \overline{\xi''^2 S_{l,1}} = \widetilde{\xi''^2}\left(\frac{1-2\tilde{\xi}}{\tilde{\xi}}\right)\bar{S}_{l,1}. \tag{2.42}$$

Defining the effective exchange coefficient $\Gamma_{\xi''^2,\text{eff}} = \Gamma_{\xi''^2,t}+\Gamma_M$, the Eq. (2.35) is reduced to

$$\begin{aligned}\frac{\partial(\bar{\rho}\widetilde{\xi''^2})}{\partial t} &+ \frac{\partial(\bar{\rho}\tilde{u}_i\widetilde{\xi''^2})}{\partial x_i} - \frac{\partial}{\partial x_i}\left(\Gamma_{\xi''^2,t}\frac{\partial\widetilde{\xi''^2}}{\partial x_i}\right)\\ &= 2\Gamma_{\xi''^2,t}\left(\frac{\partial\tilde{\xi}}{\partial x_i}\right)^2 - 2\bar{\rho}\frac{\tilde{\epsilon}}{\tilde{k}}\widetilde{\xi''^2} + \widetilde{\xi''^2}\left(\frac{1-2\tilde{\xi}}{\tilde{\xi}}\right)\bar{S}_{l,1}.\end{aligned} \tag{2.43}$$

The gas phase conservation equations are explained above. The thermo-chemical properties for reactive case and their interlinking with turbulence is discussed in the next sections.

2.1.2 Chemical reactions modeling

An important goal in modeling of chemical reactions is to predict the thermal properties in the space. This requires the complete understanding of the chemical reaction mechanism and its coupling with turbulent flow, which will be discussed in later sections.

The flamelet based models [58] for turbulent gas diffusion flames are well known, where the composition of gas mixture and gas temperature are defined in terms of mixture fraction and scalar dissipation rate. This is followed by the fact that a laminar gas flamelet is characterized in terms of mixture fraction and scalar dissipation rate, where scalar dissipation rate is associated to strain rate. As far as spray flames are concerned, the effects of liquid fuel evaporation are important and need consideration. Hollmann and Gutheil [65] suggested that the laminar spray flamelets are characterized by initial droplet size, initial droplet velocity and equivalence ratio in addition to mixture fraction and scalar dissipation rate.

In the present work, a turbulent methanol/air diffusion flame is considered. A spray flamelet library [77] is used, where the chemical reaction mechanism consists of 23 chemical species and 168 elementary chemical reactions [83]. The spray flamelet library consists of two droplet radii $r = 10$ µm and $r = 25$ µm with one equivalence ratio $E_r = 3$ for strain rates from $a = 55$ s^{-1} to extinction ($a = 1330$ s^{-1} for $r = 10$ µm and $a = 2000$ s^{-1} for $r = 25$ µm). The characterization of turbulent properties would be achieved through statistical description of mixture fraction and scalar dissipation rate, which will be discussed in the next section. In this section, the thermo-chemistry of gas mixture is described. Thermo-chemical state of the gas mixture is characterized by the pressure, p, temperature, T, and the mass fraction, $Y_1, Y_2, \ldots, Y_{N_s}$ of the N_s species. Assuming the ideal gas, the underlying equation of state is provided by the ideal gas law as given below

$$p = \frac{\rho R T}{M}, \tag{2.44}$$

where R is the gas constant and M is the molecular mass. Specific total stagnant enthalpy consists of the kinetic energy, sensible enthalpy, h_s, and chemical enthalpy (the enthalpy of formation), Δh_f^0 [84],

$$h = \frac{1}{2} u_i u_i + h_s + \Delta h_f^0. \tag{2.45}$$

The specific sensible enthalpy of species α is given by

$$h_{s,\alpha}(p,T) = h_{s,\alpha}^0 + \int_{298.15K}^{T} c_{p\alpha}(T')dT', \tag{2.46}$$

where $h_{s,\alpha}^0$ is the sensible enthalpy of species α at the reference temperature $T_0 = 298.15$ K. The value of $h_{s,\alpha}^0$ is taken from JANAF thermochemical data [85]. The

specific heat capacity $c_{p,\alpha}$ depends upon pressure and temperature. In case of constant-pressure, the specific heat capacity $c_{p\alpha}(p,T)$ of species α is given by a polynomial function of T

$$c_{p\alpha}(T) = \sum_{i=0}^{4} a_{i,\alpha} T^i \tag{2.47}$$

The coefficients $a_{n,i}$ are taken from the literature [86]. Having the specific sensible enthalpy $h_{s,\alpha}$of species α calculated, the specific sensible enthalpy of a gas mixture is computed as

$$h_s = \sum_{\alpha=1}^{N_s} h_{s,\alpha} Y_\alpha. \tag{2.48}$$

The chemical reaction energy source term $\dot{Q}$ is

$$\dot{Q} = -\sum_{\alpha=1}^{N_s} \Delta h^0_{f,\alpha} S_\alpha, \tag{2.49}$$

where S_α is the net chemical reaction rate for species α and can be written as

$$S_\alpha = M_\alpha \dot{\omega}_\alpha. \tag{2.50}$$

Assumed as a Newtonian fluid, the viscosity coefficient μ is given as a function of temperature. Effect of bulk viscosity is neglected. The dynamic viscosity of species α is

$$\ln \mu_\alpha = \sum_{i=0}^{3} a_{i,\alpha} (\ln T)^i. \tag{2.51}$$

The coefficients $a_{n,i}$ is taken from [87]. The dynamic viscosity of a gas mixture is given as [87]

$$\mu = \frac{1}{2}\left[\sum_{\alpha=1}^{N_s} X_\alpha \mu_\alpha + (\sum_{\alpha=1}^{N_s} \frac{X_\alpha}{\mu_\alpha})^{-1}\right], \tag{2.52}$$

where X_α is the mole fraction of the species α. Similarly, thermal conductivity λ_α is given as a function of temperature, too, and is determined from a polynomial form with the coefficients $d_{i,\alpha}$ [87]

$$\ln \lambda_\alpha = \sum_{i=1}^{4} d_{i,\alpha} (\ln T)^{i-1}. \tag{2.53}$$

The coefficients $d_{i,\alpha}$ are taken from [87]. The thermal conductivity of a gas mixture is determined using

$$\lambda = \frac{1}{2}\left[\sum_{\alpha=1}^{N_s} X_\alpha \lambda_\alpha + (\sum_{\alpha=1}^{N_s} \frac{X_\alpha}{\lambda_\alpha})^{-1}\right]. \tag{2.54}$$

Binary diffusion coefficient $D_{\alpha\beta}$ depends on the temperature and pressure, and at constant pressure, it is evaluated using a polynomial form with the coefficients $b_{i,\alpha\beta}$ [87]

$$\ln D_{\alpha\beta} = \sum_{i=1}^{4} b_{i,\alpha\beta} (\ln T)^{i-1}. \tag{2.55}$$

The coefficients $b_{i,\alpha\beta}$ is taken from the table in [87]. The diffusion coefficient of species α in a mixture is estimated from Hirschfelder-Curtiss (or zeroth-order) approximation [88]

$$D_{\alpha,M} = \frac{1 - Y_\alpha}{\sum_{\beta \neq \alpha} \frac{X_\alpha}{D_{\alpha\beta}}}. \tag{2.56}$$

The modeling of chemical reactions and thermo chemical properties is discussed in this section above. An important aspect in inclusion of chemical reactions is their coupling to turbulent flow. This is discussed in the next section.

2.2 Probability density function methods

The turbulence in combustion systems makes the application of stochastic techniques inevitable, which rely on the statistical fluctuations of the characteristic variables. In the realm of stochastic processes, the PDF methods are widely applied. These methods provide mathematical tools to describe complex processes and therefore, facilitate the description of a collection of data in a more lucid and convenient way, so that it may be grasped rather easily. The PDF methods can be based upon either presumed or transported PDF's.

2.2.1 Presumed PDF methods

Usually, the procedure of the presumed PDF method is

- collecting the samples from experimental data, or simulations
- arranging the samples to form a distribution
- calculating sample statistics e.g., mean, variance
- choosing an appropriate PDF to represent the empirical data
- estimating the parameters of this PDF from the calculated sample statistics
- analyzing the predictive ability of PDF by conducting particular tests

The shape and parameters of PDF will largely depend upon the sample and the way it is chosen. To avoid any bias error, valid samples should be independent and identically distributed.

In gas flames, turbulence and chemistry are interlinked by using a laminar flamelet library, where each of the laminar flamelets is characterized by mixture fraction ξ and scalar dissipation χ rate so that we may write

$$\widetilde{\phi} = \int_0^\infty \int_0^1 \phi \widetilde{P}(\xi, \chi) \mathrm{d}\xi \mathrm{d}\chi, \tag{2.57}$$

where $\widetilde{\phi}$ is a Favre averaged scalar variable. In spray flames, the effect of evaporation must also be taken into account. Hollmann and Gutheil [67] discussed the dependency of spray flames on initial equivalence ratio, initial droplet size and initial droplet velocity in addition to mixture fraction and scalar dissipation rate. Thus

$$\widetilde{\phi} = \int_0^\infty \int_0^\infty \int_0^\infty \int_0^\infty \int_0^1 \phi \widetilde{P}(\xi, \chi, E, r_0, v_0) \mathrm{d}\xi \mathrm{d}\chi \mathrm{d}E \mathrm{d}r_0 \mathrm{d}v_0. \tag{2.58}$$

The key question is to define $\widetilde{P}(\xi, \chi, E, r_0, v_0)$. The droplet size r_0, droplet velocity v_0 and equivalence ratio E_r are treated through their inclusion in flamelet library [77], therefore it is important to establish the statistical expressions of ξ and χ. Assuming that ξ and χ are statistically independent, their joint PDF can be defined as a product of marginal PDFs

$$P(\xi, \chi) = P_\xi(\xi) P_\chi(\chi). \tag{2.59}$$

Thus the statistical distributions of ξ and χ in a turbulent flow field are needed. There exist several distributions that are applied within the scope of fluid mechanics. While keeping the discussion of this section limited to spray combustion only,the distributions used in the present work are discussed here.

2.2.1.1 Log-normal distribution

The term log-normal arises from the definition that its the PDF of a random variable, whose logarithm follows a normal distribution, i.e., if $X(\mu, \sigma^2)$ is normally distributed then $\exp(X)$ follows the log-normal distribution. Thus using the rule of change of variable, the log-normal PDF of X can be written as

$$P_X(x; \mu_{\log}, \sigma) = \frac{1}{x\sigma\sqrt{2\pi}} \exp\left[-\frac{1}{2\sigma^2}(\ln x - \mu_{\log})^2\right] \;\; ; \;\; x > 0. \tag{2.60}$$

The parameters $\mu_{\log}$ and σ are the mean and standard deviation of corresponding normal distribution of $\ln(X)$ respectively. The mean $E(X)$ and variance $Var(X)$ of

the log-normal distribution are given by

$$E(X) = \exp(\mu_{\log} + \frac{1}{2\sigma^2}), \tag{2.61}$$

$$\begin{aligned} Var(X) &= \left(\exp(\sigma^2) - 1\right) \exp(2\mu_{\log} + \sigma^2) \\ &= \left(\exp(\sigma^2) - 1\right) \left(E(X)\right)^2. \end{aligned} \tag{2.62}$$

Log-normality of diffusive scalars has been assumed extensively in order to assure the consistency of random variation of local scalar dissipation in case of homogeneous turbulence [70,89]. Kolmogorov [89] first proposed the hypothesis that the local scalar dissipation χ_A averaged over the cell size A is log normally distributed. Thus

$$P_\chi(\chi_A) = \frac{1}{(\chi_A \sigma_{\log}\sqrt{2\pi})} \exp\left[-\frac{1}{2\sigma^2}(\ln\chi_A - \mu_{\log})^2\right], \tag{2.63}$$

where the A and χ_A are inter-related through the expression

$$\frac{\mathrm{d}^2(\ln\chi_A)}{\mathrm{d}A^2} = A_1 + \sigma^2 \ln\left(\frac{L}{A}\right), \tag{2.64}$$

where L is the largest scale of the flow, A_1 depends upon the flow geometry and σ^2 is treated as constant. The value of σ^2 can be taken as 2 [69,70]. Following this definition, the mean scalar dissipation rate is given by

$$\tilde{\chi} = \exp(\mu_{\log} + \frac{1}{2\sigma^2}). \tag{2.65}$$

2.2.1.2 β distribution

In probability theory, β distribution (also called β distribution of first kind) refers to a family of continuous probability distributions defined over the interval [0,1]. In Bayesian analysis, it serves as conjugate prior of Binomial, Bernoulli and geometric distributions. There are two parameters of β distribution namely a and b, which appear as exponents of random variable and control the shape of PDF. The PDF of random variable X is defined as

$$P_X(x; a, b) = \frac{x^{a-1}(1-x)^{b-1}}{B(a,b)}, \tag{2.66}$$

where $B(a,b)$ is the beta function of a and b given by

$$B(a,b) = \int_0^1 t^{a-1}(1-t)^{b-1}\mathrm{d}t = \frac{\Gamma(a)\Gamma(b)}{\Gamma(a+b)}. \tag{2.67}$$

The mean $E(X)$ and variance $Var(X)$ are given by

$$E(X) = \frac{a}{a+b}, \tag{2.68}$$

$$Var(X) = \frac{E(X)(1-E(X))}{1+a+b}. \tag{2.69}$$

Following the fact that β distribution domain lies between 0 and 1, and it can produce a variety of PDF shapes including bell-shaped, U shaped, J shaped and reverse J taped PDFs, a straight forward approach is to assume that the PDF of ξ follows β distribution [66]. Thus

$$P_\xi(\xi) = \frac{\Gamma(a+b)}{\Gamma(a)\Gamma(b)}\xi^{a-1}(1-\xi)^{b-1}. \tag{2.70}$$

Using the local values of $\widetilde{\xi}$ and $\widetilde{\xi''^2}$ in Eqs. (2.68) and (2.69), the shape parameters a and b are calculated as

$$a = \widetilde{\xi}\left[\frac{\widetilde{\xi}(1-\widetilde{\xi})}{\widetilde{\xi''^2}} - 1\right], \tag{2.71}$$

$$b = (1-\widetilde{\xi})\left[\frac{\widetilde{\xi}(1-\widetilde{\xi})}{\widetilde{\xi''^2}} - 1\right]. \tag{2.72}$$

2.2.1.3 Modified β distribution

Ge and Gutheil [68] suggested that the standard β distribution is not a suitable choice for evaporating sprays as well as reactive flows since the local value of $\widetilde{\xi}$ is less than unity in the flow field. Thus a four parameter β distribution defined over an interval $\xi_{\min}$ and $\xi_{\max}$ may be a suitable choice. This can be done by replacing the mixture fraction ξ with a rescaled mixture fraction $\frac{\xi-\xi_{\min}}{\xi_{\max}-\xi_{\min}}$ in the standard β distribution, which leads to the following definition of PDF

$$P_\xi(\xi) = \frac{\Gamma(a+b)}{\Gamma(a)\Gamma(b)}(\xi_{\max}-\xi_{\min})^{1-a-b}(\xi-\xi_{\min})^{a-1}(\xi_{\max}-\xi)^{b-1}. \tag{2.73}$$

The mean and variance of modified β distribution can be calculated by using the rule of change of variables, which yields

$$\widetilde{\xi} = \xi_{\min} + \frac{a}{a+b}(\xi_{\max}-\xi_{\min}), \tag{2.74}$$

$$\widetilde{\xi''^2} = \frac{(\widetilde{\xi}-\xi_{\min})(\xi_{\max}-\widetilde{\xi})}{1+a+b}. \tag{2.75}$$

The shape parameters are calculated using Eqs. (2.74) and (2.75) through the expressions

$$a = \frac{(\widetilde{\xi} - \xi_{\min})}{(\xi_{\max} - \xi_{\min})} \left[\frac{(\widetilde{\xi} - \xi_{\min})(\xi_{\max} - \widetilde{\xi})}{\widetilde{\xi''^2}} - 1 \right], \tag{2.76}$$

$$b = \frac{(\xi_{\max} - \widetilde{\xi})}{(\xi_{\max} - \xi_{\min})} \left[\frac{(\widetilde{\xi} - \xi_{\min})(\xi_{\max} - \widetilde{\xi})}{\widetilde{\xi''^2}} - 1 \right]. \tag{2.77}$$

An obvious question that arises is how to choose $\xi_{\min}$ and $\xi_{\max}$. A straight forward intuition is to assume the PDF to lie in the domain which is symmetric about mean and spreads about standard deviation in positive and negative directions i.e.,

$$\xi_{\min} = \widetilde{\xi} - \sqrt{\widetilde{\xi''^2}}, \tag{2.78}$$

$$\xi_{\max} = \widetilde{\xi} + \sqrt{\widetilde{\xi''^2}}. \tag{2.79}$$

This assumption may be generalized to assume

$$\xi_{\min} = \widetilde{\xi} - n\sqrt{\widetilde{\xi''^2}}, \tag{2.80}$$

$$\xi_{\max} = \widetilde{\xi} + n\sqrt{\widetilde{\xi''^2}}, \tag{2.81}$$

where $n \in \mathbb{Z}^+$. But it follows from Eqs. (2.76) and (2.77) that such an assumption would eventually enforce $a = b$. Therefore, one may conclude that assuming $\xi_{\min}$ and $\xi_{\max}$ to be symmetric about $\widetilde{\xi}$ would always result in the symmetric shape of PDF. Luo *et al.* [32] adapted the modified β distribution by assuming $\xi_{\min} = 0$ and $\xi_{\max} = \widetilde{\xi} + 2\sqrt{\widetilde{\xi_C''^2}}$. This idea may be generalized to assuming

$$\xi_{\min} = 0, \tag{2.82}$$

$$\xi_{\max} = \widetilde{\xi} + n\sqrt{\widetilde{\xi''^2}}, \quad ; \quad n \in \mathbb{Z}^+. \tag{2.83}$$

2.2.2 Transported PDF methods

In transported PDF methods, the PDF is determined by solving its transport equation [64, 68, 90, 91]. The PDF transport equation for scalar quantities of gas phase may be derived by considering instantaneous conservation equations for the gas phase. Basic idea of the transported PDF method is to describe the state of the flow at the location $\mathbf{x} = (x_1, x_2, x_3)$ at the time t in terms of a probability density function f. This f can be a one-variable PDF or a joint multi-variable PDF. The variables are physical quantities of the flow such as velocity, mixture fraction or turbulence frequency. The transport equation of the PDF is deduced from the Navier-Stokes equations [71, 92].

Appropriate physical models are adapted to model unclosed conditional expectations. The PDF transport equation is solved using a Monte-Carlo approach [93]. The sample space consists of a large number of gas particles, which represent the PDF. The development of the particles in sample space is described by a set of stochastic differential equations, which are obtained from the modeled PDF transport equation. Thus, the gas particles exhibit the same PDF as the solution of the modeled PDF transport equation. Statistics of the flow fields are obtained by integrating the particle properties over the whole sample space. In the present work, gas phase conservation equations with spray source terms are considered to derive the PDF transport equation [94]. A joint PDF of enthalpy and mixture fraction [68] is used and its transport equation is derived. For future work, a trivariate PDF of enthalpy, gas velocity and mixture fraction is proposed and its transport equation is given in Appendix A.

2.2.2.1 Derivation of PDF transport equation

To deduce the joint PDF, a fine-grained, one-point one-time Eulerian, joint mixture fraction and enthalpy PDF $f^*(\zeta, \eta; \mathbf{x}, t)$ is defined for the gas phase of turbulent spray flames as

$$f^*(\zeta, \eta; \mathbf{x}, t) = \delta(\xi(\mathbf{x}, t) - \zeta)\delta(h(\mathbf{x}, t) - \eta). \tag{2.84}$$

Here the ξ and h are mixture fraction and enthalpy in physical space, and ζ and η the corresponding values in sample space. The ensemble averaging of this fine-grained PDF can be written as

$$f(\zeta, \eta; \mathbf{x}, t) = \langle f^*(\zeta, \eta; \mathbf{x}, t)\rangle = \langle \delta(\xi(\mathbf{x}, t) - \zeta)\delta(h(\mathbf{x}, t) - \eta)\rangle, \tag{2.85}$$

where the conditional mean of any function $Q = Q(\mathbf{x}, t)$ could be related to PDF $f(\zeta, \eta; \mathbf{x}, t)$ by

$$\langle Q(\mathbf{x}, t) f^*(\zeta, \eta; \mathbf{x}, t)\rangle = \langle Q(\mathbf{x}, t)|\zeta, \eta\rangle f(\zeta, \eta; \mathbf{x}, t). \tag{2.86}$$

In terms of the properties of the Dirac-delta function, the material derivative of the fine-grained PDF has the relation as

$$0 = \frac{Df^*}{Dt} = \frac{\partial f^*}{\partial t} + \frac{\partial f^*}{\partial \mathbf{x}}\frac{d\mathbf{x}}{dt} + \frac{\partial f^*}{\partial \zeta}\frac{d\zeta}{dt} + \frac{\partial f^*}{\partial \eta}\frac{d\eta}{dt}. \tag{2.87}$$

With the shifting property of Dirac-delta function, Eq. (2.87) can be written as

$$\begin{aligned} \rho\frac{\partial f^*}{\partial t} + \rho u_j \frac{\partial f^*}{\partial x_j} &= -\rho\frac{\partial f^*}{\partial \zeta}\frac{d\zeta}{dt} - \rho\frac{\partial f^*}{\partial \eta}\frac{d\eta}{dt} \\ &= -\frac{\partial}{\partial \zeta}\left(\rho\frac{d\xi}{dt}f^*\right) - \frac{\partial}{\partial \eta}\left(\rho\frac{dh}{dt}f^*\right). \end{aligned} \tag{2.88}$$

The following can be obtained by using the Eqs. (2.85) and (2.86),

$$\rho\frac{\partial f}{\partial t}+\rho u_j\frac{\partial f}{\partial x_j}=-\frac{\partial}{\partial\zeta}\left(\rho\left\langle\frac{d\xi}{dt}|\zeta,\eta\right\rangle f\right)-\frac{\partial}{\partial\eta}\left(\rho\left\langle\frac{dh}{dt}|\zeta,\eta\right\rangle f\right). \tag{2.89}$$

Substitution of the instantaneous conservation of mass (c.f. Eq. (2.1)) into the above equation and considering the joint mass density function $F(\zeta,\eta;\mathbf{x},t)=\rho f(\zeta,\eta;\mathbf{x},t)$, the following expression is yielded

$$\frac{\partial F}{\partial t}+\frac{\partial(u_jF)}{\partial x_j}-\left\langle\frac{S_{l,1}}{\rho}|\zeta,\eta\right\rangle F=-\frac{\partial}{\partial\zeta}\left(\left\langle\frac{\mathrm{d}\xi}{\mathrm{d}t}|\zeta,\eta\right\rangle F\right)-\frac{\partial}{\partial\eta}\left(\left\langle\frac{\mathrm{d}h}{\mathrm{d}t}|\zeta,\eta\right\rangle F\right). \tag{2.90}$$

In the above transport equation of mass density function F, the terms on the right hand side are unclosed, and based on the instantaneous conservation equations for the enthalpy and mixture fraction (c.f. Eqs. (2.2) and (2.10)). These terms can be expanded as following

$$\begin{aligned}
-&\frac{\partial}{\partial\zeta}\left(\left\langle\frac{\mathrm{d}\xi}{\mathrm{d}t}|\zeta,\eta\right\rangle F\right)=-\frac{1}{\rho}\langle(1-\xi)S_{l,1}\rangle\frac{\partial F}{\partial\zeta}\\
-&\frac{\partial}{\partial\zeta}\left(\frac{1}{\rho}\left\langle\frac{\partial}{\partial x_j}(\rho D_M\frac{\partial\xi}{\partial x_j})+{S_{l,1}}'+\langle\xi S_v\rangle-\xi S_{l,1}|\zeta,\eta\right\rangle F\right),
\end{aligned} \tag{2.91}$$

$$\begin{aligned}
-&\frac{\partial}{\partial\eta}(\langle\frac{\mathrm{d}h}{\mathrm{d}t}|\zeta,\eta\rangle F)=-\frac{1}{\rho}\langle S_{l,h}-hS_{l,1}\rangle\frac{\partial F}{\partial\eta}\\
-&\frac{\partial}{\partial\eta}\left(\frac{1}{\rho}\left\langle\frac{\partial}{\partial x_j}(\rho D_h\frac{\partial h}{\partial x_j})+{S_{l,h}}'+\langle hS_{l,1}\rangle-hS_{l,1}|\zeta,\eta\right\rangle F\right),
\end{aligned} \tag{2.92}$$

so the modeled joint PDF transport equation can be written as

$$\begin{aligned}
\frac{\partial F}{\partial t}+\frac{\partial(u_jF)}{\partial x_j}-\frac{\langle S_{l,1}\rangle}{\rho}F\ &+\ \frac{1}{\rho}\langle(1-\xi)S_{l,1}\rangle\frac{\partial F}{\partial\zeta}+\frac{1}{\rho}\langle S_{l,h}-hS_{l,1}\rangle\frac{\partial F}{\partial\eta}\\
&=\ -\frac{\partial}{\partial\zeta}\left(\frac{1}{\rho}\left\langle\frac{\partial}{\partial x_j}(\rho D_M\frac{\partial\xi}{\partial x_j})+S'_\xi|\zeta,\eta\right\rangle F\right)\\
&-\ \frac{\partial}{\partial\eta}\left(\frac{1}{\rho}\left\langle\frac{\partial}{\partial x_j}(\rho D_h\frac{\partial h}{\partial x_j})+S'_h|\zeta,\eta\right\rangle F\right),
\end{aligned} \tag{2.93}$$

and the effects of fluctuation of spray source terms

$$S'_\xi = (1-\xi')S_{l,1}, \tag{2.94}$$

$$S'_h = (1-h')S_{l,h}. \tag{2.95}$$

In equation (2.93) the terms on the right hand side appear in unclosed form. They denote the effects of the molecular diffusion and the fluctuation in spray source terms, respectively. To close these terms, additional models are needed. These are discussed in the next subsection.

2.2.2.2 Mixing models

Suitable mixing models are required to describe the effects of the molecular and thermal diffusion. A precise and accurate study of molecular diffusivity is very important in order to analyze the effects of molecular mixing on turbulent reactive and non reactive spray flows. There are some models available in literature, including the interaction-by-exchange-with-the-mean (IEM) [72], modified Curl's model [74], Euclidean minimum spanning tree (EMST) mixing model [76]. In the scope of spray flows, the simplest model–the IEM model is used [95]. With the IEM model, the mixture fraction and enthalpy of the particle evolve by

$$\frac{d\xi^*(t)}{dt} = -\frac{1}{2}\frac{\widetilde{\epsilon}}{\widetilde{k}}C_\phi[\xi^*(t) - \widetilde{\xi}] + [1 - \xi^*(t)]\frac{\langle S_{l,1}\rangle}{\langle\rho\rangle}, \tag{2.96}$$

$$\frac{dh^*(t)}{dt} = -\frac{1}{2}\frac{\widetilde{\epsilon}}{\widetilde{k}}C_\phi[h^*(t) - \widetilde{h}] + \frac{\langle S_{l,h}\rangle - \langle hS_{l,1}\rangle}{\langle\rho\rangle}. \tag{2.97}$$

Here $C_\phi = 2.0$ is the standard model constant [64]. The first term on the right hand side represents the mixing process. The last term is for the source term due to the spray evaporation.

Cao *et al.* [100] investigated the validity and efficiency of mixing models on gas flames. They found that IEM should be replaced with Euclidean minimal spanning tree (EMST) or modified Curl (MC) mixing model for jet flames. So an extended modified Curl (MC) is also employed in order to evaluate the effects of micro-mixing. MC [74] is based upon Curl's particle interaction model [73]. The two equal-weight stochastic particles, denoted by p_1 and p_2, are selected at random from the ensemble and after mixing, their mixture fractions and enthalpies are given by

$$\xi^{(p_1,new)} = \xi^{(p_1)} + \frac{1}{2}a(\xi^{(p_2)} - \xi^{(p_1)}), \tag{2.98}$$

$$\xi^{(p_2,new)} = \xi^{(p_2)} + \frac{1}{2}a(\xi^{(p_1)} - \xi^{(p_2)}), \tag{2.99}$$

$$h_s^{(p_1,new)} = h_s^{(p_1)} + \frac{1}{2}a(h_s^{(p_2)} - h_s^{(p_1)}), \tag{2.100}$$

$$h_s^{(p_2,new)} = h_s^{(p_2)} + \frac{1}{2}a(h_s^{(p_1)} - h_s^{(p_2)}), \tag{2.101}$$

where the coefficient a is a random number, which lies between 0 and 1.

2.2.3 Boundary conditions

Accuracy and applicability of the numerical schemes are constrained to the imposed boundary conditions. For distinguishing the directions, x_1 is denoted by x and x_2 is denoted by r. The computation domain for an axisymmetric 2D configuration is bounded by the inlet plane $x = 0$, exit plane $x = L$, axis of symmetry $r = 0$ and

the wall $r = M$. The inlet plane is characterized by the initial conditions, which are generated from the experimental data and explained in the next chapter.

Due to axial symmetry, the radial velocity and the correlation $\widetilde{u_x''u_r''}$ are taken to be zero at the axis of symmetry i.e., $\tilde{u}_r = 0$ and $\widetilde{u_x''u_r''} = 0$ [64]. For all other variables $\widetilde{\phi}$, the property of symmetry at the axis $r = 0$ leads to the Neumann boundary condition, $\frac{\partial\tilde{\phi}}{\partial r} = 0$ [64, 101].

For the exit plane $x = L$, the length of the wall i.e., L is so chosen the fluid properties do not change anymore or equivalently, the system is in equilibrium. This leads to the zero gradient boundary condition, $\frac{\partial\widetilde{\phi}}{\partial x} = 0$.

The wall $r = M$ is the fixed boundary, where the boundary conditions are not homogeneous. Logarithmic law of the wall is applied for the variables $\widetilde{u}_x$, $\widetilde{u}_r$, $\widetilde{k}$, $\widetilde{\epsilon}$, $\widetilde{u}_x''$ and $\widetilde{u}_r''$. The temperature at the wall T_M is a known and fixed quantity for the simulations. Therefore the enthalpy at the wall can be calculated using the specific heat i.e $\widetilde{h} = C_pT_M$. For the mixture fraction and its variance, the boundary conditions at the wall are given by $\frac{\partial\widetilde{\xi}}{\partial r} = 0$ and $\frac{\partial\widetilde{\xi''^2}}{\partial r} = 0$ [77]. The correlations $\widetilde{u_x''u_r''}$, $\widetilde{u_x''\xi_j''}$, $\widetilde{u_r''\xi_j''}$, $\widetilde{u_x''h''}$ and $\widetilde{u_r''h''}$ are all set to zero.

2.3 Liquid phase flow

The transport of a liquid droplet in dry or a vapor stream is a very complex phenomena from mathematical point of view due to strong influence of physical processes like droplet collisions, breakup, evaporation and interaction with surrounding gas. The properties of liquid droplets in spray flows may depend on various aspects, which include the droplet atomization at nozzle exit, the dispersion of the droplets in surrounding gas, droplet evaporation and heat exchange with surrounding gas as well as the effects of turbulence. In the present work, the liquid phase of an evaporating water/air spray is modeled using DQMOM [13] and DDM [67], while the liquid phase of methanol/air spray flame is modeled using DDM only. In both models, the droplet motion, droplet evaporation and droplet heating are included. In DDM, the droplet collisions are neglected due to modeling limitations whereas DQMOM considers the effects of droplet interactions by including the coalescence.

2.3.1 Direct quadrature method of moments (DQMOM)

Although studies have been performed by considering both liquid and gas phases to be continuous, which leads to similar equations for liquid phase as those of gas phase [18] but there have been shortcomings such as modeling of evaporation and effect of turbulence on physical droplet sizes. A reasonable way to develop a mathematical formu-

lation is to consider that individual droplets have a continuous behavior characterized by statistical properties with negligible deviation from spherical shape [22]. Thus a distribution function $f(\mathbf{x}, r, \mathbf{v}, t)\mathrm{d}\mathbf{x}\mathrm{d}r\mathrm{d}\mathbf{v}$ may be used to describe the spray change at time t in a neighborhood $\mathrm{d}\mathbf{x}$ of droplet position $\mathbf{x}$, $\mathrm{d}r$ of droplet radius r, and $\mathrm{d}\mathbf{v}$ of droplet velocity $\mathbf{v}$. For this distribution function, the well known spray equation [22] is extensively discussed in literature and several techniques have been introduced to solve this equation numerically [14–16, 23] as discussed in chapter 1. As a matter of numerical limitation, the equation is a high-dimensional problem considering the vector forms of $\mathbf{x}$ and $\mathbf{v}$, which is quite difficult to solve unless some additional assumptions are made. The DQMOM transport equations are derived from Williams' spray equation [22], which is given by

$$\frac{\partial f}{\partial t} + \frac{\partial (\mathbf{v} f)}{\partial \mathbf{x}} = -\frac{\partial \left(R f\right)}{\partial r} - \frac{\partial (\mathbf{F} f)}{\partial \mathbf{v}} + Q_f + \Gamma_f. \tag{2.102}$$

The equation describes the transport of the number density function $f(r, \mathbf{v}; \mathbf{x}, t)$ in terms of time, t, and Euclidean space, $\mathbf{x}$. In Eq. (2.102), $\mathbf{v}$ and $\mathbf{F}$ denote droplet velocity and drag force per unit mass whereas R is the change of the droplet radius with time, i.e., $R = dr/dt$, where r is the droplet radius. The last two terms refer to the droplet interactions. Q_f represents the increase in f with time due to droplet formation or destruction by processes such as nucleation or breakup whereas Γ_f denotes the rate of change of f caused by collisions with other droplets.

For the present study, a joint radius-velocity number density function is considered [13], which is approximated by DQMOM as sum of the product of weighted Dirac-delta functions [23] of radii and velocities [12]

$$f(r, \mathbf{v}) = \sum_{n=1}^{N} w_n \delta(r - r_n)\delta(\mathbf{v} - \mathbf{v}_n), \tag{2.103}$$

where w_n and r_n are chosen as N representative quantities of weights and radii, and $\mathbf{v}_n$ are the corresponding velocities. Application of DQMOM results in closed transport equations for droplet weights or number density, radii and velocities, respectively, which are written as [13]

$$\frac{\partial w_n}{\partial t} + \frac{\partial (w_n \mathbf{v}_n)}{\partial \mathbf{x}} = a_n, \tag{2.104}$$

$$\frac{\partial (w_n \rho_l r_n)}{\partial t} + \frac{\partial (w_n \rho_l r_n \mathbf{v}_n)}{\partial \mathbf{x}} = \rho_l b_n, \tag{2.105}$$

and

$$\frac{\partial (w_n \rho_l r_n \mathbf{v}_n)}{\partial t} + \frac{\partial (w_n \rho_l r_n \mathbf{v}_n \mathbf{v}_n)}{\partial \mathbf{x}} = \rho_l \mathbf{c}_n, \tag{2.106}$$

where a_n, b_n and $\mathbf{c}_n$ are the source terms that may account for evaporation, drag force and gravity.

The steady form of Eqs. (2.104) – (2.106) is solved simultaneously by using appropriate initial and boundary conditions to find $w_n(\mathbf{x},t)$, $r_n(\mathbf{x},t)$ and $\mathbf{v}_n(\mathbf{x},t)$., The system of equations is closed by modeling the source terms i.e., a_n, b_n and $\mathbf{c}_n$, using the physical models to account for effects of droplet evaporation, drag force and gravity. These source terms are calculated through moment transformation of phase-space terms, which yields the following linear system [13, 171]

$$P_{k,l} = \int\int r^k \mathbf{v}^l \left[-\frac{\partial(Rf)}{\partial r} - \frac{\partial(\mathbf{F}f)}{\partial \mathbf{v}} - \Gamma_f - Q_f \right] \mathrm{d}r\mathrm{d}\mathbf{v}. \tag{2.107}$$

The exact form of the DQMOM linear system relies on the choice of moments. To obtain a solution, the moments are so chosen that the resulting coefficient matrix is non-singular. In the present work, N is set to be 3 and the corresponding moment set is chosen as [23] $k \in \{1, ..., 2N\}$; $l \in \{0, 1\}$. Though this approach has been tested to model non-evaporating sprays [24–26], few studies have been carried out on evaporating sprays [23, 27, 28]. However, these studies consider a very simplified evaporation model to calculate the change in droplet size with time i.e., either as a linear function of droplet volume or non-linear function of droplet volume, which is similar to the well established but very simplified d^2 law. This has been improved [13] by implementing the advanced evaporation model. Droplet evaporation is accounted for by considering the rate of change of droplet volume as [102] (see section 2.3.4).

2.3.2 Discrete droplet model (DDM)

DDM is a well established model for for dilute sprays where droplet - droplet interactions may be neglected [18, 21, 29]. The droplet positions and velocities are captured using Lagrangian particle tracking method, which are used to calculate the source terms for extended Eulerian equations of the gas phase. The model captures the trajectories and dynamics of individual droplets, which are injected in form of parcels [77]. A parcel refers to a collection of droplets, which are described by a set of properties i.e., $(\mathbf{x}_{p,k}, r_{p,k}, \mathbf{v}_{p,k}, m_{p,k}, T_{p,k}, \Delta V_{ij})$, where $\mathbf{x}_{p,k}$ is the position, $r_{p,k}$ is the radius, $\mathbf{v}_{p,k}$ is the velocity, $m_{p,k}$ is the liquid mass and $T_{p,k}$ is the temperature of k^{th} parcel in control volume ΔV_{ij}. Having a system of parcels injected, the model captures the flow properties i.e., droplet dynamics, evaporation and heating as explained in next paragraphs.

2.3.3 Droplet dynamics

The dynamics of liquid droplets in sprays is the foundation that needs to be computed for the coupling of gas - liquid phases due to its strong dependance on the flow of

surrounding gas. The droplet velocity $\mathbf{v}$ at position $\mathbf{x}$ can be explained as following

$$\mathbf{v} = \frac{\mathrm{d}\mathbf{x}}{\mathrm{d}t} \tag{2.108}$$

The change in droplet velocity is then computed using the relation

$$\frac{\mathrm{d}\mathbf{v}}{\mathrm{d}t} = \frac{3}{8}\frac{1}{r}\frac{\bar{\rho}}{\rho_l}(\mathbf{u}-\mathbf{v})|\mathbf{u}-\mathbf{v}|C_D + \mathbf{g} \tag{2.109}$$

where $\bar{\rho}$ and $\mathbf{v}$ are the density and velocity of the surrounding gas while ρ_l, C_D and $\mathbf{g}$ are liquid density, drag coefficient and gravitational acceleration, respectively. A decomposition of gas velocity as per Eq. (2.16) i.e. $\mathbf{u} = \widetilde{\mathbf{u}} + \mathbf{u}''$ in mean and fluctuating components of the velocity allows the influence of turbulence on droplet velocity. The detailed mathematical description of this decomposition is given in the section of gas phase equations. An important quantity in Eq. (2.109) is the drag coefficient, which is computed as a function of droplet's Reynolds number Re_d as follows [103]

$$C_D = \begin{cases} \frac{24}{\mathrm{Re}_d}(1+\frac{1}{6}\mathrm{Re}_d^{0.687}) & \text{if } \mathrm{Re}_d{<}10^3 \\ 0.424 & \text{if } \mathrm{Re}_d{\geq}10^3 \end{cases} \tag{2.110}$$

The droplet Reynolds number is calculated using the definition

$$\mathrm{Re}_d = 2\bar{\rho}r\frac{|\mathbf{u}-\mathbf{v}|}{\mu_f} \tag{2.111}$$

where the mean dynamic viscosity in the film μ_f is depends upon the temperature in the film T_f, which is calculated using 1/3 rule [104] as following

$$T_f = \frac{\tilde{T} + 2T_d}{3}. \tag{2.112}$$

The quantities $\tilde{T}$ and T_d refer to Favre averaged gas temperature and droplet temperature respectively.

2.3.4 Droplet evaporation

The key change that droplet undergoes while moving in a gaseous environment is the mass transfer from liquid to gas. Intuitively, change in droplet radius along the droplet trajectory is an important phenomenon. In the present work, a two-film model developed by Abramzon and Sirignano [102] is implemented to account for evaporation, where the terminology "film" describes the vapor layer between droplet surface and surrounding gas. The radius of outer boundaries of film may be calculated as [77]

$$r_{f,T_0} = r\frac{\mathrm{Nu}_0}{\mathrm{Nu}_0 - 2}; \qquad r_{f,M_0} = r_p\frac{\mathrm{Sh}_0}{\mathrm{Sh}_0 - 2}. \tag{2.113}$$

Here index '0' refers to quiescent droplets and subscript f refer to film properties. The Nusselt number Nu_0 and Sherwood number Sh_0 are given by

$$\mathrm{Nu}_0 = 1 + (1 + \mathrm{Re}_d \mathrm{Pr}_f)^{1/3} f(\mathrm{Re}_d), \tag{2.114}$$

and

$$\mathrm{Sh}_0 = 1 + (1 + \mathrm{Re}_d \mathrm{Sc}_f)^{1/3} f(\mathrm{Re}_d), \tag{2.115}$$

where Pr_f and Sc_f are Prandtl and Schmidt numbers given by

$$\mathrm{Pr}_f = \mu_f \frac{c_{p,f}}{\lambda_f} \quad \text{and} \quad \mathrm{Sc}_f = \frac{\mu_f}{\rho_f D_f}. \tag{2.116}$$

The function $f(\mathrm{Re}_d)$ depends upon droplet Reynolds number and in case of low Reynolds number, it may be calculated as defined in [102].

The quantities μ_f, $c_{p,f}$, λ_f, ρ_f and D_f refer to mean dynamic viscosity, specific heat, thermal conductivity, density and thermal diffusivity of vapor in the film. The evaporation rate of a droplet may be then computed as [102]

$$\dot{m} = \frac{\mathrm{d}\left(\frac{4}{3}\pi\rho_l r_{p,k}^3\right)}{\mathrm{d}t} = 2\pi r \bar{\rho}_f \bar{D}_f \widetilde{\mathrm{Sh}} \ln(1 + B_M). \tag{2.117}$$

The above equation implies

$$\frac{\mathrm{d}r}{\mathrm{d}t} = \frac{\bar{\rho}_f \bar{D}_f \widetilde{\mathrm{Sh}} \ln(1 + B_M)}{2\rho_l r_{p,k}}. \tag{2.118}$$

Here B_M is the Spalding mass transfer number and $\widetilde{\mathrm{Sh}}$ is the modified Sherwood number, which is calculated as

$$\widetilde{\mathrm{Sh}} = 2 + \frac{\mathrm{Sh}_0 - 2}{B_M} (1 + B_M) \ln(1 + B_M). \tag{2.119}$$

Spalding mass transfer number is calculated as following

$$B_M = \frac{Y_{Ls} - Y_{L\infty}}{1 - Y_{Ls}}, \tag{2.120}$$

where Y_{Ls} and $Y_{L\infty}$ are mass fractions of the vapor at droplet surface and outer boundary of film, respectively, and Y_{Ls} is given by [105]

$$Y_{Ls} = \frac{M_L}{M_L + \bar{M}(\bar{p}/p_L - 1)}. \tag{2.121}$$

The quantities M_L and p_L denote molar mass and pressure of water vapor while $\bar{M}$ and $\bar{p}$ represent molar mass and mean pressure of the surrounding gas, respectively. Vapor pressure for water is calculated using Antoine's equation as [106]

$$\log_{10} p_L = 10.11564 - \frac{1687.537}{T_d - 42.83}, \tag{2.122}$$

whereas for methanol, the vapor pressure is given by [107]

$$p_F = p_{\text{crit}} \exp\left(\frac{f(T_{d,\text{ref}})}{1 - T_{d,\text{ref}}}\right), \tag{2.123}$$

with

$$T_{d,\text{ref}} = 1 - \frac{T_d}{T_{\text{crit}}}; \tag{2.124}$$

$$f(T) = -8.54796T + 0.76982T^{1.5} - 3.1085T^3 + 1.54481T^6. \tag{2.125}$$

2.3.5 Droplet heating

Although the initial temperatures of gas and the droplet are equal in evaporating case, the droplet temperature is subject to change due to evaporation, and its time evolution is computed using the infinite conductivity model [102], which is a good approximation for liquids with high volatility

$$mC_{pL}\frac{\mathrm{d}T_s}{\mathrm{d}t} = \dot{m}\left[\frac{C_{pL}(T_s - T_g)}{B_T} - L_V(T_s)\right], \tag{2.126}$$

where C_{pL} is the specific heat capacity of the liquid, T_s is the temperature at droplet surface, T_g is temperature of the surrounding gas and L_V is the temperature dependent latent heat of vaporization. B_T is the Spalding heat transfer number, which is calculated in terms of the mass transfer number using the relation [102]

$$B_T = (1 + B_M)^{\phi} - 1, \tag{2.127}$$

where the exponent ϕ is given by [102]

$$\phi = \frac{C_{pL}}{C_{pg}}\frac{\widetilde{\mathrm{Sh}}}{\widetilde{\mathrm{Nu}}}\frac{1}{\mathrm{Le}}. \tag{2.128}$$

Here C_{pg} is the specific heat capacity of the gas and $\widetilde{\mathrm{Nu}}$ is the modified Nusselt number and it is given by

$$\widetilde{\mathrm{Nu}} = 2 + \frac{\mathrm{Nu}_0}{(1 + B_T)^{-0.7}}. \tag{2.129}$$

2.3.6 Droplet collisions

As it is known as a major drawback of DDM, that implementation of droplet collisions is not an easy task. In the present work, droplet coalescence is taken into account for DQMOM in order to investigate the effect of droplet collisions on evaporating sprays

while the process of breakup is currently neglected [13], since the liquid mass is quite low in the present work. The coalescence is modeled as given in [7,108]. To emphasize upon coalescence, standard assumptions [108] have been employed. These include each binary collision leading to coalescence ($Ec = 1$) or rebound ($Ec = 0$), where E_c is the coalescence efficiency. Furthermore, the mass and momentum of colliding droplets are conserved before and after the collision. In addition, the mean collision time is assumed to be smaller than the inter-collision time. Thus, for two colliding droplets with radii r_1 and r_2, and velocities $\mathbf{v}_1$ and $\mathbf{v}_2$ respectively, the coalescence function can be written as [7,108]

$$\Gamma_f = Q_c^+ + Q_c^-, \tag{2.130}$$

where Q_c^+ and Q_c^- are calculated as

$$Q_c^- = -\int_{-\infty}^{\infty}\int_{0}^{\infty} f(t,\mathbf{x};r,\mathbf{v})f(t,\mathbf{x};r_1,\mathbf{v}_1)B(|\mathbf{v}-\mathbf{v}_1|)\mathrm{d}r_1\mathrm{d}\mathbf{v}_1, \tag{2.131}$$

$$Q_c^+ = \frac{1}{2}\int_{-\infty}^{\infty}\int_{0}^{r} f(t,\mathbf{x};r_1,\mathbf{v}_1)f(t,\mathbf{x};r_2,\mathbf{v}_2)B(|\mathbf{v}-\mathbf{v}_1|)\mathrm{d}r_1\mathrm{d}\mathbf{v}_1, \tag{2.132}$$

where $B(|\mathbf{v}-\mathbf{v}_1|)$ is given by

$$B(|\mathbf{v}-\mathbf{v}_1|) = \pi(r_1+r_2)^2|\mathbf{v}_2-\mathbf{v}_1|E_c. \tag{2.133}$$

In above equations, $(r,\mathbf{v})$ refer to post-collision properties, which are related to pre-collision properties $(r_1,\mathbf{v}_1)$ and $(r_2,\mathbf{v}_2)$ through the relations given as [7,108]

$$\mathbf{v} = \frac{r_1^3\mathbf{v}_1 + r_2^3\mathbf{v}_2}{r_1^3+r_2^3}, \tag{2.134}$$

$$r^3 = r_1^3 + r_2^3. \tag{2.135}$$

2.3.7 Source terms

To calculate the source terms due to spray evaporation for Eqs. (2.18), (2.19), (2.20), (2.22), (2.24) and (2.25), the droplet number density needs to be calculated at first. Since the gas phase equations are solved for DDM only, therefore the equation for droplet number density n can be written as following while neglecting the droplet–droplet interactions,

$$\frac{\partial n}{\partial t} + \frac{\partial(u_i n)}{\partial x_i} = 0. \tag{2.136}$$

The source terms are then written as

- Source term for continuity equation

  $\bar{S}_{l,1} = n\dot{m}$

- Source term for momentum equation in i-direction

  $S_{l,\tilde{u}_x} = n\dot{m}v_i$

- Source term for energy equation

  $\bar{S}_{l,\tilde{h}} = n\dot{m}H_d$, where $H_d = \left(h(T_d) + \frac{\mathbf{v}^2}{2} + \frac{1}{2}(\mathbf{v} - \tilde{\mathbf{u}})^2 - \mathbf{v}(\tilde{\mathbf{u}} + \mathbf{u}'') - L_v(T_d)\right)$

- Source term for transport equation of turbulent kinetic energy

  $\bar{S}_{l,\tilde{k}} = \mathbf{u}''(n\dot{m}(\mathbf{v} + \mathbf{u}''))$

- Source term for dissipation rate of turbulent kinetic energy

  $\bar{S}_{l,\tilde{\epsilon}} = C_s\tilde{\epsilon}/\tilde{k}\ \bar{S}_{l,k}$

- Source term for conservation equation of mixture fraction

  $\bar{S}_{l,\tilde{\xi}} = n\dot{m}$

- Source term for variance of mixture fraction

  $\bar{S}_{l,\widetilde{\xi''^2}} = \bar{S}_{l,k}\,\widetilde{\xi''^2}\left(1 - 2\widetilde{\xi}\right)/\widetilde{\xi}$

3. Numerical Schemes

A suitable numerical scheme is necessary to solve the mathematical model so that the underlying physics may be described appropriately. This requires discretization of governing equations and then implementation of a solver by means of a computer program. For any numerical method, it is very important to

- assure the physical conservation properties
- be consistent and stable for all physical configurations in question
- ensure non-negative property of quantities, where required e.g. mixture fraction
- be feasibly precise and convergent
- be computationally affordable
- independent of case specific properties

The properties of convergence, accuracy and non-negativity are all inter-related but none implies or implied by the other. In fluid mechanics, several numerical methods have been adapted, developed and improved. Naturally each method poses both advantages and disadvantages. Therefore, each application area has its own preference. In the framework of two-phase flows, it is difficult for any standard method to produce physically feasible simulations all alone, so hybrid numerical methods are tested and adapted widely. In hybrif methods, the major concerns are the consistency and stability, therefore an analysis of stability and consistency is required.

The commonly applied methods include a variety of mathematical backgrounds, which consist of particle methods, characteristic methods, Lagrangian finite difference/finite volume methods, Eulerian finite difference/finite volume methods, finite element methods and spectral methods. The particle methods, such as smoothed particle hydrodynamics or vortex methods inherit the robustness of Lagrangian description but uncontrolled particle distortion leads to degraded accuracy and the computation of spatial differential operators on the particles is highly inefficient [151]. Method of characteristics is the oldest and nearly exact method but it can be applied to hyperbolic equations only, therefore it deals with inviscid fluids [152]. In recent years, the finite difference and finite element methods are applied extensivly. In finite difference

methods, the diffusion coefficients are calculated at the mid points of the grid cell faces, which is feasible as long as diffusion coefficients are sufficiently smooth. More precisely, a second order accuracy is achieved if the diffusion coefficients are differentiable to order 3 [153]. In case the diffusion coefficients are not highly differentiable or discontinuous, then integration based discretization schemes such as finite element and finite volume methods are a better choice. The finite element method is applied extensively in fluid mechanics. it is very stable method and it can capture complex geometries [154]. But it needs special care to ensure the conservation properties. Furthermore, it has much higher computational cost [154] as compared to contemporary finite volume method.

Alike finite difference method or finite element method, values are calculated at discrete places on a meshed geometry in finite volume method (FVM). The term "finite volume" refers to the control volume surrounding each node point on a mesh. In FVM, volume integrals that contain a divergence term are converted to surface integrals, using the divergence theorem. These terms are then evaluated as fluxes at the surfaces of each finite volume. Since the flux entering a given volume is the same as that leaving the adjacent volume, therefore these methods are conservative. Another advantage of the finite volume method is that it can be easily implemented to unstructured meshes. Many computational fluid dynamics softwares use FVM. A major characteristic of FVM is that it combines the advantages of both the finite difference method and finite element method i.e., it is flexible geometrically as well as in defining the discrete flow field. Generally, the solutions obtained by finite volume method are relatively smooth and computationally efficient as compared to other numerical schemes. It can capture complex geometries and construct high order discretized formulations. In the present work, a finite volume method based on SIMPLER algorithm [155] is used to solve the mean conservation equations of the gas phase flow while the discrete droplet model for liquid phase is solved using stochastic parcel method.

3.1 Finite volume method for gas phase conservation equations

Conservation equations are the fundamental laws of fluid mechanics, which state the conservation of mass, momentum and energy in a control volume encapsulated by a surface. These conservation equations can be represented in different ways. It is important to note that the divergence condition for the velocity is satisfied by the continuity equation for incompressible flows, whereas in case of compressible flows, the energy equation satisfies the divergence condition. Since both reactive and non-reactive cases are considered in the present work, the compressibility conditions are different from incompressible limit. It has been shown [156] that standard numerical schemes

$\tilde{\phi}$	$\bar{S}_{g,\phi}$	$\bar{S}_{l,\phi}$
1	0	$\sum_{k=1}^{N_p}(n\dot{m})_{p,k}$
$\tilde{u}_x$	$-\frac{\partial\bar{p}}{\partial x} - \frac{2}{3}\frac{\partial}{\partial x}\left[\mu_{\text{eff}}\left(\frac{\partial\tilde{u}_x}{\partial x} + \frac{1}{r}\frac{\partial(r\tilde{u}_r)}{\partial r}\right)\right] + \bar{\rho}g$	$\sum_{k=1}^{N_p}(n\dot{m}v_x)_{p,k}$
$\tilde{u}_r$	$-\frac{\partial\bar{p}}{\partial r} - \frac{2}{3}\frac{\partial}{\partial r}\left[\mu_{\text{eff}}\left(\frac{\partial\tilde{u}_x}{\partial x} + \frac{1}{r}\frac{\partial(r\tilde{u}_r)}{\partial r}\right)\right] - 2\frac{\mu_{\text{eff}}\tilde{u}_r}{r^2}$	$\sum_{k=1}^{N_p}(n\dot{m}v_r)_{p,k}$
$\tilde{h}$	0	$\sum_{k=1}^{N_p}(n\dot{m}H_d)_{p,k}$
$\tilde{k}$	$G_k - \bar{\rho}\tilde{\epsilon}$	$\sum_{k=1}^{N_p}\mathbf{u}''(n\dot{m}(\mathbf{v}+\mathbf{u}''))_{p,k}$
$\tilde{\epsilon}$	$(C_1G_k - C_2\bar{\rho}\tilde{\epsilon})\tilde{\epsilon}\,/\,\tilde{k}$	$C_s\tilde{\epsilon}/\tilde{k}\ \bar{S}_{l,k}$
$\widetilde{\xi}$	0	$\sum_{k=1}^{N_p}(n\dot{m})_{p,k}$
$\widetilde{\xi''^2}$	$2\Gamma_{\widetilde{\xi''^2},\text{eff}}\frac{\partial^2\widetilde{\xi}}{\partial x_j^2} - 2\bar{\rho}\tilde{\epsilon}\,/\,\tilde{k}\,\widetilde{\xi''^2}$	$\bar{S}_{l,k}\,\widetilde{\xi''^2}\left(1-2\widetilde{\xi}\right)/\widetilde{\xi}$

Tab. 3.1: Governing equations of the gas flow with a dilute spray [67].

for incompressible form of conservation equations may not yield physically accurate results for weakly compressible flows. Therefore, the compressible form of conservation equations is chosen.

In the present work, Favre-averaged steady axisymmetric compressible conservation equations are solved by using the methodology suggested by Patanker [155], which can be written in the following form as a generalized equation [67]

$$\frac{\partial(\bar{\rho}_g\widetilde{u}_x\tilde{\phi})}{\partial x} + \frac{1}{r}\frac{\partial(r\bar{\rho}_g\tilde{u}_r\tilde{\phi})}{\partial r} - \frac{\partial}{\partial x}\left(\Gamma_{\phi,\text{eff}}\frac{\partial\tilde{\phi}}{\partial x}\right) - \frac{1}{r}\frac{\partial}{\partial r}\left(r\Gamma_{\phi,\text{eff}}\frac{\partial\tilde{\phi}}{\partial r}\right) = \bar{S}_{g,\tilde{\phi}} + \bar{S}_{l,\tilde{\phi}}, \quad (3.1)$$

where $\tilde{\phi}$ represents the flow field variables. The source terms $\bar{S}_{g,\phi}$ and $\bar{S}_{l,\tilde{\phi}}$ are written appropriate to the variable ϕ. These source terms are approximated using particle source in cell (PSIC) method [67,78], where the droplets are considered as point sources. Table 3.1 contains the source terms of corresponding variables for the system of equations described by Eq. (3.1), where N_p denotes the number of parcels in control volume $\mathcal{V}$, n is the number of droplets in parcel, and $\dot{m}$ refers to the evaporated liquid mass (see Eq. (2.117)). Since the contribution of evaporated liquid mass $\dot{m}$ is the defining quantity in approximation of $\bar{S}_{l,\tilde{\phi}}$, a reliable evaporation computation is necessary. The method of computing droplet evaporation is explained in section 3.3.2.1.

To determine the droplet source in a control cell, the droplet position is determined at first using the relation

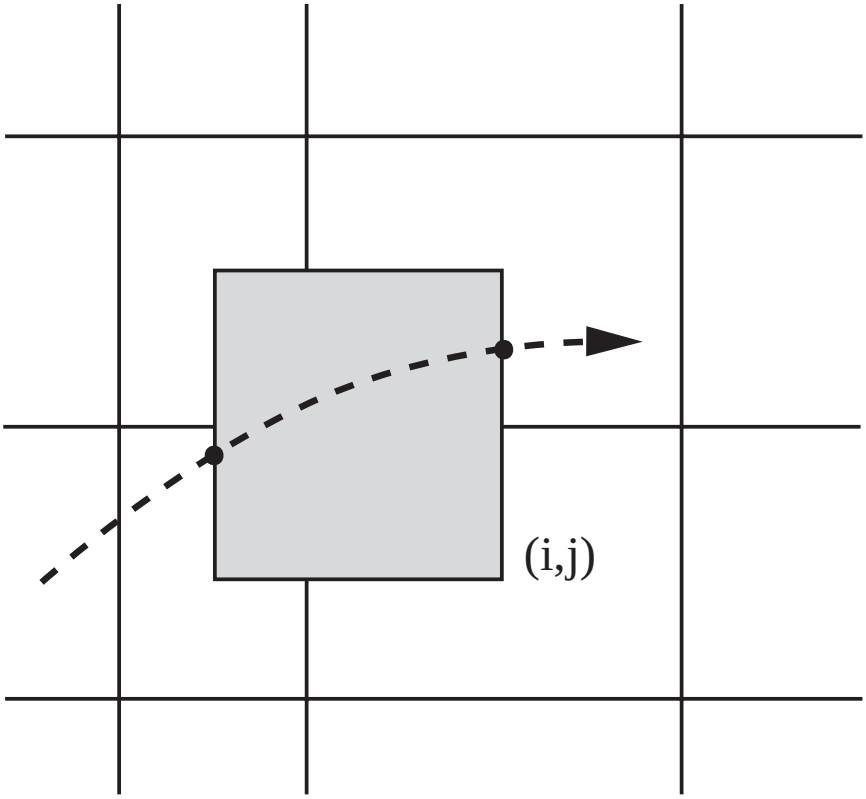

Fig. 3.1: Particle-Source-in-Cell (PSIC) model [95]

$$\mathbf{x}_p^{n+1} = \mathbf{x}_p^n + \mathbf{v}_p^n \Delta t. \tag{3.2}$$

The spray source terms for one certain control volume $\mathcal{V}$ (see Fig. 3.1) can be written as,

$$\begin{aligned} \bar{S}_{l,\phi} &= \frac{\overline{\dot{m}_{p,k}\phi}}{\mathcal{V}} \\ &= \frac{1}{\mathcal{V}} \sum_{k=1}^{N_p} [(m_{p,k}\phi_k)_{in} - (m_{p,k}\phi_k)_{out}]. \end{aligned} \tag{3.3}$$

In the present work, gas phase equations are resolved with DDM only. As it will be explained in the later sections of this chapter, DDM is solved using a Lagrangian stochastic parcel method [77].

A major concern about the present method is its applicability for non-reactive case, which represents the weakly compressible flow. It is reported that the compressible numerical schemes may be unstable at low Mach number. In the present case, Mach

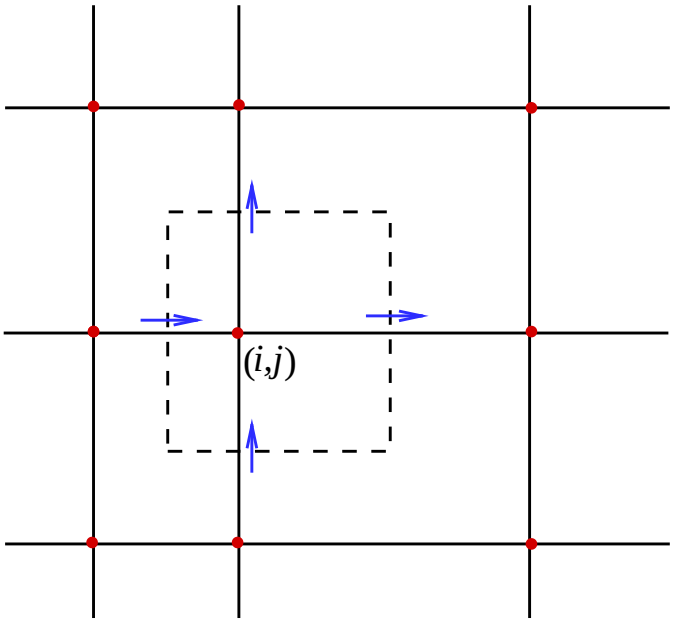

Fig. 3.2: Staggered grids in two dimensions: $\rightarrow = \tilde{u}_x$; $\uparrow = \tilde{u}_r$; $\bullet$ = scalar variables [158].

number varies between 0.1 to 0.2. Since the value of Mach number are not very close to the incompressible limit, so the compressible formulation of conservation equations seems a suitable choice. The points to address are the pressure velocity coupling and interpolation for approximation of convection terms.

It is established that decomposition of pressure over a staggered grid is suitable to address the problem of pressure velocity coupling [157], which is used in the present work. Concerning the interpolation for approximation of convection terms, an upwind scheme is a better choice than linear interpolation because it assures the non-zero diagonal of stiffness matrix, which is required for stability of the system. In the present work, a first order upwind scheme is used. Staggered grids have been used in several studies in literature. Fig. 3.2 [158] shows a staggered grid, where the control volume for the node (i, j) is shown as a dashed line. All the quantities are calculated on the grid nodes (i, j), $(i+1, j)$, $(i, j+1)$ and $(i+1, j+1)$ except the gas velocity. The gas velocity is calculated at the center of the grid cell faces to which they are normal. Pressure difference between two adjacent cells is the driving force for the velocity component at the interface of the two cells and implementation of staggered grid prevents oscillatory solutions for the pressure p. It is well established that implementation of staggered grid satisfies Poisson equation for pressure [159]. The decomposition of pressure may be attained in different ways i.e., in two components following the equation of state and

Poisson equation [157] or in three components following the asymptotic analysis [160, 161]. Since the compressible equations are used in the present work, a two component decomposition of pressure is used. There are certain disadvantages associated to the use of staggered grid too. Foremost of these disadvantages is the inconsistency of boundary conditions since at least one of the variables i.e., u_x and u_r is not defined on a particular boundary [159]. The structure of computer program is also relatively more complicated as **u** cannot be defined on the same array as other variables. In case of non rectangular grid or cartesian coordinates, the implementation is further difficult.

3.1.1 Discretized formulation

The discretized forms of conservation equations are similar except that of momentum equation because of the usage of staggered grid technique. There are several ways and techniques that can be used to discretize the governing equations. As a prerequisite of convergence, the solution must be consistent at the control volume faces i.e., the flux must be represented by the same discretization equations across the face, which is common between two adjacent cells. In the present formulation, the energy equation and the transport equations for the mixture fraction, variance of mixture fraction, turbulent kinetic energy, and its dissipation rate are solved by applying a five node formula [155] i.e., the value of an independent variable ϕ_P at a node $P = P(i, j)$ is connected with those of its two neighbors in x-direction, ϕ_E and ϕ_W, where $E = E(i + 1, j)$ and $W = W(i - 1, j)$, and its two neighbors in y-direction, ϕ_S and ϕ_N, where $N = N(i, j + 1)$ and $S = S(i, j - 1)$. The points E, W, N and S refer to east, west, north and south of the point P, respectively. Thus, any obtained equation from Eq. (3.1) can be written as

$$a_P \phi_P = \sum_{I=E,W,N,S} a_I \phi_I + b, \tag{3.4}$$

where b denotes the source term. The index $I \in \{E, W, N, S\}$ indicates the directions. The coefficients a_I represent the effects of convection and diffusion at four faces of the control volume in terms of flow rate F_I and conductivity D_I. The expressions for a_I and b are derived by integrating the differential equation (3.1) over a control volume surrounding the node p (see Fig. 3.3 [158]). The source term $S_{\tilde{\phi}} = S_{g,\tilde{\phi}} + S_{l,\tilde{\phi}}$ must be linearized, which is done by expressing it as a sum of a linear term $S_P \tilde{\phi}_P$ and a constant term S_C i.e.,

$$S_{\tilde{\phi}} = S_P \tilde{\phi}_P + S_C. \tag{3.5}$$

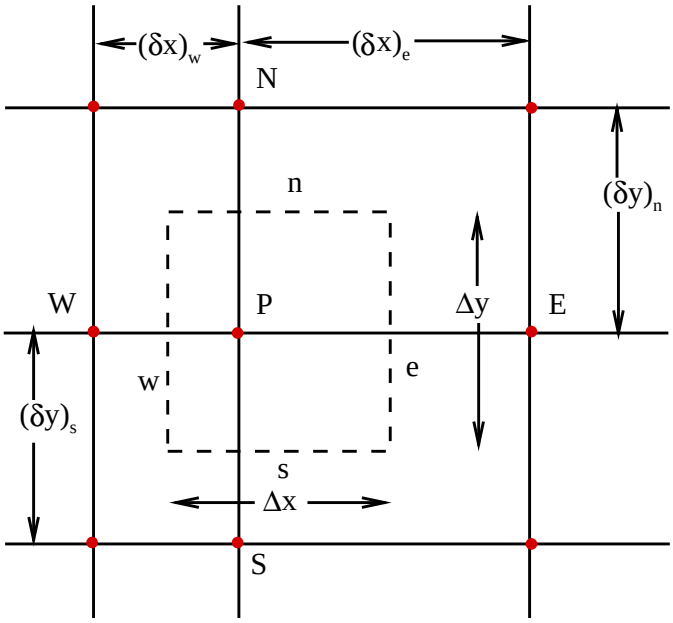

Fig. 3.3: Control volume of the grid nodes [158].

Thus,

$$a_I = D_I A(|\mathrm{P}_I|) + \frac{1}{2}\left(|E_I| - E_I\right), \; I = E, N, \tag{3.6}$$

$$a_I = D_I A(|\mathrm{P}_I|) + \frac{1}{2}\left(|E_I| + E_I\right), \; I = W, S, \tag{3.7}$$

$$a_P = \sum_I a_I - S_P \Delta x \Delta y, \tag{3.8}$$

$$b = S_C \Delta x \Delta y, \tag{3.9}$$

where $\mathrm{P_I}$ is the Peclet number, which may be defined in terms of convection and the diffusion length as

$$\mathrm{P}_I = \frac{E_I}{D_I}. \tag{3.10}$$

As it is evident that the value at a grid point is influenced by its neighboring grid points. Therefore, an increase in the value of any dependent variable at neighboring grid points of point P must increase the value of that dependent variable at point P, while the other conditions are kept unchanged. This requires that all the coefficients $a_I : I \in \{P, E, W, N, S\}$ must have the same sign, which is taken to be positive sign in this work. It can be seen in Eq. (3.8)that even if a_I are positive for $I \in \{E, W, N, S\}$, still a_P will yield a negative value for large enough S_P, which eventually will cause the

numerical computation to diverge. Thus the source term must be linearized with a negative slope i.e., $S_P < 0$.

Function $A(|\mathrm{P}|)$ depends on discretization schemes. In the present work, an upwind scheme is employed.The upwind scheme is the only approximation that unconditionally satisfies the boundedness criterion. With upwind scheme, oscillations in the solutions are avoided, i.e., the the computation is more stable. However, the upwind scheme introduces numerical diffusion as a result of the first-order truncation. A is assumed to be unity

$$A(|\mathrm{P}_I|) = 1. \tag{3.11}$$

The convection terms E_I are expressed as

$$E_I = (\bar{\rho}\tilde{u}_x)_I \Delta y,\ I = E, W, \tag{3.12}$$

$$E_I = (\bar{\rho}\tilde{u}_r)_I \Delta x,\ I = N, S. \tag{3.13}$$

The diffusion fluxes D_I are calculated using a central-difference schme and can be expressed as

$$D_I = \Gamma_I \frac{\Delta y}{(\delta x)_I},\ I = E, W; \tag{3.14}$$

$$D_I = \Gamma_I \frac{\Delta x}{(\delta y)_I},\ I = N, S. \tag{3.15}$$

3.1.1.1 Solution for conserved scalars

The solution for the conserved scalars is obtained using Tri-Diagonal-Matrix-Algorithm (TDMA) to solve the Eq. (3.4). Equation (3.4) can be rewritten as

$$\phi_P = \frac{\sum_{I=E,W,N,S} a_I \phi_I + b}{a_P}. \tag{3.16}$$

Thus setting the iterations, the following form is obtained.

$$\tilde{\phi}_P = \tilde{\phi}_P^* + \left(\frac{\sum_I (a_I \tilde{\phi}_I) + b}{a_P} - \tilde{\phi}_P^* \right). \tag{3.17}$$

Since the large changes in values of variables in successive iterations may cause computational instability, so the scalars $\tilde{\phi}_P^{n+1}$ is restricted to change only by a fraction of $\tilde{\phi}_P^n$ by using the relaxation parameters α_P i.e.,

$$\tilde{\phi}_P = \tilde{\phi}_P^* + \alpha \left(\frac{\sum_I (a_I \tilde{\phi}_I) + b}{a_P} - \tilde{\phi}_P^* \right), \tag{3.18}$$

where α_P are constants and $0 < \alpha_P < 1$.

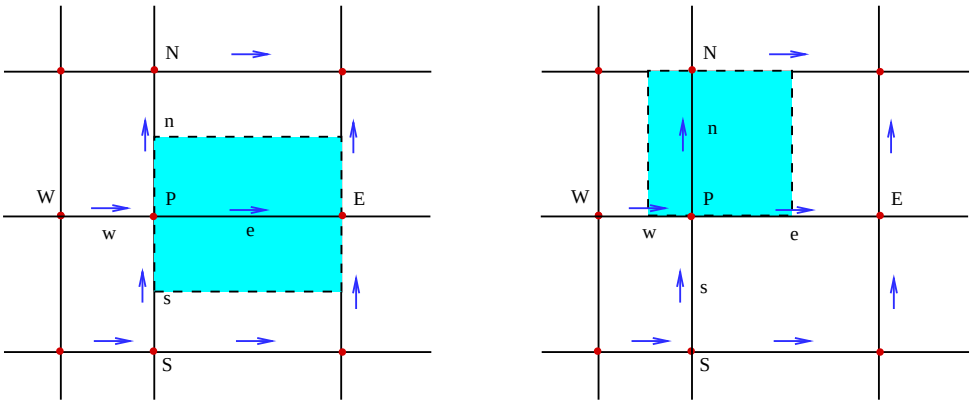

Fig. 3.4: Control volume of axial velocity (left) and radial velocity (right) [158].

3.1.1.2 Solution of momentum equation

The solution for the conserved scalars described in previous subsection is possible when density, velocity and pressure field are known. So the contiuity and momentum equations must be treated in order to obtain a solution. These equations are coupled in the physical sense, as the conservation of momentum is possible in the flow field only when the mass is conserved. The control volume for velocity $\mathbf{u}$ is shown in Fig. 3.4 [158], which is staggered in relation to the normal control volume around the grid point P and E. For the solution, pressure field must be known as the pressure difference $p_P - p_e$ is the driving force acting on the control volume for the velocity $\mathbf{u}$. The pressure gradient $-\partial\bar{p}/\partial x_i$ is considered as a source term of the momentum equation and so it is indirectly involved in continuity equation, too. The simplest way to discretize the pressure term is to consider one dimensional control volume of unity length around the point P and assume the staggered grid face at the middle of two successive grid nodes. Then using the linear interpolation for the pressure,

$$\bar{p}_w = \frac{\bar{p}_W + \bar{p}_P}{2}$$

and

$$\bar{p}_e = \frac{\bar{p}_E + \bar{p}_P}{2}.$$

So the pressure difference of velocity integration points can be described in terms of pressure difference of grid nodes as

$$\bar{p}_w - \bar{p}_e = \frac{\bar{p}_W + \bar{p}_P}{2} - \frac{\bar{p}_E + \bar{p}_P}{2} = \frac{\bar{p}_W - \bar{p}_E}{2}. \tag{3.19}$$

The problem is that while using only two of the neighboring grid points for pressure discretization, the pressure field may be constant. The same problem would arise

in case of continuity equation. Thus a correction in pressure field is needed. The calculation of the diffusion coefficient and the mass flow rate at the faces of the control volume require a treatment similar to Eq. (3.4). The resulting discretization equation is written as

$$a_e \tilde{u}^*_{x,e} = \sum a_{lb} \tilde{u}^*_{x,lb} + b + (\bar{p}^*_P - \bar{p}^*_E) A_e, \tag{3.20}$$

$$a_w \tilde{u}^*_{x,w} = \sum a_{lb} \tilde{u}^*_{x,lb} + b + (\bar{p}^*_W - \bar{p}^*_P) A_w, \tag{3.21}$$

$$a_n \tilde{u}^*_{r,n} = \sum a_{lb} \tilde{u}^*_{r,lb} + b + (\bar{p}^*_P - \bar{p}^*_N) A_n, \tag{3.22}$$

and

$$a_s \tilde{u}^*_{x,s} = \sum a_{lb} \tilde{u}^*_{r,lb} + b + (\bar{p}^*_S - \bar{p}^*_P) A_s. \tag{3.23}$$

The algebraic coefficients a_{lb} account for the combined convection-diffusion influences at the control volume faces. The source term b is defined in the same manner as in Eq. (3.4). As the correction is needed in pressure calculation, the corrected pressure $\bar{p}^*$ differs from mean effective pressure $\bar{p}$ i.e.

$$\delta p = \bar{p} - \bar{p}^*, \tag{3.24}$$

where δp is called pressure corrector. Using this correction, the velocity components calculated using Eqs. (3.20) - (3.23) are also corrected as

$$\tilde{u}_{x,e} = \tilde{u}^*_{x,e} + \frac{A_e}{a_e}(\delta p^*_P - \delta p^*_E), \tag{3.25}$$

$$\tilde{u}_{x,w} = \tilde{u}^*_{x,w} + \frac{A_w}{a_w}(\delta p^*_P - \delta p^*_E), \tag{3.26}$$

$$\tilde{u}_{r,n} = \tilde{u}^*_{r,n} + \frac{A_n}{a_n}(\delta p^*_P - \delta p^*_E), \tag{3.27}$$

$$\tilde{u}_{r,s} = \tilde{u}^*_{r,s} + \frac{A_s}{a_s}(\delta p^*_P - \delta p^*_E). \tag{3.28}$$

The calculation of pressure corrector can be aided by using the discretized form of continuity equation

$$\left[(\bar{\rho}\widetilde{u_x})_e - (\bar{\rho}\widetilde{u_x})_w\right] A_e + \left[(\bar{\rho}\widetilde{u_r})_n - (\bar{\rho}\widetilde{u_r})_s\right] A_n = \bar{S}_{l,1}. \tag{3.29}$$

Using Eqs. (3.25) - (3.28) in Eq. (3.29), following expression for pressure corrector is obtained

$$a_P \delta p_P = \sum_{I \in \{E,N,S,W\}} a_I \delta p_I + b, \tag{3.30}$$

where the coefficients and source term are given by

$$\begin{aligned} a_I &= \bar{\rho}_I d_I A_I, \\ a_p &= \sum_I a_I, \\ b &= \left[(\bar{\rho}\widetilde{u_x})_e - (\bar{\rho}\widetilde{u_x})_w\right] A_e + \left[(\bar{\rho}\widetilde{u_r})_n - (\bar{\rho}\widetilde{u_r})_s\right] A_n + (\rho g_i + \bar{S}_{l,1})\Delta V, \\ d_I &= A_I / a_I. \end{aligned}$$

3.1.2 Solution algorithm

The numerical algorithm applied to obtain a solution is abbreviated as "SIMPLER", which stands for "Semi-Implicit Method for Pressure-Linked Equations - Revised" [155]. The semi implicit algorithms were extensively applied for numerical simulations of fluid flows in the last decades. In the present work, SIMPLER algorithm is used to calculate the pressure and to ensure the validity of the continuity equation. Some modifications in the SIMPLER algorithm have been suggested in [162].

SIMPLER algorithm relies on the finite volume discretization using the staggered grids, which are incorporated in the present work. The solutions of the discretized equations are obtained through iterative procedures. The iterative procedure can be interpreted as a pseudo-transient treatment of the unsteady momentum conservation equations in discrete form to obtain the steady-state solution [155].

1. Estimation of a pressure field p^*;
2. Calculation of gas velocity ${u_x}^*$ and u_r^* using the Eqs. (3.20) - (3.23);
3. Calculation of δp using Eq. (3.30);
4. correction of calculated velocity using the Eqs. (3.25) - (3.28)
5. Obtaining pressure at next grid node i.e., $p^{n+1} = p^n + \delta p$;
6. Calculating the scalar variables
7. checking whether the source term b in Eq. (3.30) is zero. If not, returning to the step 2 and repeating until convergence is achieved.

3.1.3 Stability

The stability of applied numerical scheme is essential. In case of weakly compressible flows, the stability of numerical schemes is a known question [156]. In particular, the pressure velocity coupling needs to be treated properly. This is achieved by applying

the staggered grid in the present work. For weakly compressible flows, the compressible scheme without any modification would tend to fail due to large difference between the flow and sound velocities. When Mach number is greater than 0.3, the compressible scheme may be used without any modification. For smaller Mach numbers, explicit compressible schemes are not suitable for spray flows [57]. To be precise, incorporating small Mach numbers having high velocity of sound leads to very small time steps. This can be treated through application of semi implicit or fully implicit numerical scheme. The aspect that requires special attention is that the pressure velocity coupling in incompressible limit must ensure the divergence free constraint.

To address the aforementioned, SIMPLE-type methods have often been used in literature [160] and adapted in the present work as well. The pressure is decomposed in constant and fluctuating components. The constant part is used to calculate the equations of state. The much smaller part guarantees the divergence constraint for the velocity. Besides, the linear interpolation is not suitable for high velocity of sound in the flow. Therefore, an upwind scheme is used in the present work.

The round off error in n^{th} iteration for conserved scalars and the velocity at point P is defined by

$$e_P^n = \tilde{\phi}_P^{\text{exact}} - \tilde{\phi}_P^n. \tag{3.31}$$

Thus there relative error of successive iterations can be defined as

$$\begin{aligned} e_P^{n+1} - e_P^n &= \tilde{\phi}_P^{\text{exact}} - \tilde{\phi}_P^{n+1} - (\tilde{\phi}_P^{\text{exact}} - \tilde{\phi}_P^n) \\ &= \tilde{\phi}_P^n - \tilde{\phi}_P^{n+1}. \end{aligned} \tag{3.32}$$

Using Eq. (3.18) in Eq. (3.32), the above relation can be derived as

$$e_P^{n+1} - e_P^n = \tilde{\phi}_P^n - \left\{ \tilde{\phi}_P^n + \alpha \left(\frac{\sum_I (a_I \tilde{\phi}_I^n) + b}{a_P} - \tilde{\phi}_P^n \right) \right\}, \tag{3.33}$$

where α is the relaxation parameter and its value lies between 0 and 1. Therefore the absolute value of relative error can be written as

$$\left| e_P^{n+1} - e_P^n \right| = \alpha \left| \frac{\sum_I (a_I \tilde{\phi}_I^n) + b}{a_P} - \tilde{\phi}_P^n \right|. \tag{3.34}$$

Since $0 < \alpha < 1$, so the above equation may be transformed to the following inequality

$$\left| e_P^{n+1} - e_P^n \right| \leq \left| \frac{\sum_I (a_I \tilde{\phi}_I^n) + b}{a_P} - \tilde{\phi}_P^n \right|. \tag{3.35}$$

In the above inequality, the spray source is represented by the quantity b. Since the initial data i.e., at $n = 0$ is known and generated from experimental data, the relative error is bounded by the known quantities.

The SIMPLER based finite volume numerical scheme for the solution of gas phase conservation equations is explained. In the present work, gas phase conservation equations are solved for both non reactive and reactive cases. The reactive case is modeled using PDF method as well. In the next section, the numerical method for the solution of PDF transport equation is described.

3.2 Monte-Carlo particle method for the PDF transport equation

The PDF transport equation is a high dimensional problem and it can not be solved directly. Therefore, Monte-Carlo methods including Eulerian Monte-Carlo methods [163] and Lagrangian Monte-Carlo methods [64] are applied for its solution. The PDF is represented using stochastic Eulerian fields in Eulerian Monte-Carlo methods [163] while in Lagrangian Monte-Carlo methods, the stochastic particles are used to represent the PDF [64]. In two phase flows, the particle methods are particularly useful as the dispersed phase is often solved by particle methods, where the particles may represent droplets, bubbles or solid particles.

In the present work, a Lagrangian Monte-Carlo particle method is used for PDF transport equation, where one point PDF is represented by a finite number of gas particles. These Monte-Carlo/stochastic gas particles are created and activated according to the local flow properties at the inlet plane. The total mass of the stochastic gas particles in one control cell calculated from the mass flux during the current time step [95]

$$m^*_{\text{tot}} = \rho_0 u_{x,0} S_0 \Delta t, \tag{3.36}$$

where S_0 is the area of the control cell at inlet profile while the initial density ρ_0 and initial axial velocity $u_{x,0}$ are taken from experimental data. Each gas particle is associated to a set of properties. The set of these properties is not unique as it may vary depending upon the formulation of the PDF transport equation such as mass m^*, position $\mathbf{x}^*$, velocity $\mathbf{u}^*$, mixture fraction ξ^*_j and enthalpy h^*. The superscript * refers to sample properties. The position of gas particle i.e., $\mathbf{x}^*$ evolves according to the following equation:

$$\frac{\partial \mathbf{x}^*}{\partial t} = \mathbf{u}^*(\mathbf{x}^*), \tag{3.37}$$

where $\mathbf{u}^*(\mathbf{x}^*)$ is the instantaneous velocity of the particle. The instantaneous velocity of the particle is written as

$$\mathbf{u}^*(\mathbf{x}^*) = \tilde{\mathbf{u}}(\mathbf{x}^*) + \mathbf{u}^{''}(\mathbf{x}^*, t), \tag{3.38}$$

where $\tilde{\mathbf{u}}$ is computed by the finite volume method and is interpolated into the particle's position $\mathbf{x}^*$. A first-order interpolation is used in the present work i.e., if the particle is located in the cell e with four vertices (i,j), $(i+1,j)$, $(i,j+1)$, and $(i+1,j+1)$, then the value of function ϕ at the particle position (x_1,x_2) is interpolated from the values stored at the nodes

$$\begin{aligned}\phi^*(x_1,x_2) &= g_{i,j}(x_1,x_2)\phi_{i,j} + g_{i+1,j}(x_1,x_2)\phi_{i+1,j} \\ &+ g_{i,j+1}(x,y)\phi_{i,j+1} + g_{i+1,j+1}(x_1,x_2)\phi_{i+1,j+1}, \end{aligned} \tag{3.39}$$

where $g_{i,j}(x_1,x_2)$ is the linear basis function coefficient of node (i,j) to the particle position (x_1,x_2) in the cell e. The linear basis function coefficient is defined as

$$g_{i,j}(x_1,x_2) = \frac{(x_{1,i+1}-x_1)(x_{2,i+1}-x_2)}{(x_{1,i+1}-x_{1,i})(x_{2,i+1}-x_{2,i})}, \tag{3.40}$$

$$g_{i+1,j}(x,y) = \frac{(x_1-x_{1,i})(x_{1,i+1}-x_2)}{(x_{1,i+1}-x_{1,i})(x_{2,i+1}-x_{2,i})}, \tag{3.41}$$

$$g_{i,j+1}(x,y) = \frac{(x_{1,i+1}-x_1)(x_2-x_{2,i})}{(x_{1,i+1}-x_{1,i})(x_{2,i+1}-x_{2,i})}, \tag{3.42}$$

$$g_{i+1,j+1}(x,y) = \frac{(x_1-x_{1,i})(x_2-x_{2,i})}{(x_{1,i+1}-x_{1,i})(x_{2,i+1}-x_{2,i})}. \tag{3.43}$$

The sum of these four coefficients equals to unity:

$$\sum_{\alpha=1}^{4} g_\alpha(x_1,x_2) = 1.$$

If the gas particle is not in the cell e, then the linear basis function coefficients equal zero:

$$g_\alpha(x_1,x_2) = 0.$$

To determine the value of the fluctuating velocity is through a Monte-Carlo method, it is assumed that the fluctuating velocity $\vec{u}''$ follows a Gaussian distribution with the mean zero and the variance of $2k/3$:

$$f(u'') = \left(\frac{4}{3}\pi\tilde{k}\right)^{-\frac{1}{2}} \exp\left(-\frac{3}{4\tilde{k}}u''^2\right). \tag{3.44}$$

The turbulent kinetic energy is interpolated from grids into the gas particle's position using Eq. (3.39). A second-order algorithm is used to solve Eq. (3.37) [93]. The mid-point $\mathbf{x}^{*^{n+\frac{1}{2}}}$ is computed by

$$\mathbf{x}^{*^{n+\frac{1}{2}}} = \mathbf{x}^{*^n} + \frac{\Delta t}{2}\left(\tilde{\mathbf{u}}^n(\mathbf{x}^{*^n}) + \mathbf{u}^n\right). \tag{3.45}$$

The superscript n denotes the n^{th} time step. Thus, the new mean velocity $\mathbf{u}^n(\mathbf{x}^{*^{n+\frac{1}{2}}})$ and fluctuating velocity $\mathbf{u}^{''n+1}$ at position $\mathbf{x}^{*^{n+\frac{1}{2}}}$ are computed. The particle's position at $(n+1)$th time step is calculated by

$$\mathbf{x}^{*^{n+1}} = \mathbf{x}^{*^n} + \Delta t \left(\tilde{\mathbf{u}}^n(\mathbf{x}^{*^{n+\frac{1}{2}}}) + \frac{1}{2}(\mathbf{u}^{''n} + \mathbf{u}^{n+1}) \right). \tag{3.46}$$

In particulate form, the IEM model for the k^{th} particle can be written as

$$\mathrm{d}\xi_k^* = -\frac{1}{2}\frac{C_\phi}{t_\tau(\mathbf{x}_k^*)}(\xi_k^* - \tilde{\xi}(\mathbf{x}_k^*))\mathrm{d}t + [1-\xi_k^*]\frac{\langle S_{l,1}\rangle}{\langle\rho\rangle}\mathrm{d}t, \tag{3.47}$$

$$\mathrm{d}h_k^* = -\frac{1}{2}\frac{C_\phi}{t_\tau(\mathbf{x}_k^*)}(h_k^* - \tilde{h}(\mathbf{x}_k^*))\mathrm{d}t + \frac{\langle S_{l,h}\rangle - \langle hS - l, 1\rangle}{\langle\rho\rangle}\mathrm{d}t \tag{3.48}$$

where the local turbulent fluctuating time scale $t_\tau(\mathbf{x}_k^*)$ is interpolated from the grid nodes. The exact increment in ϕ_k^* in terms of $\tilde{\phi}$ over time Δt is [95]

$$\Delta\phi_k^* = -d_k(\phi_k^* - \tilde{\phi}(\mathbf{x}_k^*)) \tag{3.49}$$

with

$$d_k = 1 - e^{-\frac{1}{2}C_\phi \Delta t/t_\tau}. \tag{3.50}$$

The quantity $\tilde{\phi}(\mathbf{x}_k^*)$ is interpolated from the grid node by

$$\tilde{\phi}(\mathbf{x}_k^*) = \sum_\alpha g_\alpha(\mathbf{x}_k^*)\hat{\phi}_\alpha, \tag{3.51}$$

where $g_\alpha(\mathbf{x}_k^*)$ is the linear basis function coefficient of node α to the particle position $\mathbf{x}_k^*$ with

$$\sum_\alpha g_\alpha(\mathbf{x}_k^*) = 1. \tag{3.52}$$

Thus

$$\Delta\phi_k^* = -d_k(\phi_k^* - \sum_\alpha g_\alpha(\mathbf{x}_k^*)\hat{\phi}_\alpha). \tag{3.53}$$

The global change in ϕ must be zero during the whole mixing process. However, if the value of $\hat{\phi}$ is directly taken from $\tilde{\phi}$ which is stored at the grid nodes, the global change may not be zero [64]. Thus, the value of $\hat{\phi}$ must be estimated by setting the global change to zero,

$$\begin{aligned}
0 = \Delta G &\equiv \sum_k m_k^*\Delta\phi_k^* = -\sum_k m_k^* d_k \left(\phi_k^* - \sum_\alpha g_\alpha(\mathbf{x}_k^*)\hat{\phi}_\alpha\right) \\
&= -\sum_k m_k^* d_k \left(\sum_\alpha g_\alpha(\mathbf{x}_k^*)\phi_k^* - \sum_\alpha g_\alpha(\mathbf{x}_k^*)\hat{\phi}_\alpha\right) \\
&= -\sum_k \sum_\alpha \left(g_\alpha(\mathbf{x}_k^*) m_k^* d_k \left(\phi_k^* - \hat{\phi}_\alpha\right)\right) \\
&= \sum_\alpha \left(-\left(\sum_k g_\alpha(\mathbf{x}_k^*) m_k^* d_k \phi_k^*\right) + \hat{\phi}_\alpha \left(\sum_k g_\alpha(\mathbf{x}_k^*)\mathbf{m}_\mathbf{k}^*\mathbf{d}_\mathbf{k}\right)\right).
\end{aligned} \tag{3.54}$$

Therefore, $\hat{\phi}_\alpha$ can be determined by

$$\hat{\phi}_\alpha = \frac{\sum_k g_\alpha(\mathbf{x}_k^*) m_k^* d_k \phi_k^*}{\sum_k g_\alpha(\mathbf{x}_k^*) m_k^* d_k}. \tag{3.55}$$

The mean values are evaluated from the results of the transported PDF method at each node. The computation is via the linear basis function coefficient. For an arbitrary function Φ, its mean value at the node α is calculated from its value of the gas particles

$$\tilde{\Phi} = \frac{\sum_e \sum_k g_\alpha(\mathbf{x}_k^*) \Phi_k^*}{\sum_e \sum_k g_\alpha(\mathbf{x}_k^*) m_k^*}. \tag{3.56}$$

The first sum is over the cells e enclosed by nodes α.

Time step is restricted by Courant – Friedrichs – Lewy (CFL) condition [164]. Physically, the CFL condition indicates that a fluid particle should not travel more than one control volume in one time step. The global time step is computed by the following formula:

$$\Delta t = C_{\mathrm{CFL}} \cdot \min \left\{ \frac{\Delta x_{1,i}}{|\tilde{u_{1i}}|}, \frac{\Delta x_{2,i}}{|\tilde{u_{2i}}|}, \frac{\tilde{k}_i}{\tilde{\epsilon}_i}, \dots \right\}, \quad i = 1, \dots, N_g, \tag{3.57}$$

where N_g is the total number of the grid points, $\Delta x_{1,i}$ and $\Delta x_{2,i}$ are the lengths of the control volume of node i in axial and radial directions respectively, and u_1 and u_2 are the axial and radial gas velocities. k and ϵ are the turbulent kinetic energy and its dissipation rate. The constant C_{CFL} should not be larger than 1 to satisfy the von Neumann stability condition. Here, C_{CFL} is set to 0.5. The resulting time step is serves for both the finite volume method and the particle method.

In transported PDF method, the statistics of the flow field are evaluated at each cell. It is reported [165] that the statistical error is proportional to $N^{-1/2}$, where N is the number of sample values. Thus the statistical error will be quite large if corresponding total number of gas particles in one cell is too low. On the other hand, if the total number of gas particles in one cell is too large, it would cause computational problems. To avoid such cases, special strategy [64] is needed to keep the gas particle number of every cell in a certain range, $[N_{\min}, N_{\max}]$. In the present work, a split/discard algorithm is used [68] to ensure the number of stochastic particles to fall in the desired range, which is set to $N_{\min} = 60$ and $N_{\max} = 100$.

3.3 Liquid phase

3.3.1 Stochastic parcel method for DDM

For the application of thefinite volume method discussed earlier, appropriate approximation of spray source terms described in Table 3.1 is needed. These source terms

describe the contribution of the evaporated liquid mass towards the gas flow properties. For this purpose, the liquid phase is modeled through DDM [18,21,29], where the droplet properties are computed using stochastic parcel method [77]. A droplet parcel is a set of droplets represented by identical properties and position i.e., $(\mathbf{x}_{p,k}, \mathbf{v}_{p,k}, r_{p,k}, m_{p,k})$ represent the position, velocity, droplet radius and liquid mass of k^{th} parcel. Droplet radius, velocity, temperature and evaporated mass are calculated as described in sections 3.3.2.1 and 3.3.2.2. These calculations are used to compute the spray source terms described in section 2.3.7 and table 3.1.

3.3.2 Finite difference scheme for DQMOM

In the present work, DQMOM is not coupled to gas phase rather inlet gas flow properties are used for computations. A generalized model for 3-dimensional physical space has been discussed for application to evaporating sprays [13]. Here DQMOM is discussed in 2-dimensional physical space considering axisymmetric configuration. Thus the DQMOM equations can written in component form by taking $\mathbf{v} = [v_x, v_r]$ and $\mathbf{x} = [x, r]$. Eqs. (2.104) – (2.106) can be represented in generalized form in each geometrical direction given by,

$$\frac{\partial W_x}{\partial t} + \frac{\partial W_x v_x}{\partial x} = S_x, \tag{3.58}$$

$$\frac{\partial W_r}{\partial t} + \frac{\partial W_r v_r}{\partial r} = S_r, \tag{3.59}$$

where

$$\begin{aligned} (W_x, S_x) &\in \{(w_n, a_n), (w_n \rho_l r_n, \rho_l b_n), (w_n \rho_l r_n v_{xn}, \rho_l c_{n,x})\}, \\ (W_r, S_r) &\in \{(w_n, a_n), (w_n \rho_l r_n, \rho_l b_n), (w_n \rho_l r_n v_{rn}, \rho_l c_{n,r})\}. \end{aligned}$$

The choice of numerical scheme is important. It has been shown [13] that a two step predictor-corrector numerical formula i.e., McCormac method [168] is accurately applicable and computationally efficient for DQMOM in one dimensional physical space. For two-dimensional geometrical space, a better numerical scheme is needed. The purpose is to solve the transport equations of DQMOM only, since the liquid properties such as droplet temperature, evaporated mass, droplet velocities and droplet radii are computed in the same way as discussed in earlier sections of this chapter. Furthermore, DQMOM is not fully coupled to gas phase, since the gas phase equations are not solved for DQMOM rather only inlet gas flow properties are used for computations. Therefore, keeping the computational efficiency, ease of application and numerical accuracy, a second order finite difference scheme is applied to solve the Eqs. (3.58) – (3.59) [169]. The scheme uses central difference approach, therefore the neighboring points of node

P are denoted by S, N in $x-$direction and W, E in $r-$ direction. Thus the solution formulae may be written as

$$\begin{aligned} W_{x,i}^{j+1} &= W_{x,i}^{j} && (3.60)\\ &- \frac{\Delta t}{\Delta x_i}\left[-W_{x,i+1}^{j}(v_{x,i+1}^{j})_L + W_{x,i}^{j}(v_{x,i}^{j})_L + W_{x,i}^{j}(v_{x,i}^{j})_R - W_{x,i-1}^{j}(v_{x,i-1}^{j})_R\right], \\ W_{x,i}^{j+1}v_{x,i}^{j+1} &= W_{x,i}^{j}v_{x,i}^{j} && (3.61)\\ &- \frac{\Delta t}{\Delta x_i}\left[W_{x,i+1}^{j}(v_{x,i+1}^{j})_L^2 + W_{x,i}^{j}(v_{x,i}^{j})_L^2 - W_{x,i}^{j}(v_{x,i}^{j})_R^2 - W_{x,i-1}^{j}(v_{x,i-1}^{j})_R^2\right], \\ W_{r,i}^{j+1} &= W_{r,i}^{j} && (3.62)\\ &- \frac{\Delta t}{\Delta r_i}\left[-W_{r,i+1}^{j}(v_{r,i+1}^{j})_L + W_{r,i}^{j}(v_{r,i}^{j})_L + W_{r,i}^{j}(v_{r,i}^{j})_R - W_{r,i-1}^{j}(v_{r,i-1}^{j})_R\right], \\ W_{r,i}^{j+1}v_{r,i}^{j+1} &= W_{r,i}^{j}v_{r,i}^{j} && (3.63)\\ &- \frac{\Delta t}{\Delta r_i}\left[W_{r,i+1}^{j}(v_{r,i+1}^{j})_L^2 + W_{r,i}^{j}(v_{r,i}^{j})_L^2 - W_{r,i}^{j}(v_{r,i}^{j})_R^2 - W_{r,i-1}^{j}(v_{r,i-1}^{j})_R^2\right]. \end{aligned}$$

The above formulation is applied to an equidistant rectangular grid, where the size of each grid cell is 1.5 10^{-3} m in radial direction and 1.0 10^{-4} in radial direction, resulting in a maximum of 80 $\times$ 1000 grid nodes.

3.3.2.1 Evaporation

The detailed description of the model is already given (c.f. section 2.3.4). Droplet radius and temperature need to be computed to close the evaporation model in Eqs. (2.118) and (2.117), which are calculated using a second order Runge – Kutta scheme given below

$$r^{n+1} = r^{n+1} + \Delta t \frac{\mathrm{d}r}{\mathrm{d}t}\Big|_{n+\frac{1}{2}}, \tag{3.64}$$

$$T_d^{n+1} = T_d^{n+1} + \Delta t \frac{\mathrm{d}T_d}{\mathrm{d}t}\Big|_{n+\frac{1}{2}}. \tag{3.65}$$

When the droplet radius is small enough i.e.,

$$r < \max\{0.1r, 1\mu m\}, \tag{3.66}$$

then the droplet is assumed to have evaporated completely becuase the liquid mass, being the cube function of droplet radius becomes negligible.

3.3.2.2 Droplet velocity

Usually the droplet velocity is computed using an explicit numerical scheme [81]. In the present work, an implicit scheme is adapted for the calculation of droplet velocity [167]. The direction of the acceleration of gravity is taken as the positive x-axis. The droplet

velocity in the z-direction is assumed to be zero without the loss of generality, since the geometrical configuration is axisymmetric. At time $t = t_0$, the droplet velocities in the axial and radial directions are

$$v_x = v_{x0},\ v_r = v_{r0}. \tag{3.67}$$

Two positive constants are introduced and defined as

$$C = \frac{3}{8}\frac{\bar{\rho}}{\rho_l}\frac{C_d}{r_d},$$

$$a = \sqrt{\frac{g}{C}},$$

where r_d is the droplet radius. Using these constants, Eq. (2.109) along the x-axis (parallel to the direction of gravity) can be written as

$$\frac{\mathrm{d}v_x}{dt} = -C|v_x - u_x|(v_x - u_x) + Ca^2. \tag{3.68}$$

There are two possible cases. First, the drag force is in the same direction as the acceleration of gravity. In this case, the droplet velocity must be smaller than the gas velocity i.e., $v_{p,x} < u_x$ so Eq. (3.68) turns to be

$$\frac{\mathrm{d}v_x}{\mathrm{d}t} = C(v_x - u_x)^2 + Ca^2. \tag{3.69}$$

Integrating the above equation, the droplet velocity at the time $t = t_0 + \Delta t$ can be determined by the help of initial condition:

$$v_x = u_x + a \cdot \tan\left(\arctan\left(\frac{v_{x0} - u_x}{a}\right) + aC\Delta t\right). \tag{3.70}$$

Equations (3.69) and (3.70) hold only when $v_x < u_x$. Therefore, Δt should be smaller than the time required by the droplet velocity come in equilibrium with gas velocity i.e., t_l

$$t_l = -\frac{1}{aC}\arctan\left(\frac{v_{p,x0} - u_x}{a}\right). \tag{3.71}$$

When $t = t_0 + t_l$, the droplet velocity equals to the gas velocity i.e., $v_x = u_x$, and therefore the drag force is zero. Because of gravitational force, the droplet velocity would keep increasing, which leads to the second case. In this case, the drag force is in the opposite direction of the acceleration of gravity ($v_{x0} > u_x$). Eq. (3.68) takes the form

$$\frac{\mathrm{d}v_x}{\mathrm{d}t} = -C(v_x - u_x)^2 + Ca^2. \tag{3.72}$$

Integrating the above equation, the droplet velocity at the time $t = t_0 + \Delta t$ can be evaluated from the initial condition:

$$v_x = u_x + a + \frac{2a}{\frac{v_{x0} - u_x + a}{v_{x0} - u_x - a}\exp(2aC\Delta t) - 1}. \tag{3.73}$$

When $\Delta t \to \infty$, the droplet velocity v_x approaches to $u_x + a$. When $v_x = u_x + a$, the gravitational force is balanced by the drag force. The expression $v_x - u_x - a$ would keep the same sign during the whole procedure i.e.

$$(v_x - u_x - a)(v_{x0} - u_x - a) \geq 0. \tag{3.74}$$

In the radial direction (perpendicular to the direction of gravity), the Eq. (2.109) can be written as

$$\frac{\mathrm{d}v_r}{\mathrm{d}t} = -C|v_r - u_r|(v_r - u_r). \tag{3.75}$$

Integrating the above equation, the droplet velocity at the time $t = t_0 + \Delta t$ can be determined from the initial condition:

$$v_r = \frac{v_{r0} + C\Delta t|v_{r0} - u_r|u_r}{1 + C\Delta t|v_{r0} - u_r|}. \tag{3.76}$$

When $\Delta t \to \infty$, the droplet velocity v_r approaches to the gas velocity u_r. The direction of the drag force will not change in this case, too. The expression $v_r - u_r$ will be positive during the whole procedure i.e.

$$(v_r - u_r)(v_{r0} - u_r) \geq 0. \tag{3.77}$$

The scheme was tested for different cases in [167] and found to be accurate and robust, where the errors induced by the time integration are minimized.

4. Results and Discussion

Two different test cases have been investigated in the present work. At first, an evaporating water/air spray in steady axisymmetric configuration was simulated through DDM and DQMOM. Secondly, a methanol/air turbulent diffusion flame was simulated using presumed and transported PDF methods. In this chapter, the results from these studies are presented and discussed.

4.1 Evaporating Water/Air Spray

Evaporating sprays are of special interest as those occur not only in many industrial applications but also constitute the defining physical phenomena in spray combustion and spray drying processes. Therefore, having models validated for evaporating sprays motivate their application in simulations of spray drying and spray combustion processes. A water spray injected through a hollow cone Delavan SDX-90 nozzle in a vertical spray chamber and carried by air was modeled by DDM and DQMOM. The starting data for the simulations were taken from experimental data, where the experiments were conducted by the group of Prof. G. Brenn at TU Graz, Austria. The experimental facility is explained in the next section. The generation of initial data is discussed in the following section. The results are from DQMOM and DDM are compared with experiment [13, 171] and discussed.

4.1.1 Experimental setup

A series of experiments had been carried out at TU Graz by the group of Prof. G. Brenn. A water spray in air was studied for different liquid mass inflow rates with different liquid densities. Various atomizers with different dimensions of swirl chambers and exit diameters were used. The droplet sizes and velocities were recorded at various cross sections for different liquid inflow rates using phase Doppler anemometry (PDA) [170]. The present simulations concern the experimental data generated using the Delavan nozzle SDX-SD-90 with an internal diameter of 0.002 m and an outer diameter of 0.012 m at the nozzle throat and 0.016 m at the top for liquid inflow rates of 80 kg/h and 120 kg/h. A water spray was injected into a cylindrical spray chamber of diameter 1 m. The carrier gas was air at room temperature and atmospheric pressure. Measurements

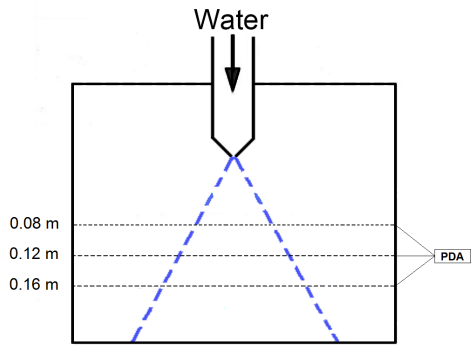

Fig. 4.1: Schematic of experimental setup

were recorded at cross sections of 0.08 m, 0.12 m and 0.16 m. Figure 4.1 illustrates the schematic of the experimental setup. The data at 0.08 m were taken as starting point for initial data generation for computations, and results were compared at later cross sections.

4.1.2 Initial data generation

The experimental data at the closest position to the nozzle is used to generate initial data for the numerical computations. The nearest experimental position is 0.08 m from

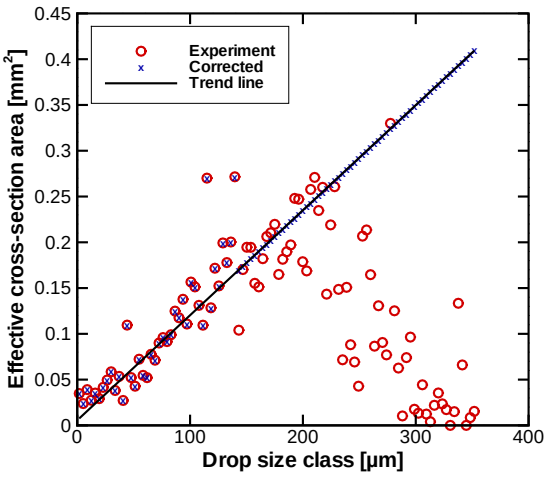

Fig. 4.2: Profile of effective cross-section area of the probe volume for measured droplet size.

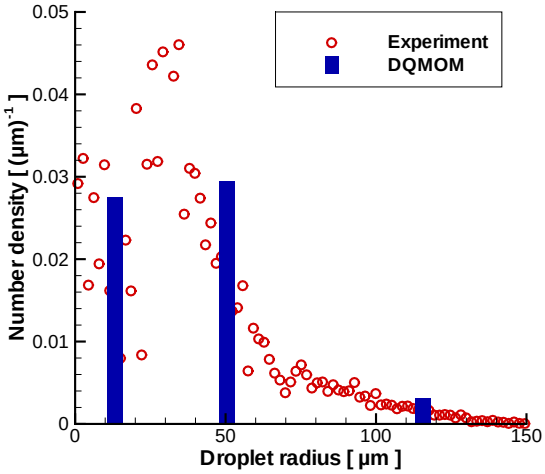

Fig. 4.3: Experimental and DQMOM approximation of droplet number density for a water spray.

nozzle,where the measurements are available at radial positions separated by 1.5 $10^{-}3$ m distance. The PDA data at every radial position consists of droplet radius, velocities in axial and radial directions and the time elapsed for each measurement, which gives the total time carried out over a period. These data is grouped into 100 droplet size classes. The effective cross-sectional area of the probe volume is computed. The result of the calculation for a water flow rate of 80 kg/h, at a position of 0.066 m from the center is shown in Fig. 4.2. The trajectory length exhibits strong fluctuations, which increase with the droplet size. Furthermore, the number of droplets in the size classes for the larger diameters is typically much lower than in the smaller size classes. Therefore, the properties such as droplet trajectory lengths through the probe volume are statistically unreliable for drops with sizes greater than a certain threshold value [173]. In particular, the decrease of the effective probe volume size with increasing drop size such as from 200 µm as shown in Fig. 4.2 is unphysical. The effective cross-section area is therefore calculated using a linear trend line from a threshold diameter. In the first step, the linear trend line is calculated using a linear regression scheme based on the data in the drop size classes up to 60% of the maximum droplet size.

In the second step, for all drop size classes from 40% of the maximum drop size class for this experimental position on, the values of the effective cross section area are obtained as values of the linear trend line. There is, therefore, an overlap of the size class ranges used for computing the trend line and those whose probe volume cross-section areas are calculated using the trend line. Once the effective cross-sectional area probe volume is corrected, the number density is corrected correspondingly. Then, the

moment sets of droplet size and velocities are computed, which in turn are used to calculate the initial weights (number densities), radii and velocities using a product - difference algorithm [172]. In the present study, DQMOM approximates the spray distribution by three-node closure, which implies that the required number of moments is 12 (3 each: weights, droplet radii, axial velocities, radial velocities). The same procedure is followed at every radial position for the cross-section of 0.08 m. Figure 4.3 shows the experimental distribution of droplets and DQMOM approximation at 0.066 m from the center of the spray for 80 kg/h water flow rate. The problem of negative moments is handled by employing the adaptive Wheeler algorithm wherever necessary [177]. The experimental data are also used to generate a system of parcels for DDM, where the properties of k^{th} parcel are denoted by (x_k, r_k, u_k, m_k). The liquid mass of kth parcel is computed considering the spherical symmetry of the droplets, i.e.

$$m_k = \sum_i \frac{4}{3}\rho_l \pi r_i^3, \tag{4.1}$$

where subscript i refers to the number of droplets in the parcel.

4.1.3 Results

Droplet properties including size and velocity are computed using both models and compared with the experiment at the cross sections of 0.12 m and 0.16 m away from

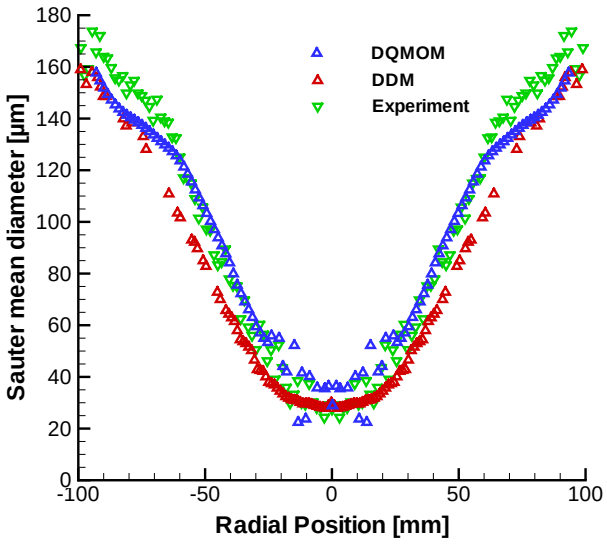

Fig. 4.4: Experimental and numerical profiles of the Sauter mean diameter at the cross section of 0.12 m distance from the nozzle exit for 80 kg/h.

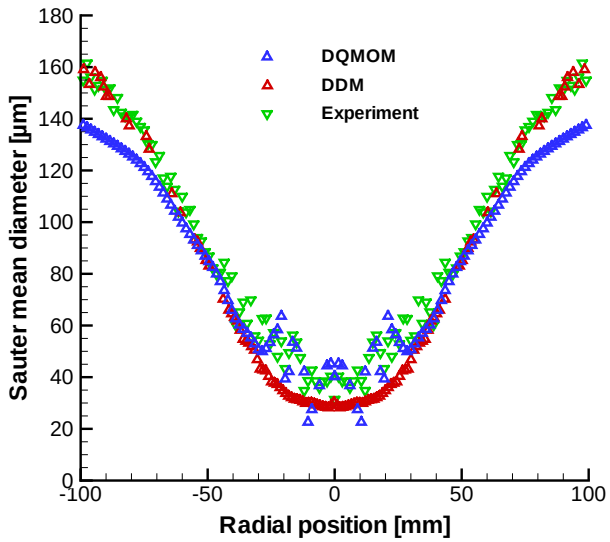

Fig. 4.5: Experimental and numerical profiles of the Sauter mean diameter at the cross section of 0.16 m distance from the nozzle exit for 80 kg/h.

nozzle exit. Figures 4.4 and 4.5 show the computed and experimental profiles of the Sauter mean diameter at cross sections 0.12 m and 0.16 m away from nozzle exit for 80 kg/h. The DDM simulation result matches quite well the experiment at the center of the spray at 0.12 m away from nozzle exit, but slightly under-predicts towards the periphery of the spray. A good agreement is observed at 0.16 m cross section between DDM and experiment. The DQMOM simulation results are in good agreement with experiment at 0.12 m downstream the nozzle exit, and it is closer to the experimental data at higher radial distance. Further downstream, at 0.16 m from the nozzle exit, the DQMOM simulations reveal some scattering near the centerline, and at higher radial distances, they under-predict the experimental results. This discrepancy may result from the numerical scheme which employs an explicit finite difference method to solve the transport equations of DQMOM; the results can be improved by implementing an implicit method. The post processing of experimental data may be the reason of the deviation, too.

For a liquid inflow rate of 120 kg/h, the computed and experimental profiles of Sauter mean diameter at cross sections of 0.12 m and 0.16 m away from nozzle exit are shown in Figs. 4.6 and 4.7. At the cross section of 0.12 m, it can be seen that DQMOM improves the DDM results as DDM over predicts the experimental values. The scattering behavior of simulation results near the centerline is observed in this case too. As the droplets move to the next cross section, a decrease in large size droplets

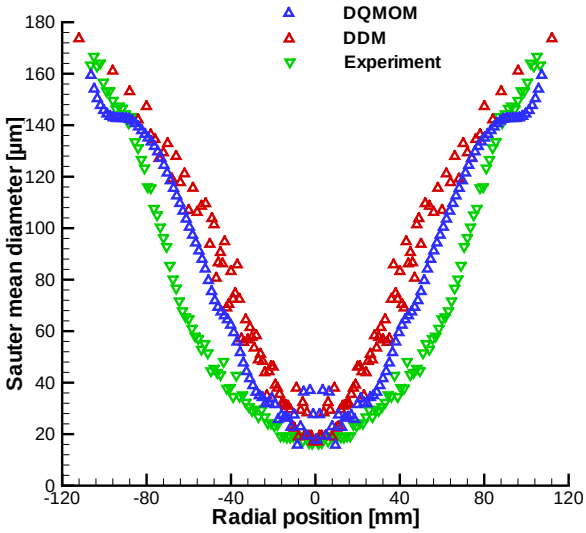

Fig. 4.6: Experimental and numerical profiles of the Sauter mean diameter at the cross section of 0.12 m distance from the nozzle exit for 120 kg/h.

is evident, which is predicted by both DQMOM and DDM. The results show that DQMOM shows better agreement with experiment, while DDM predicts a somewhat

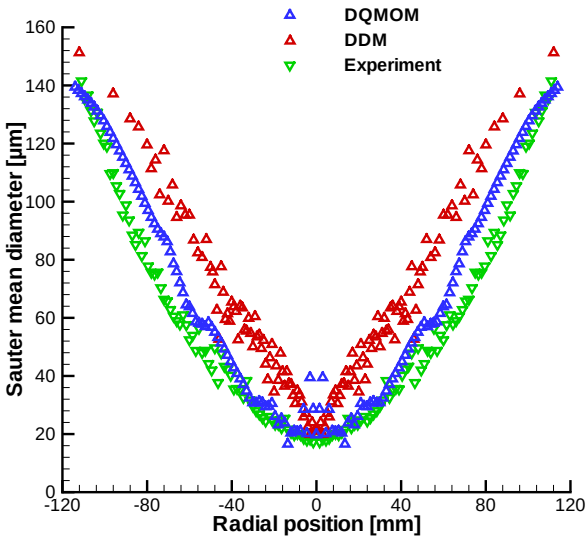

Fig. 4.7: Experimental and numerical profiles of the Sauter mean diameter at the cross section of 0.16 m distance from the nozzle exit for 120 kg/h.

higher values than experiment at corresponding radial positions.

The overall shape of a hollow cone spray is captured quite nicely by both methods, although some deviations are observed in particular in DQMOM as compared to experimental profile, possibly due to the post-processing of the experimental data in order to correct the number frequency at every measuring position to rule out the fluctuations in the effective cross section area of the measuring volume for the larger droplet sizes [173]. This correction of experimental data is position dependent, whereas the DQMOM and DDM results account for these corrections for the initial condition but not at positions further downstream. Another reason for the discrepancies in the DQMOM results may be the fact that the spray equations are not yet fully coupled to the gas phase.

Comparing the maximum values of the Sauter mean diameter at the two cross sections displayed in Figs. 4.4, 4.5, 4.6 and 4.7, a decrease in large size droplets is observed as the droplets move away from nozzle. Even though the process of evaporation is considered in the present models, the major reason for the decrease in droplet size may be attributed to the influence of drag force applied by the surrounding gas, because significant evaporation may not occur at the present room temperature condition. This decrease is more evident in the large droplet size region, where the dynamic interaction of droplet with surrounding gas dominates as observed in profiles of mean droplet velocity (see Figs. 4.12 and 4.13).

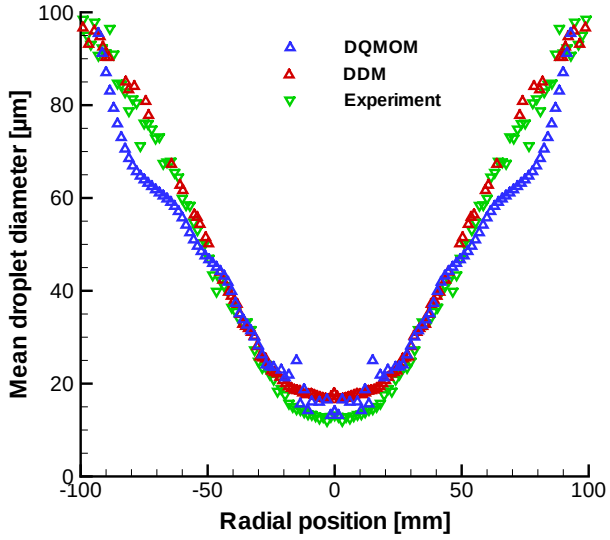

Fig. 4.8: Experimental and numerical profiles of the mean droplet diameter at the cross section of 0.12 m distance from the nozzle exit for 80 kg/h.

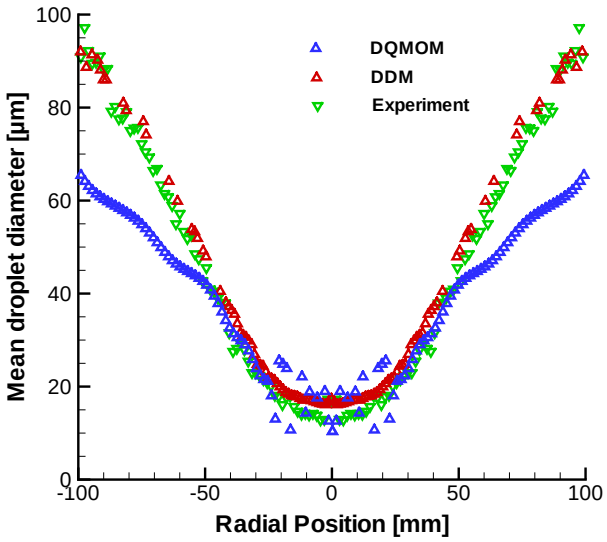

Fig. 4.9: Experimental and numerical profiles of the mean droplet diameter at the cross section of 0.16 m distance from the nozzle exit for 80 kg/h.

Besides the Sauter mean radius, in many technical applications such as particle size analysis in powder sampling or pharmaceutical industries, the mean droplet diameter is an important physical quantity. Radial profiles of the mean droplet diameter are shown and compared with experiment in Figs. 4.8 and 4.9 for 80 kg/h. DDM results are in very good agreement with the experiment. A slight decrease in the mean droplet diameter is observed as the droplets move away from nozzle indicating some mass transfer from liquid to gas, which is attributable to gas - liquid interactions. The DQMOM results are in very good agreement with experiment at the cross section of 0.12 m near the centerline, and there, they improve the DDM results. At 75 mm radial position, the DQMOM results are below experimental values, which may stem from the explicit finite difference technique. At the cross section of 0.16 m, a good agreement is observed between DQMOM and experiment near the axis of symmetry, even though some scattering is obtained.

In Figs. 4.8 and 4.9 Deviations from experiment occur in the large droplet size region, which is due to the fact that the numerical technique captures the distribution function globally, and some local discrepancies may be observed. This may be improved by solving the gas phase equations for DQMOM, which is not done in the present study, where the inlet gas flow properties are used to calculate the source terms for transport equations for DQMOM [13].

Figures 4.10 and 4.11 show the computed and experimental profiles of mean droplet

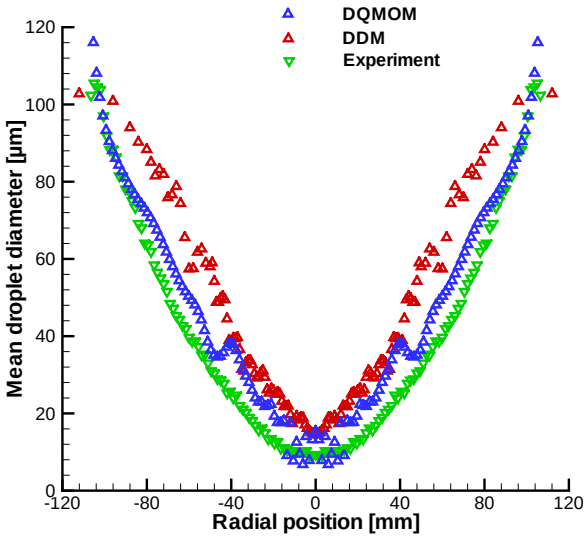

Fig. 4.10: Experimental and numerical profiles of the mean droplet diameter at the cross section of 0.12 m distance from the nozzle exit for 120 kg/h.

diameter at cross sections of 0.12 and 0.16 m away from nozzle exit for liquid inflow rate of 120 kg/h. At 0.12 m away from nozzle exit, both DDM and DQMOM agree

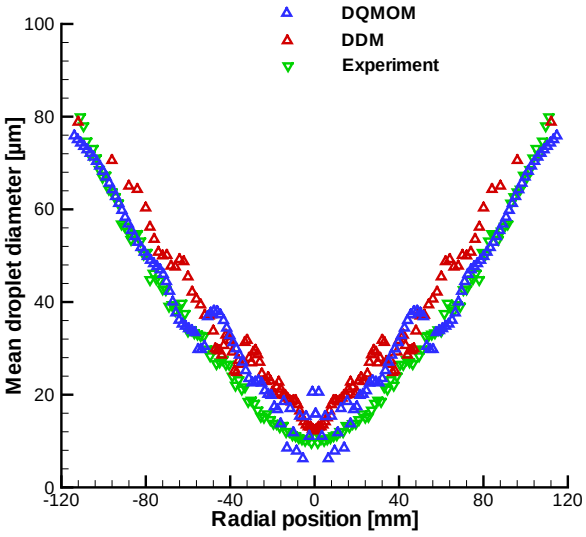

Fig. 4.11: Experimental and numerical profiles of the mean droplet diameter at the cross section of 0.16 m distance from the nozzle exit for 120 kg/h.

well with each other near the centerline, where they show somewhat higher values than the experiment. At the radial positions away from the centerline, DQMOM is in good agreement with experiment, and it improves the DDM results. As the droplets move away from nozzle exit, a decrease in size can be observed at the cross section of 0.16 m away from nozzle exit, which is similar to the case of liquid flow rate of 80 kg/h. Near the centerline at 0.16 m away from nozzle exit, both DQMOM and DDM show the same behavior and predict slightly higher values than experiment. At higher radial positions, DDM values are a little high as compared to DQMOM and experiment, where DQMOM coincides with experimental data.

In Figs. 4.12 and 4.13, the radial profiles of mean droplet velocity are displayed. It can be seen that the droplet velocity is higher for larger droplets as anticipated. Interestingly, the small size droplets near to the axis of symmetry also move at a higher velocity as observed in the experiment and thus making the velocity profile bimodal, which is predicted quite nicely by both models. A closer look reveals that the width of the jet is captured by the DQMOM, whereas the DDM predicts somewhat broader profiles with a lower maximum value at the centerline. At the spray edge, a judgement of the numerical methods is difficult, since the experimental data are somewhat spread in the case of the smaller distance from the nozzle exit. At 0.16 m, the slopes of the numerical results deviate from the experimental data, which show the highest error in experimental data processing [173]. Comparing the velocity profiles at the two different

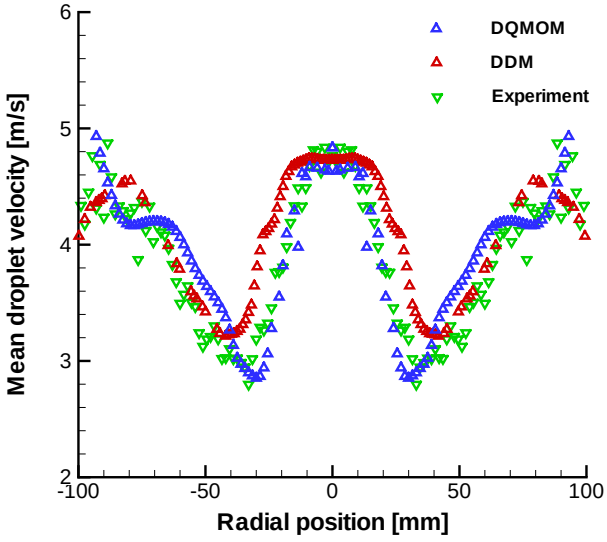

Fig. 4.12: Experimental and numerical profiles of the mean droplet velocity at the cross section of 0.12 m distance from the nozzle exit.

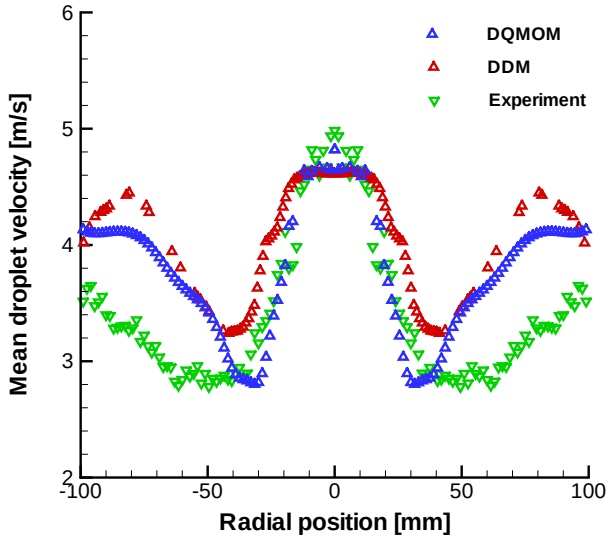

Fig. 4.13: Experimental and numerical profiles of the mean droplet velocity at the cross section of 0.16 m distance from the nozzle exit.

cross sections, it is seen that the velocity decreases as droplets move away from nozzle. This is because the droplets are strongly decelerated by the dynamic interaction with the surrounding gas. The gas around the spray stagnates and is driven into motion only due to the spray entrainment. The gas motion driven by the spray arises at the expense that the droplet loses momentum.

The droplet properties are predicted quite well by the present simulations, which confirms their applicability for spray flows. There are some deviations between simulation and experimental results, which are attributable to the post processing of the experimental data as discussed before. In case of DDM, neglecting droplet interactions may need reconsideration. For DQMOM, the improved numerical scheme and the simultaneous solution of the gas phase equations may improve the simulation results. For DQMOM,

4.2 Methanol/Air Spray Flame

A turbulent methanol/air diffusion spray flame is modeled using transported PDF method and the results are compared with presumed PDF approach and experiment. In transported PDF method, a joint mixture fraction-enthalpy PDF [68] is used and its transport equation is derived. An extended IEM and an extended modified Curl's model are proposed as described in section 2.2.2.2. A detailed methanol/air combustion

mechanism is implemented through a spray flamelet model [65]. The mechanism [83] consists of 23 species and 168 elementary reactions. The spray flamelet library is pre-calculated from laminar counterflow spray flame. The library [65] consists of the data with two different initial droplet radii of 25 µm and 10 µm, and one equivalence ratio $E_r = 3$, one initial spray velocity $v_0 = 0.44$ m/s. The species concentrations of a gas particle are determined from the spray flamelet library. The droplet size is determined by interpolating the local Sauter mean radius at the nodes into the gas particle's position. The instantaneous dissipation rate of the gas particle, χ^*, is described using a log-normal distribution. The parameter $\mu_{\log}$ in the log-normal distribution (c.f. Eq. (2.63)) is calculated from the mean of the dissipation rate, which is computed from the local variance of the mixture fraction. The properties of the gas particle, ξ^*, χ^*, r^*, E_{l0} and v_0, are computed by interpolating the data from the spray flamelet library. The temperature of the gas particle is computed from the composition

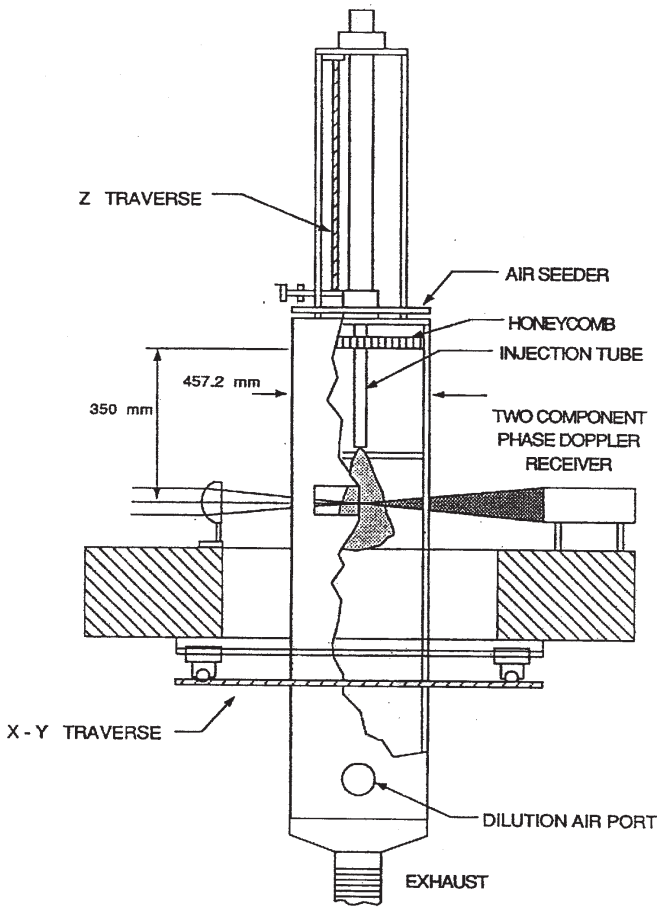

Fig. 4.14: Schematic of the methanol/air experimental setup.

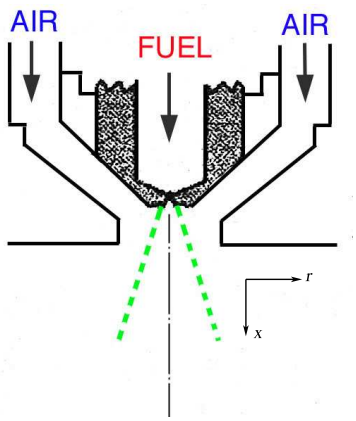

Fig. 4.15: Sketch of the fuel injector.

properties and the enthalpy h_s^*.

4.2.1 Experimental Setup

The experiments were carried out by McDonell and Samuelsen [174,175], where a dilute methanol spray is injected into a turbulent air flow. Figure 4.14 illustrates the overall geometry of the methanol/air spray burner [175]. Inlet mass flow rate of the liquid fuel is 1.32 g/s whereas the air flow results in a pressure drop of 3.73 kPa. Figure 4.15 shows the sketch of the fuel injector [175]. The gas and droplet velocities, droplet size distribution, liquid flux, gas temperature and concentration of methanol vapor are measured at the cross sections of 7.5 mm, 25 mm, 50 mm, 100 mm, and 150 mm away from the nozzle exit. The gas velocity, droplet velocity and droplet size are measured using phase Doppler interferometry (PDI). The concentration of the methanol vapor is measured using infrared extinction/scattering (IRES). The experimental data at the cross section of 7.5 mm away from the nozzle exit are taken as the inlet profiles for numerical computations. The results are compared at the cross sections further down stream.

4.2.2 Results

In the PDF simulation, the Dirac delta profile is prescribed for the particles' mixture fraction at the inlet. Liu's [165] study of numerical accuracy in transported PDF methods shows that the number of particle per cell, *Npc*, should not be smaller than 50 to keep the bias error below 5% . In the present transported PDF method, *Npc* is set to 80, so that the bias error is kept below 4%. In the present work, the simulation results of transported PDF method obtained using modified Curl's mixing model are compared with IEM model as well as presumed standard β function.

Calculations of the spray and gas flow are sensitive to the initial conditions. In the present work, the inlet for computation locates near the nozzle ($x = 0.0075$ m), where the flow structure is very complex. Little disturbance of the initial conditions in spray or gas flow may result in a quite different field. The interaction between spray and gas flow is very strong. The coarse measurements of the droplet size distribution at the inlet profile cause uncertainties in the results of spray and consequently in the results of gas flow.

To assure the precision of numerical scheme, the computed profiles of axial gas velocity are compared with experiment. Figure 4.16 shows the computed and experimental profiles of axial gas velocity at the cross section of 0.025 m. The modified Curl's result is shown in blue solid line, IEM result is shown using a dash dot red line and standard β distribution result is shown using a black dashed line. The experimental

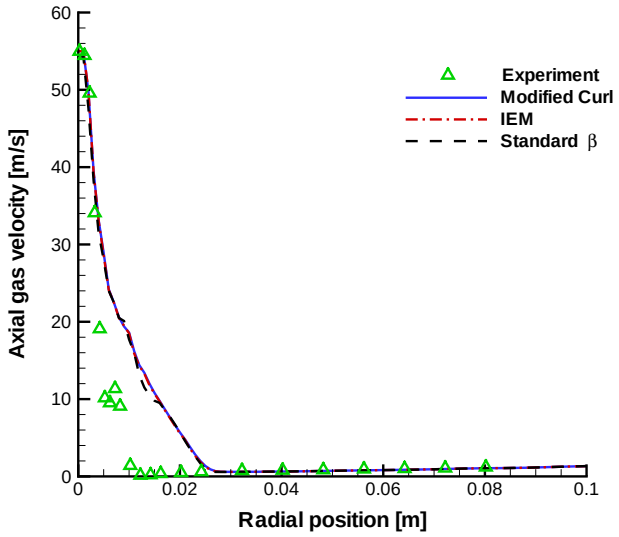

Fig. 4.16: Experimental and numerical profiles of the axial gas velocity at the cross section of 0.025 m distance from the nozzle exit.

values are shown using green symbols. It can be seen that the velocity is quite high at the centerline whereas it monotonically decreases towards the farther radial positions. This trend is captured quite well by the simulation results although deviations can be

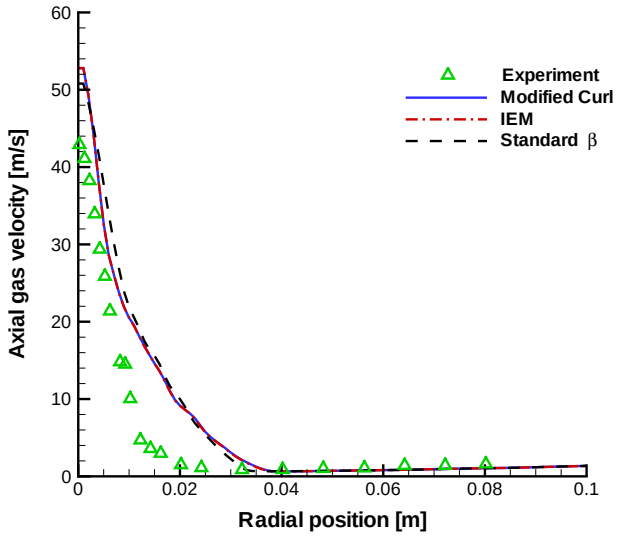

Fig. 4.17: Experimental and numerical profiles of the axial gas velocity at the cross section of 0.05 m distance from the nozzle exit.

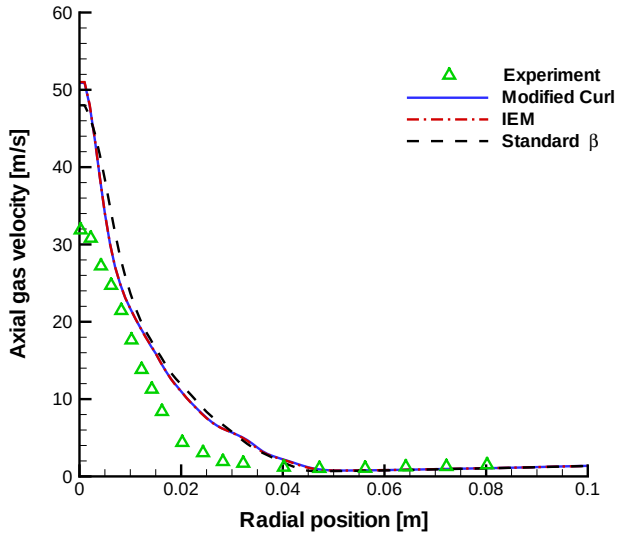

Fig. 4.18: Experimental and numerical profiles of the axial gas velocity at the cross section of 0.075 m distance from the nozzle exit.

observed between simulation and experimental results between the radial positions of 0.005 m and 002 m. This might have resulted from coarse experimental measurements at the cross section of 0.0075 m, which is used to generate the starting data of the simulations.

The gas velocity at the cross sections of 0.050 m, 0.075 m, 0.1 m and 0.15 m away from nozzle exit is shown in the Figs. 4.17 – 4.20. The profiles exhibit the monotonically decreasing behavior in increasing radial direction with their maximum at the centerline. This trend is predicted quite well in the simulation results. In Figs. 4.17– 4.19, it can be seen that the simulation results are somewhat higher at the centerline as compared to experimental value. This might have resulted from the first order truncation error caused by the applied upwind scheme.

Figure 4.20 shows the computed and experimental profiles of axial gas velocity at the cross section of 0.15 m away from the nozzle exit. It can be seen that transported PDF method improves the result of presumed PDF method at the centerline, where presumed PDF result is somewhat higher than experimental value.

The deviations between simulation results and the experiment are attributed to the first order truncation caused by the applied numerical scheme. The stability issues in solution of the momentum equation have brought the staggered grid and the upwind interpolation scheme into play. An alternative can be to use a trivariate joint transported PDF of gas velocity, enthalpy and mixture fraction. This will imply the gas velocity to be computed by applying a physical model. In this thesis, a trivariate joint PDF of

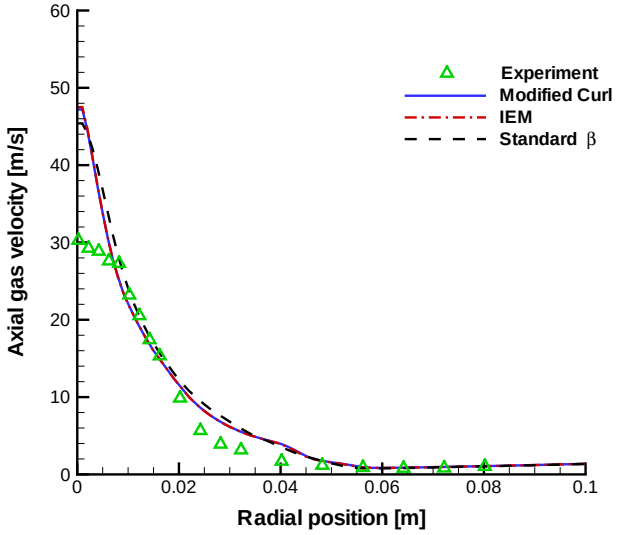

Fig. 4.19: Experimental and numerical profiles of the axial gas velocity at the cross section of 0.1 m distance from the nozzle exit.

gas velocity, enthalpy and mixture fraction is proposed and its transported equation is derived (see Appendix), where the gas velocity is modeled using an extended simplified Langevin model [95].

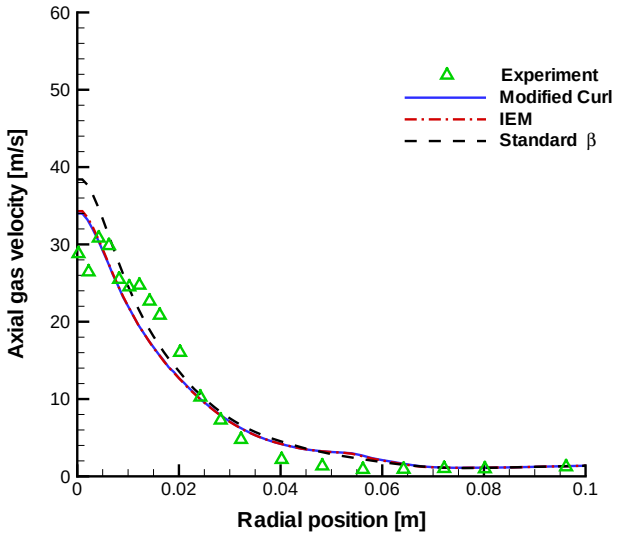

Fig. 4.20: Experimental and numerical profiles of the axial gas velocity at the cross section of 0.15 m distance from the nozzle exit.

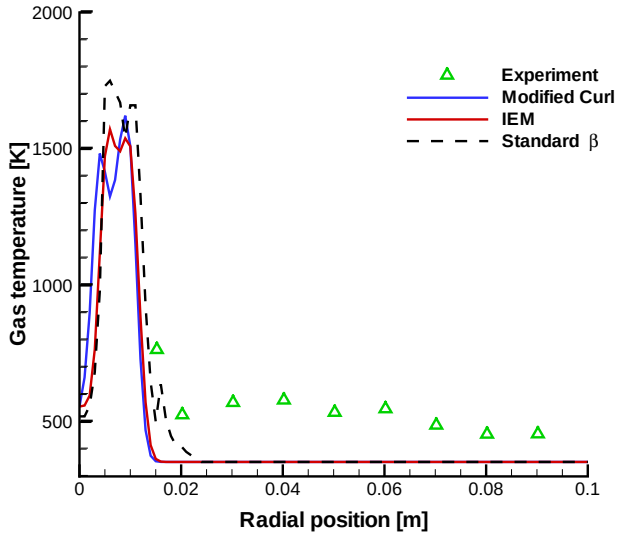

Fig. 4.21: Experimental and numerical profiles of the gas temperature at the cross section of 0.025 m distance from the nozzle exit.

Figures 4.21 – 4.25 show the profiles of gas temperature at cross sections of 0.025, 0.05, 0.075, 0.1 and 0.15 m away from the nozzle exit. The results from modified Curl's model are shown using blue lines where as the results from IEM and standard β function

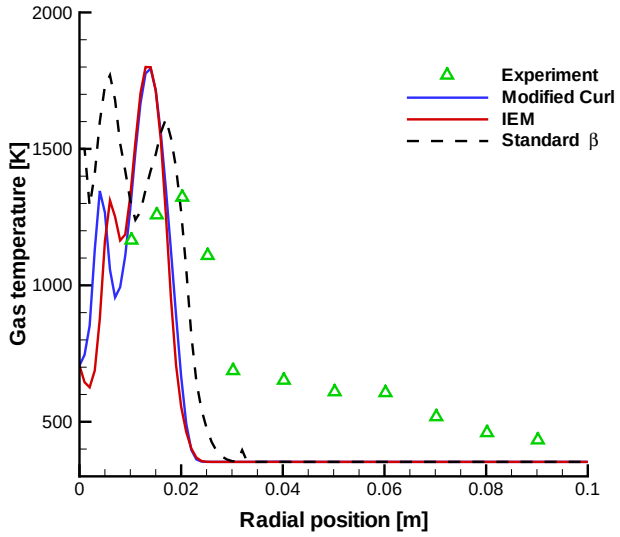

Fig. 4.22: Experimental and numerical profiles of the gas temperature at the cross section of 0.05 m distance from the nozzle exit.

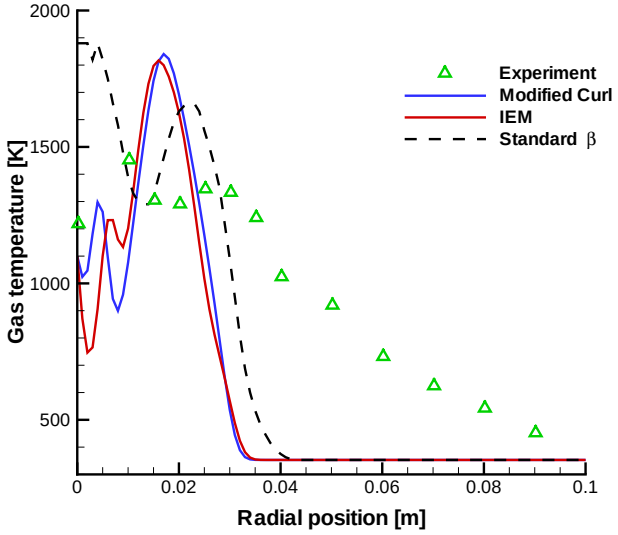

Fig. 4.23: Experimental and numerical profiles of the gas temperature at the cross section of 0.075 m distance from the nozzle exit.

are shown using red lines and black dashed lines, respectively. The symbols denote the experimental data. It can be seen in Fig. 4.21 that the experimental values are not available near the center line, which makes the comparison of the models somewhat difficult. Although standard β function seems to be slightly closer to experimental data as compared to transported PDF's at the radial positions of 0.015 and 0.02 m, the uncertainty at the center line might be a reason of the deviation between simulation and experimental results. The experimental uncertainty is observed at the cross section of 0.05 m away from nozzle exit shown in Fig. 4.22, where the experimental data is not available at the centerline.

Figure 4.23 shows the temperature profiles at the cross section of 75 mm away from nozzle exit. It can be seen that standard β distribution over-predicts the temperature at centerline, where transported PDF performs better. Modified Curl slightly improves the results of IEM in the region between the radial positions of 0.01 and 0.03 m away from centerline.

In Fig. 4.24 the results from IEM and standard β distribution over-predict the experimental value at centerline while the result form modified Curl's model is closer to experimental value at the cross section of 0.1 m. At the cross sections of 0.1 and 0.15 m away from nozzle exit, the profiles obtained using the modified Curl's model improve the IEM and standard β distribution between about 0.02 and 0.05 m from the centerline as shown in Figs. 4.24 and 4.25.

Although the simulation results are in the same data range as of experimental

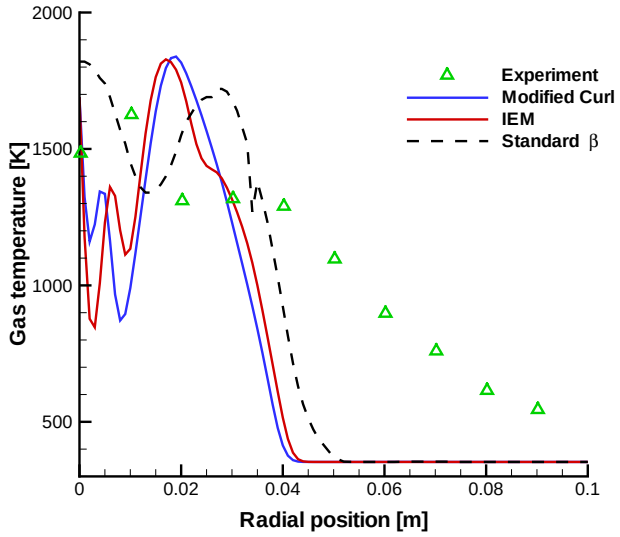

Fig. 4.24: Experimental and numerical profiles of the gas temperature at the cross section of 0.1 m distance from the nozzle exit.

values, and they capture the trend of experimental profiles, the obvious discrepancies are observed. These discrepancies may be due to the inappropriate initial distribution of the liquid flux, which is caused by experimental uncertainties. Also, the experimental

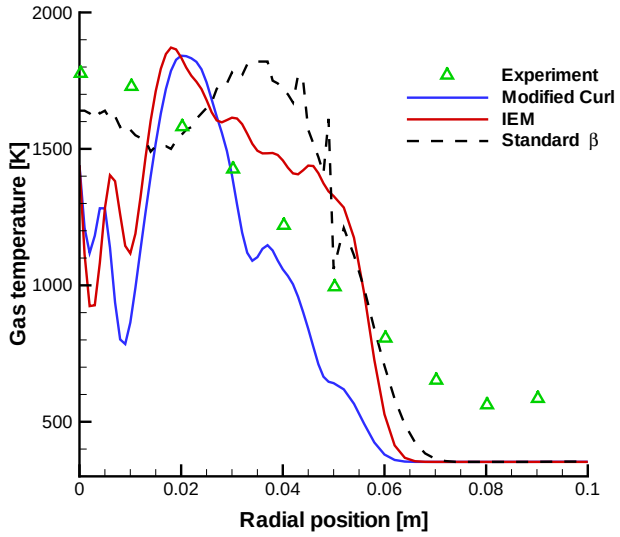

Fig. 4.25: Experimental and numerical profiles of the gas temperature at the cross section of 0.15 m distance from the nozzle exit.

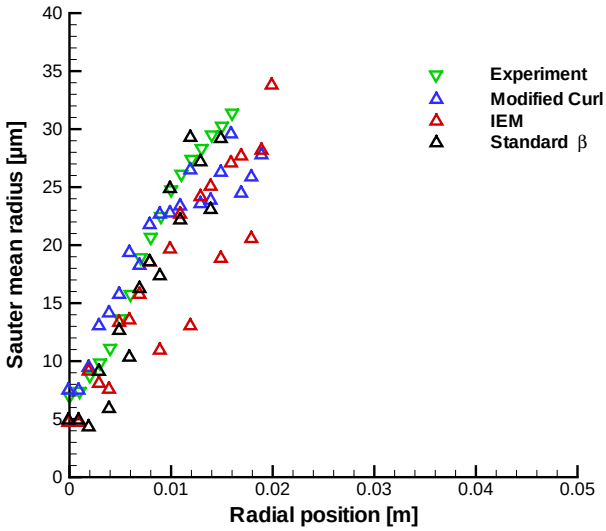

Fig. 4.26: Experimental and numerical profiles of Sauter mean radius at the cross section of 0.025 m distance from the nozzle exit.

measurements of temperature are not available near the center line at the cross sections nearer to the nozzle exit. The improved experimental data would help. Furthermore, the computed profiles of gas temperature are quite fluctuating. As described earlier, laminar flamelet library is used in the present work, where two different initial droplet radius, $r_0 = 25$ µm and 10 µm are considered.

When the local Sauter mean radius is larger than 10 µm, the library with $r_0 = 25$ µm is used. When the local Sauter mean radius is smaller than 10 µm and larger than 1 µm, the library with $r_0 = 10$ µm is used. Therefore, the droplet properties are very important in describing the spray flames. Figure 4.26 shows the computed and experimental values of Sauter mean radius at the cross section of 0.025 m away from nozzle exit. The results from modified Curl's model, IEM and standard β distribution are shown using blue, red and black triangles pointing up while the experimental values are shown using green downward pointing triangles. It can be seen that the modified Curl's model improves the results of IEM and standard β distribution. As it can be seen in Figs. 4.21 – 4.25, the fluctuations in the results of both of transported PDF methods and moment closure method occur in the region near the centerline, where the Sauter mean radius is less than 25 µm. An improvement in spray flamelet library with more initial droplet radii will help improving the results.

In the transported PDF and presumed PDF methods, the major difference is about statistical description of fluctuations in mixture fraction space. In the present work, a standard β distribution is applied as presumed PDF. In Fig. 4.27, the shapes of

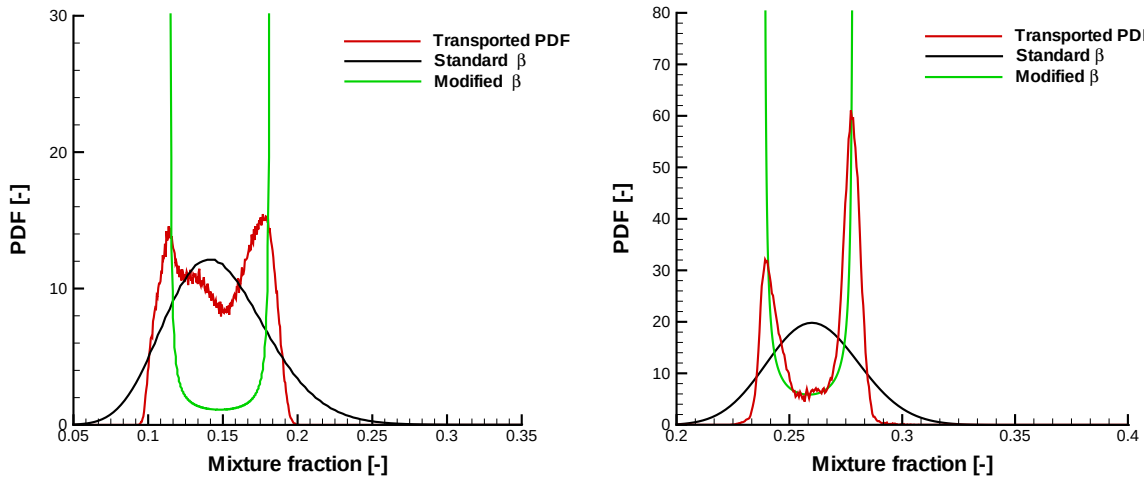

Fig. 4.27: Transported and presumed PDF shapes at axial location of 0.025 m and radial location of 0.01 m (left) as well as at axial location of 0.05 m and radial location of 0.01 m (right).

transported and presumed PDFs at axial location of 0.025 m and radial location of 0.01 m (left) as well as at axial location of 0.05 m and radial location of 0.01 m (right) are shown. For modified β distribution, the additional parameters are chosen

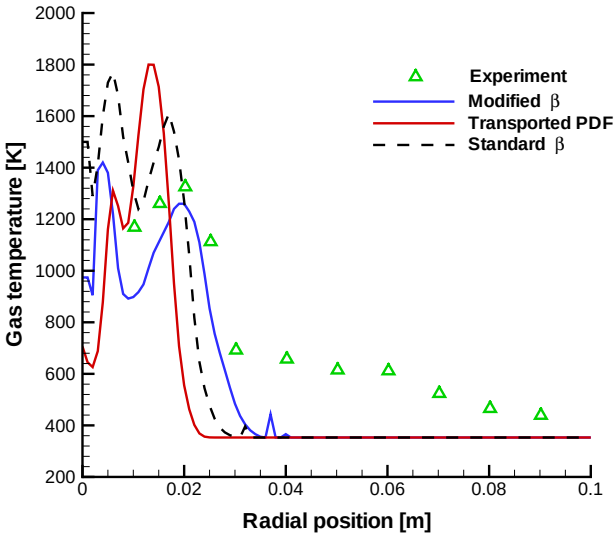

Fig. 4.28: Comparison of modified β with standard β and transported PDF methods for gas temperature at the cross section of 0.05 m distance from the nozzle exit.

to be $\xi_{\max} = \tilde{\xi} + \sqrt{\widetilde{\xi''^2}}$ and $\xi_{\min} = \tilde{\xi} - \sqrt{\widetilde{\xi''^2}}$. The transported PDF profiles show the bimodal shape, which is not reflected by standard β distribution whereas the modified β distribution captures the bimodal behavior of the PDF. Thus, application of modified β distribution may improve presumed PDF method. The choice of additional parameters, namely $\xi_{\max}$ and $\xi_{\min}$ is still an open question, which needs further investigation.

Figures 4.28 shows a comparison of modified β distribution with standard β distribution and transported PDF method, where the profiles of gas temperature at cross section of 0.05 m are shown. The additional two parameters for modified β distribution are taken to be $\xi_{\max} = \tilde{\xi} + \sqrt{\widetilde{\xi''^2}}$ and $\xi_{\min} = 0$. It can be seen that the modified β distribution improves the results of standard β distribution. Further investigation about the choice of $\xi_{\max}$ and $\xi_{\min}$ may help to form better presumed PDF model.

The simulation results captured the overall trend and data range of experimental profiles, where the results from modified Curl's model improve the results from IEM and presumed PDF method. The deviations are observed, too. For gas velocity, the application of a joint trivariate transported PDF of gas velocity, enthalpy and mixture fraction will bring an interesting comparison of results. The temperature profiles may be smoothed by introducing a spray flamelet library with more droplet radii. The experimental uncertainty near the centerline also need to be treated so that more reliable starting data may be generated.

5. Conclusions and Outlook

In this dissertation, an evaporating water/air spray is modeled using DQMOM and DDM while a methanol/air spray flame is modeled using transported PDF method.

In the case of water/air spray, the mathematical formulation of DQMOM, accounting for droplet size and velocity, is derived, and a numerical solution procedure is developed. For DDM, the gas phase is described by Favre-averaged Navier – Stokes equations considering the droplets as point sources, which are calculated using the PSIC model. Convective droplet heating and evaporation as well as velocity are modeled, and the droplet size and velocity distributions are analyzed with both DDM and DQMOM. Droplet collisions are included in DQMOM by modeling the coalescence. The DDM does not include droplet collisions due to modeling limitations, which include redistribution of droplet classes.

Numerical and experimental results are compared at different cross sections, where the experimental data of the cross section closest to the nozzle exit are used for the generation of initial conditions for the simulations. The results from both DDM and DQMOM are found in good agreement with experiment. Some deviations in case of mean droplet diameter are observed between DQMOM and experiment that might have resulted from the present DQMOM formulation, which is not yet fully coupled with the gas phase equations. Moreover, the numerical technique employed an explicit finite difference method to solve the DQMOM transport equations – an implicit scheme may lead to considerable improvement. Concerning the experimental data, a post-processing of the raw data was performed in order to correct the number frequency of large droplets with respect to the effective cross section area, leading to different correction factors for different droplet positions in experimental data away from the centerline – these different corrections cannot be reflected in the numerical results.

A methanol/air spray flame was modeled using the PDF methods. A transported joint PDF of mixture fraction and enthalpy for turbulent spray flows is adapted. The PDF transport equation is derived. The unclosed term of molecular mixing is described using an extended IEM model, where the standard IEM is extended to account for spray flows. Also, modified Curl's model is extended for spray flows and applied. Detailed chemistry consisting of 23 species and 168 elementary reactions is implemented through a spray flamelet model. The PDF transport equation is closed through coupling with extended $k - \epsilon$ model to account for spray flows. The PDF transport equation is

solved using a hybrid finite volume/Lagrangian Monte-Carlo particle method. The numerical results of gas velocity, gas temperature and Sauter mean radius are compared with experimental data and the results from the moment closure method, which used standard β function as presumed PDF. The numerical results of the PDF method are in good agreement with experimental data and improve the results from the moment closure method.

The choice of optimum physical models to close the PDF transport equation for spray flows is still an open topic of research. For gas flames, modified Curl's model is reported to be an efficient model, but it needs to be validated for spray flows in benchmark cases. Advanced models such as EMST should also be extended for spray flows and tested for application. In the future work, a trivariate joint velocity-enthalpy-mixture fraction PDF coupled with the spray flamelet model will be employed to simulate the turbulent spray flames. The derivation of its transport equation is given in Appendix A.

Appendix

A. Trivariate Transported PDF

A.1 Derivation of PDF transport equation

To describe the form of a PDF transport equation, a fine grained one-point one-time joint gas velocity – enthalpy – mixture fraction PDF $f^*(\mathbf{V}, \zeta, \eta; \mathbf{x}, t)$ is defined for the gas phase of turbulent spray flames as

$$f^*(\mathbf{V}, \zeta, \eta; \mathbf{x}, t) = \delta(\mathbf{u}(\mathbf{x}, t) - \mathbf{V})\delta(\xi - \zeta)\delta(h(x, t) - \eta), \tag{A.1}$$

where $\mathbf{V}$, , ζ and η are the gas velocity, mixture fraction and enthalpy in sample space and $\mathbf{u}$, ξ and h are the gas velocity, mixture fraction and enthalpy in physical space. It is important to note that the aim is to derive a transport equation for non-presumed PDF $f(\mathbf{V}, \zeta, \eta; \mathbf{x}, t)$, which may be related to fine grained PDF $f'(\mathbf{V}, \zeta, \eta; \mathbf{x}, t)$ by using the definition of mean and properties of delta function (fine grained merely means a function that is written as product of delta functions). More precisely, the mean of any function $Q(\mathbf{x}, t)$ is given by

$$\langle Q(\mathbf{x}, t)\rangle = \int\int\int Q(\mathbf{x}, t) f(\mathbf{V}, \zeta, \eta; \mathbf{x}, \mathbf{t}) \mathrm{d}\mathbf{V}\mathrm{d}\zeta\mathrm{d}\eta. \tag{A.2}$$

It is known that delta functions satisfy shifting property i.e.

$$\int\int\int g(\mathbf{x})\delta(\mathbf{x} - \mathbf{y})\mathrm{d}\mathbf{x} = g(\mathbf{y}), \tag{A.3}$$

where $\delta(\mathbf{x} - \mathbf{y}) = \delta(x_1 - y_1)\delta(x_2 - y_2)\delta(x_3 - y_3)$. Replacing $Q(\mathbf{u}(\mathbf{x}, t), \xi_C(\mathbf{x}, t), h(\mathbf{x}, t))$ with $\delta(\mathbf{u}(\mathbf{x}, t) - \mathbf{V})\delta(\xi - \zeta)\delta(h - \eta)$ in Eq. (A.2), the following equation is obtained

$$\langle f^*(\mathbf{V}, \zeta, \eta; \mathbf{x}, t)\rangle = \int\int\int \delta(\mathbf{u}(\mathbf{x}, t) - \mathbf{V})\delta(\xi - \zeta)\delta(h - \eta) f(\mathbf{V}, \zeta, \eta; \mathbf{x}, t)\mathrm{d}\mathbf{V}\mathrm{d}\zeta\mathrm{d}\eta. \tag{A.4}$$

Transforming the integral variables $\mathbf{V} \longrightarrow \mathbf{V}^*$, $\zeta \longrightarrow \zeta^*$ and $\eta \longrightarrow \eta^*$, and replacing $Q(\mathbf{u}(\mathbf{x}, t), \xi(\mathbf{x}, t), h(\mathbf{x}), t)$ with $Q(\mathbf{V}^*, \zeta^*, \eta^*)$ in above equation, the following is yielded

$$\begin{aligned} \langle f^*(\mathbf{V}, \zeta, \eta; \mathbf{x}, t)\rangle &= \int\int\int \delta(\mathbf{V}^* - \mathbf{V})\delta(\zeta^* - \zeta)\delta(\eta^* - \zeta) f(\mathbf{V}^*, \zeta^*, \eta^*; \mathbf{x}, t)\mathrm{d}\mathbf{V}^*\mathrm{d}\zeta^*\mathrm{d}\eta^* \\ &= f(\mathbf{V}, \zeta, \eta; \mathbf{x}, \mathbf{t}). \end{aligned} \tag{A.5}$$

The last step follows from Eq. (A.3). Therefore, the conditional mean may be related to PDF $f(\mathbf{V},\zeta,\eta;\mathbf{x},\mathbf{t})$ as

$$\langle Q(\mathbf{x},t)f^*(\mathbf{V},\zeta,\eta;\mathbf{x},t)\rangle = \langle Q(\mathbf{x},t)|\mathbf{V},\zeta,\eta\rangle f(\mathbf{V},\zeta,\eta;\mathbf{x},t). \tag{A.6}$$

In terms of the properties of the Dirac-delta function, the material derivative of the fine-grained PDF can be written as

$$0 = \frac{\mathrm{D}f^*}{\mathrm{D}t} = \frac{\partial f^*}{\partial t} + \frac{\partial f^*}{\partial \mathbf{x}}\frac{\mathrm{d}\mathbf{x}}{\mathrm{d}t} + \frac{\partial f^*}{\partial \zeta}\frac{\mathrm{d}\zeta}{\mathrm{d}t} + \frac{\partial f^*}{\partial \eta}\frac{\mathrm{d}\eta}{\mathrm{d}t} + \frac{\partial f^*}{\partial \mathbf{V}}\frac{\mathrm{d}\mathbf{V}}{\mathrm{d}t}. \tag{A.7}$$

Using the shifting property of Dirac-delta function, Eq. (A.8) can be written as

$$\begin{aligned}\rho\frac{\partial f^*}{\partial t} + \rho u_j\frac{\partial f^*}{\partial x_j} &= -\rho\frac{\partial f^*}{\partial \zeta}\frac{\mathrm{d}\zeta}{\mathrm{d}t} - \rho\frac{\partial f^*}{\partial \eta}\frac{\mathrm{d}\eta}{\mathrm{d}t} - \rho\frac{\partial f^*}{\partial \mathbf{V}}\frac{\mathrm{d}\mathbf{V}}{\mathrm{d}t} \\ &= -\frac{\partial}{\partial\zeta}(\rho\frac{\mathrm{d}\xi}{\mathrm{d}t}f^*) - \frac{\partial}{\partial\eta}(\rho\frac{\mathrm{d}h}{\mathrm{d}t}f^*) - \frac{\partial}{\partial\mathbf{V}}(\rho\frac{\mathrm{d}\mathbf{u}}{\mathrm{d}t}f^*).\end{aligned} \tag{A.8}$$

Using Eqs. (A.5) and (A.6), in Eq. (A.8), the following can be obtained

$$\rho\frac{\partial f}{\partial t} + \rho u_j\frac{\partial f}{\partial x_j} = -\frac{\partial}{\partial\zeta}(\rho\langle\frac{\mathrm{d}\xi}{\mathrm{d}t}|\mathbf{V},\zeta,\eta\rangle f) - \frac{\partial}{\partial\eta}(\rho\langle\frac{\mathrm{d}h}{\mathrm{d}t}|\mathbf{V},\zeta,\eta\rangle f) - \frac{\partial}{\partial\mathbf{V}}(\rho\langle\frac{\mathrm{d}\mathbf{u}}{\mathrm{d}t}f|\mathbf{V},\zeta,\eta\rangle). \tag{A.9}$$

Substitution of the instantaneous conservation of mass (c.f. Eq. (2.1)) into the above equation and considering the joint mass density function $F(\mathbf{V},\zeta,\eta;\mathbf{x},t) = \rho f(\mathbf{V},\zeta,\eta;\mathbf{x},t)$, the following expression is yielded

$$\begin{aligned}\frac{\partial F}{\partial t} + \frac{\partial(u_jF)}{\partial x_j} - \langle\frac{S_{l,1}}{\rho}|\zeta,\eta\rangle F = &- \frac{\partial}{\partial\zeta}(\langle\frac{\mathrm{d}\xi}{\mathrm{d}t}|\mathbf{V},\zeta,\eta\rangle F) - \frac{\partial}{\partial\eta}(\langle\frac{\mathrm{d}h}{\mathrm{d}t}|\mathbf{V},\zeta,\eta\rangle F) \\ &- \frac{\partial}{\partial\mathbf{V}}(\langle\frac{\mathrm{d}\mathbf{u}}{\mathrm{d}t}|\mathbf{V},\zeta,\eta\rangle F).\end{aligned} \tag{A.10}$$

In the above transport equation of mass density function F, the terms on the right hand side are unclosed, and based on the instantaneous conservation equations for the enthalpy and mixture fraction (c.f. Eqs. (2.2) and (2.10)). These terms can be expanded as following

$$\begin{aligned}- &\frac{\partial}{\partial\zeta}(\langle\frac{\mathrm{d}\xi}{\mathrm{d}t}|\mathbf{V},\zeta,\eta\rangle F) = -\frac{1}{\rho}\langle(1-\xi)S_{l,1}\rangle\frac{\partial F}{\partial\zeta} \\ - &\frac{\partial}{\partial\zeta}(\frac{1}{\rho}\left\langle\frac{\partial}{\partial x_j}\left(\rho D_M\frac{\partial\xi}{\partial x_j}\right) + {S_{l,1}}' + \langle\xi S_v\rangle - \xi S_{l,1}|\mathbf{V},\zeta,\eta\right\rangle F),\end{aligned} \tag{A.11}$$

$$\begin{aligned}- &\frac{\partial}{\partial\eta}(\langle\frac{\mathrm{d}h}{\mathrm{d}t}|/bfV,\zeta,\eta\rangle F) = -\frac{1}{\rho}\langle S_{l,h} - hS_{l,1}\rangle\frac{\partial F}{\partial\eta} \\ - &\frac{\partial}{\partial\eta}(\frac{1}{\rho}\left\langle\frac{\partial}{\partial x_j}\left(\rho D_h\frac{\partial h}{\partial x_j}\right) + {S_{l,h}}' + \langle hS_{l,1}\rangle - hS_{l,1}|\mathbf{V},\zeta,\eta\right\rangle F),\end{aligned} \tag{A.12}$$

and

$$
\begin{aligned}
- \quad & \frac{\partial}{\partial \eta}(\langle \frac{\mathrm{d}\mathbf{u}}{\mathrm{d}t} | \mathbf{V}, \zeta, \eta \rangle F) = -\frac{1}{\rho} \langle S_{l,u_j} - \mathbf{u} S_{l,1} \rangle \frac{\partial F}{\partial \mathbf{V}} \\
- \quad & \frac{\partial}{\partial \mathbf{V}}(\frac{1}{\rho} \left\langle \frac{\partial}{\partial x_j} \left(\rho D_u \frac{\partial \mathbf{u}}{\partial x_j} \right) + S_{l,u_j}{}' + \langle \mathbf{u} S_{l,1} \rangle - \mathbf{u} S_{l,1} | \mathbf{V}, \zeta, \eta \right\rangle F). \qquad \text{(A.13)}
\end{aligned}
$$

Neglecting the fluctuating parts of the source terms i.e. $S_{l,1}{}'$, $S_{l,h}{}'$ and $S_{l,u_i}{}'$, the the modeled joint PDF transport equation is written as

$$
\begin{aligned}
\frac{\partial F}{\partial t} + \frac{\partial (u_j F)}{\partial x_j} - \frac{\langle S_{l,1} \rangle}{\rho} F \quad + \quad & \frac{1}{\rho} \langle (1-\xi) S_{l,1} \rangle \frac{\partial F}{\partial \zeta} + \frac{1}{\rho} \langle S_{l,h} - h S_{l,1} \rangle \frac{\partial F}{\partial \eta} + \frac{1}{\rho} \langle S_{l,u_j} - \mathbf{u} S_{l,1} \rangle \frac{\partial F}{\partial \mathbf{V}} \\
= \quad - \quad & \frac{\partial}{\partial \zeta} \left(\frac{1}{\rho} \left\langle \frac{\partial}{\partial x_j} (\rho D_M \frac{\partial \xi}{\partial x_j}) + S'_\xi | \zeta, \eta \right\rangle F \right) \\
- \quad & \frac{\partial}{\partial \eta} \left(\frac{1}{\rho} \left\langle \frac{\partial}{\partial x_j} (\rho D_h \frac{\partial h}{\partial x_j}) + S'_h | \zeta, \eta \right\rangle F \right) \\
- \quad & \frac{\partial}{\partial \mathbf{V}} (\frac{1}{\rho} \left\langle \frac{\partial}{\partial x_j} \left(\rho D_u \frac{\partial \mathbf{u}}{\partial x_j} \right) + S'_{u_i} | \mathbf{V}, \zeta, \eta \right\rangle F). \qquad \text{(A.14)}
\end{aligned}
$$

In Eq. (A.14), the terms on the right hand side appear in unclosed form. To close the first two terms on the right hand side, the models are discussed in the section 2.2.2.2. For the third term, a velocity model is needed, which is discussed in the next section.

A.2 Velocity model

PDF methods represent the gas flow using stochastic particles, so that it may be treated as a particulate system. To model the velocity in Eq. (A.14), the fluid particle velocity $\mathbf{u}(t)$ is represented by the stochastic particle velocity $\mathbf{u}^*(t)$. In literature, Various models are available to model the evolution of the particles in the velocity sample space [64, 97, 98, 150]. A suitable model to generate the stochastic process of turbulent dispersion is the Langevin equation [150]. The generalized Langevin model [150] can be written as

$$
\mathrm{d}u_i^*(t) = \frac{1}{\rho} \frac{\partial \langle p \rangle}{\partial x_i} dt + G_{ij}(u_j^*(t) - \langle u_j \rangle)\mathrm{d}t + (C_0 \epsilon)^{1/2} \mathrm{d}W_i(t). \qquad \text{(A.15)}
$$

The first term on the right-hand side describes the acceleration due to the mean pressure gradient. The effects of viscous stress tensor and Wiener process are represented in second and third term respectively, where Wiener process represents the effects of fluctuating pressure gradients. $\mathrm{d}W_i(t) = W_i(t + \mathrm{d}t) - W_i(t)$ is a normal distribution with the mean $\langle \mathrm{d}W_i(t) \rangle = 0$ and the variance $\langle \mathrm{d}W_i(t) \mathrm{d}W_j(t) \rangle = \mathrm{d}t \delta_{ij}$ [150]. The coefficient $G_{ij}(\mathbf{x}, t)$ depends on the local spatial and temporal values and is given by

$$
G_{ij} = -\left(\frac{1}{2} + \frac{3}{4} C_0 \right) \frac{\epsilon}{k} \delta_{ij}. \qquad \text{(A.16)}
$$

The above equation forms widely known simplified Langevin model (SLM) [64]. There are other models as well such as isotropization-of-production model, which defines G_{ij} as

$$G_{ij} = -\frac{1}{2}C_R\frac{\epsilon}{k}\delta_{ij} + C_2\frac{\partial\langle u_i\rangle}{\partial x_j}, \tag{A.17}$$

where C_R and C_2 are constants [150]. In simplified Langevin model, the effect of the mean velocity gradient is neglected. The stochastic particle's velocity is modeled by

$$\begin{aligned} \mathrm{d}u_i^*(t) &= \frac{1}{\bar{\rho}}\left(\bar{\rho}g_i - \frac{\partial\bar{p}}{\partial x_i} + \bar{S}_{l,u_i}\right)\mathrm{d}t \\ &- \left(\frac{1}{2} + \frac{3}{4}C_0\right)\frac{\tilde{\epsilon}}{\tilde{k}}\left(u_i^*(t) - \tilde{u}_i\right)\mathrm{d}t + \left(C_0\tilde{\epsilon}\right)^{1/2}\mathrm{d}W_i(t), \end{aligned} \tag{A.18}$$

where $C_0 = 2.1$ is the model constant [64]. The acceleration due to the body force (gravitational force) is included in the first term on right hand side. The second term is for the acceleration due to the mean pressure gradient while the third term is for the spray source respectively. The fourth term is the viscous stress tensor. The last term represents the diffusion process in which $\mathbf{W}(t)$ is a Wiener process.

B. Nomenclature

Symbol	Unit	Description
A	m^2	Surface area of control volume
B_M	-	Spalding mass transfer number
B_T	-	Spalding heat transfer number
C_0	-	Constant in Langevin model
C_{CFL}	-	Constant in Courant–Friedrichs–Lewy condition
C_D	-	Drag coefficient in spray model
C_{pg}	J/(kg K)	Specific heat capacity of gas
C_{pL}	J/(kg K)	Specific heat capacity of liquid
$C_{p\alpha}$	J/(kg K)	Constant-pressure specific heat of species α
C_s	-	Constant in extended $k-\epsilon$ model for spray flows
C_ϕ	-	Constant in IEM model
c_{tr}	-	Constant in spray model
$c_{\epsilon,1}$	-	Constant in $k-\epsilon$ model
$c_{\epsilon,2}$	-	Constant in $k-\epsilon$ model
c_μ	-	Constant in $k-\epsilon$ model
$a_n, b_n, \mathbf{c}_n$		Source terms for DQMOM
D	m^2/s	Diffusion coefficient
$D(x)$		Cumulative distribution function
D_M	m^2/s	Mean diffusion coefficient of mixture
E_r	-	Equivalence ratio in counterflow spray flame
$\mathrm{erfc}(x)$		Error function
$\mathbf{F}$	$\mathrm{m/s}^2$	Drag force per unit mass
$\mathbf{F}$		Vector of convective terms
f		Probability density function
f		Droplet distribution function
G_{ij}		Coefficient in velocity model for trivariate PDF
G_k	$\mathrm{kg/(m\ s}^3)$	Generation term for turbulent kinetic energy
Δh_f^0	J/g	Specific enthalpy of formation

$h_{s,\alpha}$	J/g	Specific sensible enthalpy of species α
h_t	J/g	Specific total non-chemical enthalpy
$h_{t,c}$	J/g	Specific total enthalpy
$\mathbf{J}_q^c$	J/(m^2 s)	Heat flux due to thermal conductivity
$\mathbf{J}_q^d$	J/(m^2 s)	Heat flux due to molecular diffusion
k	m^2/s^2	Turbulent kinetic energy
L	m	Turbulent length scalar
L_v	J/g	Latent heat of liquid
$\dot{M}_{d,k}$	kg/s	Liquid mass flux represented by k-th droplet parcel
N	-	Particle number, sample number
$\mathbf{N}$		Vector of viscious terms
$N_{\max}$	-	Maximum particle number in one cell
$N_{\min}$	-	Minimum particle number in one cell
N_s	-	Species number
$\widetilde{\mathrm{Nu}}$	-	Modified Nusselt number
Nu_0	-	Nusselt number
p	Pa	Pressure
P		Presumed probability density function
p_{crit}	Pa	Critical pressure of liquid phase
p_F	Pa	Vapor pressure
Pr	-	Prandtl number
r	m	Droplet radius
$r_{p,k}$	m	Droplet radius in kth parcel
R_α	J/(mol K)	Gas constant of species α
Re	-	Reynolds number
Re_d	-	Droplet Reynolds number
r_0	m	Initial droplet radii in counterflow spray flame
$\mathbf{S}$		Vector of source terms
S_g		Source term due to gas phase
S_l		Source term due to liquid phase
S_α	kg/s	Chemical production rate of species α in mass
Sc	-	Schmit number
$\widetilde{\mathrm{Sh}}$	-	Modified Sherwood number
Sh	-	Sherwood number
T	K	Temperature
T_{crit}	K	Critical temperature of liquid phase
T_d	K	Droplet temperature
t	s	Time

$\mathbf{u}$	m/s	Gas velocity in physical space
$\mathbf{V}$	m/s	Gas velocity in sample space
$\mathbf{v}$	m/s	Droplet velocity
u_x	m/s	Axial component of gas velocity
u_r	m/s	Radial component of gas velocity
v_x	m/s	Axial component of droplet velocity
v_r	m/s	Radial component of droplet velocity
$\mathbf{V}$	m/s	Velocity in sample space
$\mathbf{W}$		Vector of conservation variables
W_α	kg/mol	molecular weight of species α
X_α	-	Mole fraction of species α
$\mathbf{x}$	m	Geometrical coordinates
Y_{Ls}	-	Mass fraction of liquid vapor at droplet surface
Y_α	-	Mass fraction of species α
Z_A	-	Mass fraction of element A
ϵ	$\mathrm{m}^2/\mathrm{s}^3$	Dissipation rate of turbulent kinetic energy
ζ	-	Mixture fraction in sample space
λ	J/(m s K)	Thermal conductivity
μ	kg/(m s)	Viscosity coefficient
μ_t	kg/(m s)	Turbulent viscosity coefficient
μ_l	kg/(m s)	Laminar viscosity coefficient
μ_eff	kg/(m s)	Effective viscosity coefficient
ξ	-	Mixture fraction
ρ	$\mathrm{kg/m}^3$	mass density
σ_k	-	Effective Schmidt number for k
σ_ϵ	-	Effective Schmidt number for ϵ
χ	s^{-1}	Dissipation rate of mixture fraction
Γ_f		Droplet coalescence function
$\Gamma(x)$	-	Gamma function
Γ_h	kg/(m s)	Thermal diffusion coefficient
$\Gamma_{h,\mathrm{eff}}$	kg/(m s)	Effective thermal diffusion coefficient
$\Gamma_{h,t}$	kg/(m s)	Turbulent thermal diffusion coefficient
$\Gamma_{k,\mathrm{eff}}$	kg/(m s)	Effective exchange coefficient for k
$\Gamma_{\epsilon,\mathrm{eff}}$	kg/(m s)	Effective exchange coefficient for ϵ
Γ_M	kg/(m s)	Mean mass diffusion coefficient of the mixture
$\Gamma_{M,\mathrm{eff}}$	kg/(m s)	Effective mean mass diffusion coefficient of the mixture
$\Gamma_{M,t}$	kg/(m s)	Turbulent mean mass diffusion coefficient of the mixture
Δt	s	Time step
$\mathcal{V}$	m^{-3}	Control volume

Subscripts and Superscripts

Symbol	Quantity
C	Carbon
d	Droplet
F	Fuel
l	Liquid
O	Oxygen
p	Parcel
s	Species, sensible
$\tilde{}$	Favre average
$\bar{}$	Time average
$''$	Fluctuating component in Favre average
$'$	Fluctuating component in time average
$*$	Sample properties
$\langle\ \rangle$	Ensemble average
$\hat{}$	Estimated property

Physical Constants

Symbol	Quantity
$\mathcal{R} = 8.31451$ J/(mol K)	Universal gas constant
$g = 9.81$ m/s^2	Gravitational acceleration

Bibliography

[1] Mao, C.-P, Szekely Jr., G. A., Faeth, G. M., *Evaluation of locally homogeneous flow model for spray combustion*. NASA Contractor Report 3202 (1980).

[2] Mao, C.-P, Szekely Jr., G. A., Faeth, G. M., Evaluation of locally homogeneous flow model for spray combustion. *Journal of Energy*, **4(2)**: 78-87(1980).

[3] Shearer, A. J., Faeth, G. M., *Evaluation of locally homogeneous flow model for spray evaporation*. NASA Contractor Report 3198 (1979).

[4] Hennick, E. A., Lightstone, M., F., A Comparison of Stochastic Separated Flow Models for Particle Dispersion in Turbulent Flows. *Energy & Fuels* **14(1)**: 95-103 (2000).

[5] Lightstone, M. F., Stainsby, E. A., An improvement to the SSF model for the prediction of light particle dispersion. *Chemical Engineering Communications* **193(12)**:1605-1611 (2006).

[6] Laurent, F., Massot, M., Multi-fluid modelling of laminar polydisperse spray flames: origin, assumptions and comparison of sectional and sampling methods. *Combustion Theory and Modelling* **5**(4):537-572 (2001).

[7] Laurent, F., Massot, M., Villidieu, P., Eulerian multi-fluid modeling for the numerical simulation of coalescence in polydisperse dense liquid sprays. *Journal of Computational Physics* **194**(2):505-543 (2004).

[8] Dufour, G., Villidieu, P., A second-order Multi-Fluid model for evaporating sprays. *Mathematical Modeling and Numerical Analysis* **39**(5):931-936 (2005).

[9] Marchisio, D. L., Pikturna, J. T., Fox, R. O., Vigil, R. D., Barresi, A. A., Quadrature method of moments for population-balance equations. *AIChE Journal* **49**:1266-1276 (2003).

[10] McGraw, R., Description of aerosol dynamics by the quadrature method of moments. *Aerosol Science and Technology* **27**(2):255-265 (1997).

[11] Marchisio, D. L., Vigil, R. D., and Fox, R. O., Quadrature method of moments for aggregation-breakup. *Journal of Colloid and Interface Science* **258**(2):322-334 (2003).

[12] Marchisio, D. L., Fox, R. O., Solution of population balance equations using direct quadrature method of moments. *Journal of Aerosol Science* **36**:43-73 (2005).

[13] Gopireddy, S. R., Humza, R. M., Gutheil, E., Modeling and simulation of evaporating spray flows with coalescence in an Eulerian framework. *Chemie Ingenieur Technik* **84**(3):349-356 (2011).

[14] Gouesbet, G., Berlemont, A., Eulerian and Lagrangian approaches for predicting the behaviour of discrete particles in turbulent flows. *Progress in Energy and Combustion Science* **25**:133-159 (1999).

[15] Mashayek, F., Pandya, R. V. R., Analytical description of particle/droplet-laden turbulent flows. *Progress in Energy and Combustion Science* **29**:329-378 (2003).

[16] Loth, E., Numerical approaches for motion of dispersed particles, droplets and bubbles. *Progress in Energy and Combustion Science* **26**:161-223 (2000).

[17] Beck, J. C., Watkins, A. P., The droplet number moments approach to spray modelling: The development of heat and mass transfer sub-models. *International Journal of Heat and Fluid Flow* **24**:242-259 (2003).

[18] Faeth, G. M., Evaporization and combustion of sprays. *Progress in Energy and Combustion Science* **9**:1-76 (1983).

[19] Faeth, G. M., Mixing, transport and combustion in sprays. *Progress in Energy and Combustion Science* **13**:293-345 (1987).

[20] Faeth, G. M., Spray combustion phenomena. *Proceedings of Combustion Institute* **26**:1593-1612 (1996).

[21] Law, C. K., Heat and mass transfer in combustion: fundamental concepts and analytical techniques. *Progress in Energy Combustion and Science* **10**:295-318 (1984).

[22] Williams, F. A., Spray combustion and atomization. *Physics of Fluids* **1**:541-545 (1958).

[23] Fox, R. O., Laurent, F., Massot, M., Numerical simulation of spray coalescence in an Eulerian framework: Direct quadrature method of moments and multi-fluid method. *Journal of Computational Physics* **227**:3058-3088 (2008).

[24] Chan, T. L., Liu, Y. H., Chan, C. K., Direct quadrature method of moments for the exhaust particle formation and evolution in the wake of the studied ground vehicle. *Journal of Aerosol Science* **41**:553-568 (2010).

[25] Selma, B., Bannari, R., Proulx, P., Simulation of bubbly flows: Comparison between direct quadrature method of moments (DQMOM) and method of classes (CM). *Chemical Engineering Science*, **65**(6):1925-1941 (2010).

[26] Mazzei, L., Marchisio, D. L., Lettieri, P., Direct quadrature method of moments for the mixing of inert polydisperse fluidized powders and the role of numerical diffusion. *Industrial Engineering and Chemistry Research*, **49**(11):5141-5152 (2010).

[27] Bruyat, A., Laurent, C., Rouzand, O., Direct quadrature method of moments for multicomponent droplet spray vaporization. *International Conference on Multiphase Flow*, Tampa, Florida, May 30 - June 4 (2010).

[28] Choi, D., Schneider, L., Spyrou, N., Sadiki, A., Janicka, J., Evaporation of tetralin spray with direct quadrature method of moments and Eulerian multifluid method. *International Conference on Multiphase Flow*, Tampa, Florida, May 30 - June 4 (2010).

[29] Sirignano, W. A., Fluid dynamics of sprays-1992 Freeman scholar lecture. *Journal of Fluids Engineering* **115**:345-378 (1992).

[30] Sirignano, W. A., *Fluid dynamics and transport of droplets and sprays*. Cambridge University Press (1999).

[31] Orszag, S. A., Analytical Theories of Turbulence, *Journal of Fluid Mechanics* **41**: 363-386 (1970).

[32] Luo, K., Pitsch, H., Pai, M. G., Desjardins, O., Direct numerical simulations and analysis of three dimensional n-heptane spray flames in a model swirl combustor. *Proceedings of the Combustion Institute* **33**:2143-2152 (2011).

[33] Baritaud, T., Poinsot, T., Baum, M., *Direct numerical simulation for turbulent reacting flows*. Paris: Editions Technip, 1996.

[34] Yeung, P. K., Pope, S. B., Lagrangian statistics for direct numerical simulations of isotropic turbulence. *Journal of Fluid Mechanics* **207**:531-586 (1989).

[35] Squires, K. D., Eaton, J. K., Measurements of particle dispersion obtained from direct numerical simulations of isotropic turbulence. *Journal of Fluid Mechanics* **226**:1-35 (1991).

[36] Boivin, M., Simonin, O., Squires, K. D., Direct numerical simulation of turbulence modulation by particles in isotropic turbulence. *Journal of Fluid Mechanics* **375**:235-263 (1998).

[37] Sundaram, S., Collins, L. R., Collision statistics in an isotropic particle-laden turbulent suspension. Part 1: direct numerical simulations. *Journal of Fluid Mechanics* **335**:75-109 (1997).

[38] Okong'o N. A., Bellan J., Direct numerical simulation of a transitional supercritical binary mixing layer: heptane and nitrogen. *Journal of Fluid Mechanics*, **464**:1-34 (2002).

[39] Moin, P., Mahesh, K., DNS: a tool for turbulence research. *Annual Review of Fluid Mechanics* **30**:539-578 (1998).

[40] Sato, Y., Deutsch, E., Simonin, O., Direct numerical simulation of heat transfer by solid particles suspended in homogeneous isotropic turbulence. *International Journal of Heat and Fluid Flow* **19**(2):187-192 (1998).

[41] Mashayek, F., Simulations of reacting droplets dispersed in isotropic turbulence. *AIAA Journal* **37**:1420-1425 (1999).

[42] Janica J, Sadiki A. Large eddy simulation of turbulent combustion systems. *Proceedings of Combustion Institute* **30**:537-547 (2005).

[43] Menon, S., fureby, C., *Computational Combustion*. In: Encyclopedia of Aerospace Engineering, John Willey & sons 2010.

[44] Okong'o N. A., Bellan J., Consistent large-eddy simulation of a temporal mixing layer laden with evaporating drops. Part 1. Direct numerical simulation, formulation and *a priori* analysis. *Journal of Fluid Mechanics* **499**:1-47 (2004).

[45] Miller R. S., Bellan J., Direct numerical simulation and subgrid analysis of a transitional droplet laden mixing layer. *Physics of Fluids* **12**:650-671 (2000).

[46] Miller RS, Harstad KG, Bellan J. Direct numerical simulations of supercritical fluid mixing layers applied to heptane - nitrogen. *Journal of Fluid Mechanics* **436**:1-39 (2001).

[47] Domingo P, Vervisch L, Réveillon J., DNS analysis of partially premixed combustion in spray and gaseous turbulent flame-bases stabilized in hot air. *Combustion and Flame* **140**:172-195 (2005).

[48] Givi P. Quality assessment of the filtered density function for large eddy simulation. *1st workshop on "Quality Assessment of Unsteady Methods for Turbulent Combustion Prediction and Validation"*, Darmstadt (Seeheim -Jugenheim), Germany, June 16- 17, 2005.

[49] Wang Q. Z., Squires K. D., Large eddy simulation of particle-laden turbulent channel flows. *Physics of Fluids* **8**(5):1207-1223 (1996).

[50] Boivin M, Simonin O, Squires, K. D., On the prediction of gas-solid flows with two-way coupling using large eddy simulation. *Physics of Fluids* **12**:2080-2090 (2000).

[51] Langford, J. A., Moser, R. D., Optimal LES formulations for isotropic turbulence, *Journal of Fluid Mechanics* **398**:321-346 (1999).

[52] Meyers, J., Geurts, B., Sagaut, P., (Eds.), *Quality and reliability of large-eddy simulations*. ERCOFTAC Series, Vol. 12, Springer (2008).

[53] Kuerten, H., Geurts, B.; Armenio, V., Fröhlich, J. (Eds.) *Direct and large-eddy simulation VIII*. ERCOFTAC Series, Vol. 15, Springer (2011).

[54] Ge, H.-W., Zhu, M.-M., Chen, Y.-L., Gutheil, E., Hybrid unsteady RANS and PDF method for turbulent non-reactive/reactive flows. *1st Workshop on Quality Assessment of Unsteady Methods for Turbulent Combustion Prediction and Validation*, Darmstadt (Seeheim-Jugenheim), June 16-17, 2005.

[55] Pakhomov, M. A., RANS simulation of effect of evaporating droplets on a turbulent heat transfer in a mist flow in a sudden pipe expansion *Computational Thermal Sciences* **2(4)**:311-321, (2010).

[56] Mashayek, F., Droplet-turbulence interactions in low mach number homogeneous shear two-phase flows. *Journal of Fluid Mechanics* **367**:163-203 (1998).

[57] Mashayek, F., Direct numerical simulation of evaporating droplet dispersion in forced low mach number turbulence. *International Journal of Heat and Mass Transfer* **41**(17):2601-2617 (1998).

[58] Peters, N., Laminar diffusion flamelet models in non-premixed turbulent combustion. *Progress in Enery and Combustion Science* **10**:319-339 (1984).

[59] Dhuchakallaya, I., Rattanadecho, P.,Watkins, P., Auto-ignition and combustion of diesel spray using unsteady flamelet model. *Applied Thermal Engineering* 52:420-427 (2013).

[60] Knudsen, E., Pitsch, H., A general flamelet transformation useful for distinguishing between premixed and non-premixed modes of combustion. *Combustion and Flame* 156:678-696 (2009).

[61] Nguyen, P., Vervish, L., Subramanian, V., Domingo, P., Multidimensional flamelet-generated manifolds for partially premixed combustion. *Combustion and Flame* 127:43-61 (2010).

[62] Franzelli, B., Fiorina, B., Darabiha, N., A tabulated chemistry method for spray combustion. *Proceedings of Combustion Institue* **34** (2012).

[63] Gutheil, E., Multiple Solutions for Structures of Laminar Counterflow Spray Flames. *Progress in Computational Fluid Dynamics* 5(7):414-419 (2005).

[64] Pope S. B., *Turbulent flows*. Cambridge: Cambridge University Press, 2000.

[65] Hollmann, C., Gutheil, E. Flamelet-modeling of turbulent spray diffusion flames based on a laminar spray flame library. *Combustion Science and Technology* **135**(1-6):175-192 (1998).

[66] Richardson, J. M., Howard, H. C., Smith, R. W., The relation between sampling-tube measurements and concentration fluctuations in a turbulent gas jet. In: *Proceedings of Combustion Institute* **4**:814-817, Baltimore (1953).

[67] Hollmann C, Gutheil E. Modeling of turbulent spray diffusion flames including detailed chmistry. *Proceedings of Combustion Institute* **26**:1731-1738(1996).

[68] Ge,H.-W., Gutheil, E., Simulation of a turbulent spray flame using coupled PDF gas phase and spray flamelet modeling. *Combustion and Flame* **153(1-2)**:173-185, (2008).

[69] Antonia, R. A., Sreenivasan, K. R., Log-Normality of temperature dissipation in a turbulent boundary layer. *Physics of Fluids* **20**: 1800-1804 (1977).

[70] Kerstein, A. R., Ashurst, W. T., *Lognormality of gradients of diffusive scalars in homogeneous, two–dimensional mixing systems*. Sandia National Laboratories, 1983.

[71] Pope S. B., PDF methods for turbulent reactive flows. *Progress in Energy and Combustion Science* **11**:119-192 (1985).

[72] Dopazo C., Probability density function approach for a turbulent axisymmetric heated jet. Centerline evolution. *Physics of Fluids* **18**:397-404 (1975).

[73] Curl, R. L., Dispersed phase mixing: 1. Theory and effects in simple reactore *AIChE Journal* **9**(2): 175-181 (1963).

[74] Janicka J., Kolbe W., Kollmann W., Closure of the transport equation for the probability density function of turbulent scalar fields. *Journal of Non-Equilibrium Thermodynamics* **4**:47-66 (1979).

[75] Eckstein J, Chen J. Y., Chou C. P., Janicka J., Modeling of turbulent mixing in opposed jet configuration: one-dimensional Monte Carlo probability density function simulation. *Proceedings of Combustion Institute* **28**:141-148 (2000).

[76] Subramaniam S., Pope S. B., A mixing model for turbulent reactive flows based on euclidean minimum spanning trees. *Combustion and Flame* **115**:487-514 (1998).

[77] Hollmann C. *Modellierung turbulenter Sprayflammen unter Verwendung detaillierter chemischer Reaktionsmechanismen*. PhD Thesis, University of Heidelberg, Heidelberg, 1997.

[78] Crowe, C. T., Sharma, M. P., Stock, D. E., The particle-source-in cell (PSI-Cell) model for gas-droplet flows. *Journal of Fluids Engineering* **99**:325-332 (1977).

[79] Gutheil, E., Williams, F. A., A Numerical and Asymptotic Investigation of Structures of Hydrogen-Air Diffusion Flames. *Western States Section/The Combustion Institute* 89-109, 1989.

[80] Launder, B. E., Spalding, D. B., *Mathematical models of turbulence*. London/New York: Academic Press, 1972.

[81] Amsden, A. A., O'Rourke, J. O.,Butler, T. D., *KIVA-II: A computer program for chemically reactive flows with sprays*. Technical Report UC-96, Los Alamos National Laboratory, May 1989.

[82] Jones, W. P., Whitelaw, J. H., Calculation methods for reacting turbulent flows: A review. *Combustion & Flame* **48**:1-26 (1982).

[83] Chevalier, C., *Entwicklung eines detaillierten Reaktionsmechanismus zur Modellierung der Verbrennungsprozesse von Kohlenwasserstoffen bei Hoch- und Niedrigtemperaturbedingungen*. Ph.D. Thesis, University of Stuttgart, Stuttgart, 1993.

[84] Poinsot, T., Veynante, D., *Theoretical and numerical combustion*. Philadelphia: Edwards, 2001.

[85] Chase, M. W., Davis, C. A., Downey, J. R., Frurip, D. J., McDonald, R. A., Syverud, A. N., JANAF Thermochemical Tables, 3rd ed. *Journal of Physical and Chemical Reference Data* **14** (1985).

[86] Burcat, A., McBride, B., *1994 ideal gas thermodynamic data for combustion and air-pollutant use.* Technical Report, Reporrt TAE 697 TECHNION - Israel Institute of Technology Haifa, Israel (1993).

[87] Kee, R. J., Warnatz, J., Miller, J. A., *A FORTRAN computer-code package for the evaluation of gas-phase viscosities, conductivities, and diffusion coefficients.* Technical Report, Report SAND 83-8209 Sandia Laboratory (1983).

[88] Hirschfelder, J. O., Curtiss, C. F., Bird, R. B., *Molecular theory of gases and liquids*. New York: John Wiley & Sons (1954).

[89] Kolmogorov, A. N. A refinement of previous hypotheses concerning the local structure of turbulence in a viscous incompressible fluid at high Reynolds number. *Journal of Fluid Mechanics* **13**: 82–85 (1962).

[90] Lou, H., Miller, R. S., On the Scalar Probability Density Function Transport Equation for Binary Mixing in Isotropic Turbulence at Supercritical Pressure. *Physics of Fluids* **13**:3386-3399 (2001).

[91] Pope, S. B., Lagrangian PDF methods for turbulent flows. *Annual Review of Fluid Mechanics* **26**:23-63 (1994).

[92] Pope, S. B.. An explanation of the turbulent round-jet/plane-jet anomaly. *AIAA Journal* **16**(3):279-281 (1978).

[93] Jenny, P., Pope, S. B., Muradoglu, M., Caughey, D. A., A hybrid algorithm for the joint pdf equation of turbulent reactive flows. *Journal of Computational Physics* **166**:218-252 (2001).

[94] Ge, H.-W., Gutheil, E., PDF Simulation of Turbulent Spray Flows. *Atomization and Sprays* **16**(5):531-542 (2006).

[95] Ge, H-.W., *Probability Density Function Modeling of Turbulent Non–reactive and Reactive Spray Flows.* Ph.D. Thesis, University Heidelberg, Heidelberg, 2006.

[96] Pope, S. B., The probability approach to the modelling of turbulent reacting flows. *Combustion and Flame* **27**(3):299-312 (1976).

[97] Pope, S. B., Stochastic Lagrangian models of velocity in homogeneous turbulent shear flow. *Physics of Fluids* **14**(5):1696-1702 (2002).

[98] Pope, S. B., A stochastic Lagrangian model for acceleration in turbulent flows. *Physics of Fluids* **14**(7):2360-2375 (2002).

[99] Raman, V., Fox, R. O., Harvey, A. D., Hybrid finite-volume/transport PDF simulations of a partially premixed methane-air flame. *Combustion and Flame* **136**:327-350 (2004).

[100] Cao, R. R., Wang, H., Pope, S. B., *The effect of mixing models in PDF calculations of piloted jet flames.* Proceedings of the Combustion Institute **31**:1543-1550 (2007).

[101] Bockhorn, H., *Zur Struktur turbulenter Diffusionsflammen.* Habilitationsschrift, TU Darmstadt (1989).

[102] Abramzon, B., Sirignano, W. A., Droplet vaporization model for spray combustion calculation. *International Journal of Heat and Mass Transfer* **32**(9):1605-1618 (1989).

[103] Schiller, L., Neumann, A. Z., A drag coefficient correlation. *VDI Zeitschrift* **77**:318-320 (1933).

[104] Hubbard, G. L., Denny, V. E., Mills, A. F., Droplet evaporation: effects of transient and variable properties. *International Journal of Heat and Mass Transfer* **18**(9):1003-1008 (1975).

[105] Atkins, P., Paula, J. D., *Atkins Physical Chemistry.* Oxford Higher Education, 7th Edition, 2001.

[106] Antoine, C., Tensions des vapeurs; nouvelle relation entre les tensions et les temperatures. *Comptes Rendus des Séances de l'Académie des Sciences* **107**: 681-684 (1888).

[107] Vargaftik, N. B. *Handbook of physical properties of liquids and gases: Pure substances and mixtures.* Washington: Hemisphere Publication Corporation (1986).

[108] Hylkema, J., Villedieu, P., Une méthode particulaire aléatoire reposant sur une équation cinétique pour la simulation numérique des sprays denses. *C.R.A.S. de Paris, t.325 série* **1**:323-328 (1997).

[109] Kuo, K. K., *Principles of combustion.* New York: John Wiley & Sons, 1986.

[110] Crowe, C. T., Chung, J. N., Troutt, T. R., Particle mixing in free shear flows. *Progress in Engery and Combustion and Science* **14**:171-194 (1988).

[111] Riley, J. J., Patterson, G. S., Diffusion experiments with numerically integrated isotropic turbulence. *Physics of Fluids* **17**:292-297 (1974).

[112] Squires, K. D., Eaton, J. K., Particle response and turbulence modification in isotropic turbulence. *Physics of Fluids* **2**(7):1191-1203 (1990).

[113] Elghobashi, S., Truesdell, G. C., On the two-way interaction between homogeneous turbulence and dispersed solid particles, I: turbulence modification. *Physics of Fluids* **5**:1790-1801 (1993).

[114] Ahmed, A. M., Elghobashi, S., On the mechanisms of modifying the structure of turbulent homogeneous shear flows by dispersed particles. *Physics of Fluids* **12**(11): 2906-2930 (2000).

[115] Tsuji, T., Narutomi, R., Yokomine, T., Ebara, S., Shimizu, A., Unsteady three-dimensional simulation of interactions between flow and two particles. *International Journal Multiphase Flow* **29**:1431-1450 (2003).

[116] Jaberi, F. A., Temperature fluctuations in particle-laden homogeneous turbulent flows. *International Journal of Heat and Mass Transfer* **41**(24):4081-4093 (1998).

[117] Jaberi, F. A., Mashayek, F., Temperature decay in two-phase turbulent flows. *International Journal of Heat and Mass Transfer* **43**(6):993-1005 (2000).

[118] Pandya, R. V. R., Mashayek, F., Non-isothermal dispersed phase of particles in turbulent flow. *Journal of Fluid Mechanics* **475**:205-245 (2003).

[119] Mashayek, F., Numerical investigation of reacting droplets in homogeneous shear turbulence. *Journal of Fluid Mechanics* **405**:1-36 (2000).

[120] Mashayek, F., Velocity and temperature statistics in reacting droplet-laden homogeneous shear turbulence. *Journal of Propulsion and Power* **17**(1): 197-202 (2001).

[121] Mashayek, F., Dynamics of evaporating drops. Part I: formulation and evaporation model. *International Journal of Heat and Mass Transfer* **44**(8):1517-1526 (2001).

[122] Mashayek, F., Dynamics of evaporating drops. Part II: free oscillations. *International Journal of Heat and Mass Transfer* **44**(8):1527-1541 (2001).

[123] Mashayek, F., Jaberi, F. A., Miller, R. S., Givi, P., Dispersion and polydispersity of droplets in stationary isotropic turbulence. *International Journal of Multiphase Flow* **23**:337-355 (1997).

[124] Abdel-Hameed, H., Bellan, J., Direct numerical simulations of two-phase laminar jet flows with different cross-section injection geometries. *Physics of Fluids* **14**(10): 3655-3674 (2002).

[125] Leboissetier, A., Okong'o, N. A., Bellan, J., Consistent large-eddy simulation of a temporal mixing layer laden with evaporating drops. Part 2. *A posteriori* modelling. *Journal of Fluid Mechanics* **523**:37-78 (2005).

[126] Le Clercq, P. C., Bellan, J., Direct numerical simulation of gaseous mixing layers laden with multicomponent-liquid drops: liquid-specific effects. *Journal of Fluid Mechanics* **533**:57-94 (2005).

[127] Varanasi, K. K., Clack, H. L., Miller, R. S., On preferential diffusion of binary component liquid droplets evaporating in a two-phase mixing layer. *International Journal of Multiphase Flow* **30**:1235-1257 (2004).

[128] Haworth, D. C., Jansen, K., Large-eddy simulation on unstructured deforming meshes: toward reciprocating IC engines. *Computers & Fluids* **29**:493-524 (2000).

[129] Pope, S. B., Ten questions concerning the large-eddy simulation of turbulent flows. *New Journal of Physics* **6**:35 (2004).

[130] Yeh, F, Liu, U., On the motion of small particles in a homogeneous turbulent shear flow. *Physics of Fluids* **3**(11):2758-2776 (1991).

[131] Aggarwal, S. K., Xiao, Y., Effects of external forcing on droplet dispersion in a developing shear layer. *Journal of Propulsion and Power* **10**:395-401 (1994).

[132] Miller, R. S., Turbulence-Flame Modification in Particle Laden Reacting Shear Flow. *AIAA paper 2001-0193, 39th Aerospace Science Meeting*, Reno, Nevada, January 8-11, 2001.

[133] Miller, R. S., Bellan, J., On the validity of the assumed probability density function method for modeling binary mixing/reaction of evaporated vapor in gas/liquid-droplet turbulent shear flow. *Proceedings of Combustion Institute* **27**:1065-1072 (1998).

[134] Miller, R. S., Bellan, J., Direct numerical simulation of a confined three-dimensional gas mixing layer with one evaporating hydrocarbon-droplet-laden stream. *Journal of Fluid Mechanics* **384**:293-338 (1999).

[135] Armenio, V., Piomelli, U., Fiorotto, V., Effect of the subgrid scales on particle motion. *Physics of Fluids* **11**(10):3030-3042 (1999).

[136] Sankaran, V., Menon, S., LES of spray combustion in swirling flows. *Journal of Turbulence* **3**(11) (2002).

[137] Pandya, R. V. R., Mashayek, F., Two-fluid large-eddy simulation approach for particle-laden turbulent flows. *International Journal of Heat and Mass Transfer*, **45**(24):4753-4759 (2002).

[138] Apte, S. V., Gorokhovski, M, Moin, P. LES of atomizing spray with stochastic modeling of secondary breakup. *International Journal of Multiphase Flow* **29**:1503-1522 (2003).

[139] Yang, C. Y., Lei, U., Role of the turbulent scales in the settling velocity of heavy particles in homogeneous isotropic turbulence. *Journal of Fluid Mechanis* **371**:179-205 (1998).

[140] Ling, W., Chung, J. N., Troutt, T. R., Crowe, C. T.. Direct numerical simulation of a three-dimensional temporal mixing layer with particle dispersion. *Journal of Fluid Mechanics* **358**:61-85 (1998).

[141] Iliopoulos, I., Mito, Y., Hanratty, T. J.. A stochastic model for solid particle dispersion in a nonhomogeneous turbulent field. *International Journal of Multiphase Flow* **29**:375-394 (2003).

[142] Akselvoll, K., Moin, P., Large-eddy simulation of turbulent confined coannular jets. *Journal of Fluid Mechanics* **315**:387-411 (1996).

[143] Borghi, R., Turbulent combustion modelling. *Progress in Energy and Combustion Science* **14**:245-292 (1988).

[144] Tolpadi, A. K., Correa, S. M., Burrus, D. L., Mongia, H. C., Monte Carlo Probability density function method for gas turbine combustor flowfield predictions. *Journal of Propulsion and Power* **13**(2):218-225 (1997).

[145] Veynante, D., Vervisch, L., Turbulent combustion modeling. *Progress in Engery and Combustion Science* **28**:193-266 (2002).

[146] Hopf, E., Statistical hydromechanics and functional calculus. *Journal of Rational Mechanics and Analysis*, **1**:87-123 (1952).

[147] Lewis, R. M., Kraichnan, R. H., A space-time functional formalism for turbulence. *Communications on Pure and Applied Mathematics*, **15**:397-411 (1962).

[148] Petty, C. A., Reed, X. B. J., Asympototic solutions of Hopf's equation for turbulent chemical reactions. *AIChE Journal* **18**:751-753 (1972).

[149] Lundgren, T. S. Distribution functions in statistical theory of turbulence. *Physics of Fluids* **10**:969-975 (1967).

[150] Haworth, D. C., Pope, S. B., A generalized Langevin model for turbulent flows. *Physics of Fluids* **29**(2):387-405 (1986).

[151] Bergdorf, M., Cottet, G.-H., Koumoutsakos, P., Multilevel adaptive particle methods for convection-diffusion equations. *Multiscale Modeling and Simulation: A SIAM Interdisciplinary Journal* **4**(1):328-357 (2005).

[152] Tannehill, J. C., Anderson, D. A., Pletcher, R. H., *Computational fluid mechanics and heat transfer*. Second ed., Taylor and Francis, 1999.

[153] Shapira, Y., *Matrix based multigrid*. Second ed., Springer New York, 2008.

[154] Pepper, D. W., Heinrich, J. C., *The finite element method: basic concepts and applications (Series in computational and physical processes in mechanics and thermal sciences)*. Second ed., Taylor & Francis, 1999.

[155] Patankar, S. V., *Numerical heat transfer and fluid flow*. Taylor & Francis, 1980.

[156] Metzner, M., *Mehrgitterverfahren für die Kompressiblen Euler- und Naiver Stoke Gleichungen mit besonderer Betrachtung des Schwach Kompressiblen Falles.* Ph. D. thesis, University of Heidelberg (2003).

[157] Bijl, H., *Computation of flow at all speeds with a staggered scheme.* Ph.D. Thesis, Technische Universität Delft (1999).

[158] Srivatsa, S.,K., *CORA2: A computer code for axisymmetrical combustion chambers*. CHAM Ltd. (1977).

[159] Fletcher, C. A. J., *Computational techniques for fluid dynamics 2. Specific techniques for different flow categories*. Berlin/New York: Springer (1991).

[160] Metzner, M., Wittum, G., Computing low Mach number flows by parallel adaptive multigrid. *Computing and Visualization in Science* **9**: 259-269 (2006).

[161] Klein, R., Munz, C. D., The multiple pressure variable (MPV) approach for numerical approximation of weakly compressible fluid flow. In: *Numerical Modelling in Continuum Mechanics*, Rannacher, R., Feistauer, M., Kozel, K. (eds.) 123-133. Charles University, Prag (1995).

[162] Doormal, J. P. V., Raithby, G. D., Enhancement of the SIMPLE method for predicting incompressible fluid flows. *Numerical Heat Transfer* **7**:147-163 (1984).

[163] Sabel'nikov, V., Soulard, O., Eulerian (field) Monte Carlo methods for solving PDF transport equations in turbulent reacting flows. In: *Handbook of Combustion*, Wiley-VCH (2010).

[164] Courant, R., Friedrichs, K., Lewy, H., Über die partiellen Differenzengleichungen der mathematischen Physik. *Mathematische Annalen* **100**(1): 32-74 (1928).

[165] Liu, K., *Joint velocity-turbulent frequency-composition probability density function (PDF) calculation of bluff body stabilized flames.* Ph.D. thesis, Cornell University, 2004.

[166] Batchelor, G. K., *An Introduction to Fluid Dynamics*. Cambridge University Press London, 1967.

[167] Ge, H.-W., Gutheil, E., An efficient numerical solution scheme for the computation of the particle velocity in two-phase flows. *Progress in Computational Fluid Dynamics* **7-8**:467-472 (2007).

[168] Bird, G. A., *Molecular gas dynamics and direct simulation of gas flows*. Oxford Science Publications **42** (1994).

[169] Bouchet, F., On zero pressure gas dynamics. *Advances in kinetic theory and computing: selected papers*, World Scientific, Singapore (1994).

[170] Tratnig, A., Brenn, G., Drop size spectra in sprays from pressure-swirl atomizers. *International Journal of Multiphase Flow* **36**(5):349-363 (2010).

[171] Humza, R. M., Gopireddy, S. R., Gutheil, E., Numerical Simulation of Evaporating Sprays in a Convective Flow Field. *ICLASS 2012, 12th Triennial International Conference on Liquid Atomization and Spray Systems*, Heidelberg, Germany, September 2-6, 2012.

[172] Gordon, R. G., Error Bounds in Equilibrium Statistical Mechanics. *Journal of Mathematical Physics* **9**: 655-663 (1968).

[173] Albrecht, H.-E., Damaschke, N., Tropea, C., *Laser Doppler and Phase Doppler Measurement Techniques*, Springer-Verlag, Berlin, 2003.

[174] McDonell, V. G., Samuelsen, G. S., *Detailed data set: PDI and IRES measurements in methanol sprays under reacting and nonreacting conditions, case A-C.* Report UCI-ARTR-90-17A-C, UCI Combustion Laboratory, Irvine, 1990.

[175] McDonell, V. G., Samuelsen, G. S., An experimental data base for computational fluid dynamics of reacting and nonreacting methanol sprays. *Journal of Fluids Engineering* **117**:145-153 (1995).

[176] Massiello, P. J., *Intermittency of the fine structure of turbulent velocity and temperature field measured at high Reynolds number.* Ph.D. thesis, University of California, San Diego, 1974.

[177] Wheeler, J. C., Modified moments and Gaussian quadratures. *Rocky Mountain Journal of Mathematics* **4**:287-296 (1974).

[178] Dukowicz, J. K. A particle-fluid numerical model for liquid sprays. *Journal of Computational Physics* **2**:111-566 (1980).